COMPUTER-AIDED AERODYNAMIC DESIGN OF SMALL SCALE HORIZONTAL AXIS WIND TURBINE BLADES

A Thesis Submitted to
the Graduate School of Engineering and Sciences of
İzmir Institute of Technology
in Partial Fulfillment of the Requirements for the Degree of

MASTER OF SCIENCE

in Mechanical Engineering

by
Tuhfe GÖÇMEN

July 2012
İZMİR

We approve the thesis of **Tuhfe GÖÇMEN**

Prof. Dr. Mehmet Barış ÖZERDEM
Supervisor

Assoc. Prof. Dr. Moghtada MOBEDI
Committee Member

Assoc.Prof. Dr. Serhan KÜÇÜKA
Committee Member

Assist. Prof. Dr. Seçil ARTEM
Committee Member

Assist. Prof. Dr. Koray ÜLGEN
Committee Member

13/07/2012

Prof. Dr. MetinTANOĞLU
Head of the Department of Mechanical Engineering

Prof. Dr. R. Tuğrul SENGER
Dean of the Graduate School of Engineering and Sciences

ACKNOWLEDGEMENTS

First of all, I would like to thank my supervisor Barış ÖZERDEM for his valuable guidance and support. I would also like to thank to my professors, Moghtada MOBEDI and Ünver ÖZKOL for their encouragement and insights throughout the study.

I wish to express my deepest gratitude and love to my mother Süriye GÖÇMEN who taught me to believe in myself from the beginning and my brother Andaç GÖÇMEN who has been one my best friends for all my life.

I would also like to thank to my friends here in IZTECH, especially to Z-46 CREW together with Eren UÇAR for their cardinalism, help and support socially and academically.

ABSTRACT

COMPUTER AIDED AERODYNAMIC DESIGN OF SMALL SCALE HORIZONTAL AXIS WIND TURBINE BLADES

In this thesis, aerodynamic design of 1, 5, 10, 25, 50, 100, 250 and 500 kW horizontal axis wind turbine generators has been performed. The design procedure starts with the design and analysis of airfoils done by programs of PROFOIL and XFOIL, respectively through which the structural, aerodynamic and aeroacoustic principles have been taken into consideration. Then, the performance parameters of designed profiles were inputted to the constructed modified blade element momentum theory (BEM) code together with the main design parameters in order to obtain 3D blade geometry. The code is validated using MIE wind turbine with a rated power of 8 kW. The generated blade geometries are then analyzed using commercial computational fluid dynamics CFD code Numeca FINE™/Turbo and the velocity and pressure distributions around the blade have been visualized, separately. Moreover, the power coefficient, Cp was calculated and the power curves of the designed wind turbine rotors were drawn.

ÖZET

KÜÇÜK ÖLÇEKLİ YATAY EKSENLİ RÜZGAR TÜRBİN PALALARININ BİLGİSAYAR DESTEKLİ AERODİNAMİK TASARIMI

Bu çalışmada, 1, 5, 10, 25, 50, 100, 250 ve 500 kW güç çıkışı olan yatay eksenli rüzgar türbinlerinin aerodinamik tasarımı yapılmıştır. Dizayn süreci PROFOIL ve XFOIL programları kullanılarak ve yapısal, aerodinamik ve aeroakustik prensipler göz önünde bulundurularak gerçekleştirilen kanat profili tasarım ve analizi ile başlamıştır. Sonrasında, tasarlanan profillerin performans parametreleri ve temel kanat tasarım özellikleri; modifiye edilmiş pala elemanı teorisi kullanılarak hazırlanan koda girilmiştir ve çıktı olarak 3 boyutlu pala geometrisi elde edilmiştir. Kullanılan kod, MIE 8 kW rüzgar türbini verilerini kullanarak doğrulanmıştır. Oluşturulan geometri, ticari bir hesaplamalı akışkanlar dinamiği HAD kodu olan Numeca FINE™/Turbo programı kullanılarak incelenmiş ve pala etrafındaki hız ve basınç dağılımları gözlemlenmiştir. Ayrıca, tasarlanmış rüzgar türbini rotorlarının güç katsayıları hesaplanmış ve güç eğrileri çizdirilmiştir.

TABLE OF CONTENTS

LIST OF FIGURES

Figure **Page**

LIST OF TABLES

LIST OF SYMBOLS

A	Rotor swept area, m^2
a	Axial induction factor at rotor plane
a'	Angular induction factor at rotor plane
B	Number of blades
c	Chord length of the airfoil
c_d	2D drag coefficient
c_D	3D drag coefficient
c_l	2D lift coefficient
c_L	3D lift coefficient
Cp	Power coefficient of wind turbine rotor
c_T	Thrust coefficient
D	Drag force, N
F	Prandtl tip loss factor
F_I	Inviscid flux vector
F_V	Viscous flux vector
l	Length scale, m
L	Lift force, N
M	Mach number
$\dot{m}$	Mass flow rate, kg/s
p	Pressure, Pa, kPa
P	Power, W, kW
Q	Rotor torque, Nm
r	Local radius, m
R	Rotor radius, m
Re	Reynolds number
T	Rotor thrust, N
U	Free stream velocity, m/s
W, w	Relative velocity, m/s
W	Work, Nm

Greek letters

λ	Tip speed ratio
ρ	Air density, kg/m^3
α	Angle of attack, deg
θ_P	Blade pitch angle, deg
θ_T	Blade twist angle, deg
φ	Angle of relative wind velocity, deg
σ	Solidity
σ'	Local solidity
v	Kinematic viscosity of air, m^2/s
v_t	Turbulent kinematic viscosity, m^2/s
μ	Dynamic viscosity of air, kg/m·s
Ω, ω	Angular velocity of the rotor, rad/s

Subscripts

design	Design variable
r	local
rel	relative
N	normal
T	tangential

Abbreviations

Re	Reynolds number
HAWT	Horizontal axis wind turbine
VAWT	Vertical axis wind turbine

CHAPTER 1

INTRODUCTION

Starting with the industrial revolution, energy has become one of the major concerns of all kind of people around the world. Because of the increasing demand of energy, several solutions have been provided including fossil fuels and nuclear power. Although those energy sources were sufficient to meet the needs of the market, they have created much bigger problems such as pollution and global warming. As a result, it has been agreed by many countries all around the world that carbon dioxide and greenhouse gasses emissions should be limited by Kyoto Protocol prepared by United Nation Framework Convention on Climate Change (UNFCCC) [1]. This has led the interest in green energy to increase tremendously and made wind turbines more popular for the investors.

1.1. History of Wind Energy Usage

Wind was also one of the most important sources to produce power in the past. Two main examples are the windmills and windwheels. They were using the torque produced by the machinery for various purposes. The windmills were basically used for milling the grains and the windwheels were used to pump water. The first windmill which rotates vertically is believed to be in use in the year of 644 A.D. in Persian – Afghan border and it is illustrated in Figure 1.1. However, it took centuries to come to Europe in where the axis of rotation was mostly horizontal. In Europe, the first windmill can be said to have been built in 1119, beginning of the twelfth century [2]. Thus, all those experiences gained in all these years will be beneficial for understanding and contributing to the development of modern wind turbine technology.

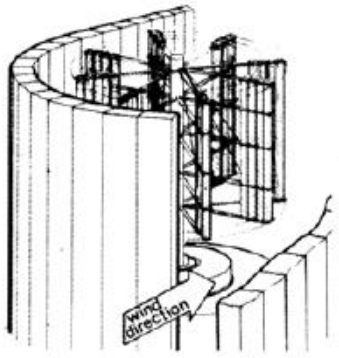

Figure 1.1 Afghan – Persian Windmill [3]

1.2. Modern Wind Turbines

Using wind for electricity started with the invention of electrical generators which happened towards the end of the nineteenth century. After their appearance, it has been thought to rotate it with a windmill and the first notable attempt was in 1891, Askov, Denmark. The first power producing turbine was designed and built by Poul La Cour and it was driving a dynamo. It should be noted that, with that turbine, he also handled the storage problem by using the direct current generated by the wind turbine to electrolyze water and store hydrogen gas where it is used in gas lamps at that time very commonly [2].

Figure 1.2.Poul La Cour's first electricity producing wind turbine [2]

In the following years, the small electrical generators have become more and more widespread, both in Europe and the USA, and the most prominent small wind turbine is three bladed with actual airfoil shapes produced by Marcellus Jacobs [3]. As can also be seen in Figure 1.2, that rotor began to shape the horizontal axis wind turbines today.

Figure 1.3.Jacobs Turbine [3]

In Europe, Denmark and Germany was the two main countries that host important technological developments in wind turbine technology in early twentieth century, especially after the First World War. In Denmark, the idea to use aerodynamic stall in power control and usage of induction generator has been developed and it can be said that, those innovations contribute a lot to modern wind turbine technology and also made Denmark one of the strongest countries in wind turbine business. In Germany, the applications of aerodynamics to the rotor technology done by Ulrich Hütter were so remarkable that some of the principles are still in use today [4].

In United States, especially after the oil crisis in 1970's, the interest in wind energy has increased. Together with the regulations about tax credit to wind turbine investors, wind energy has become profitable. Thus, individual turbines or wind farms has been constructed approximately in five years up to the capacity of 1500MW, especially in California. However, when the regulation cancelled, the momentum of wind turbine business has faded [3].

Towards the end of the twentieth century, originated from environmental, financial and also political reasons, the interest and investment in wind turbine business

has increased tremendously. As a result, technological development has reached to a level that, according to Global Wind Statistics report prepared by Global Wind Energy Council (GWEC), the installed wind power capacity is 238,351MW in total around the world by the end of 2011 [5]. It can be seen from Figure 1.4 that, even for a five year time period, the usage of wind power in order to produce electricity has increased excessively.

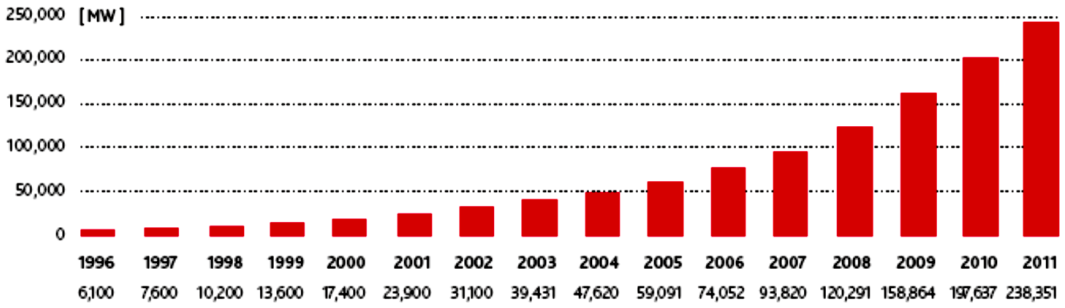

Figure 1.4.Global Cumulative Installed Wind Capacity 1996 - 2011 [5]

While world – wide improvement in terms of wind energy usage is spoken of, it should be mentioned that together with the European countries and USA, Asian countries such as China and India have contributed a lot to that increasing regime especially after year 2008. Figure 1.5 shows the sectorial growth of wind turbine industry in Asia.

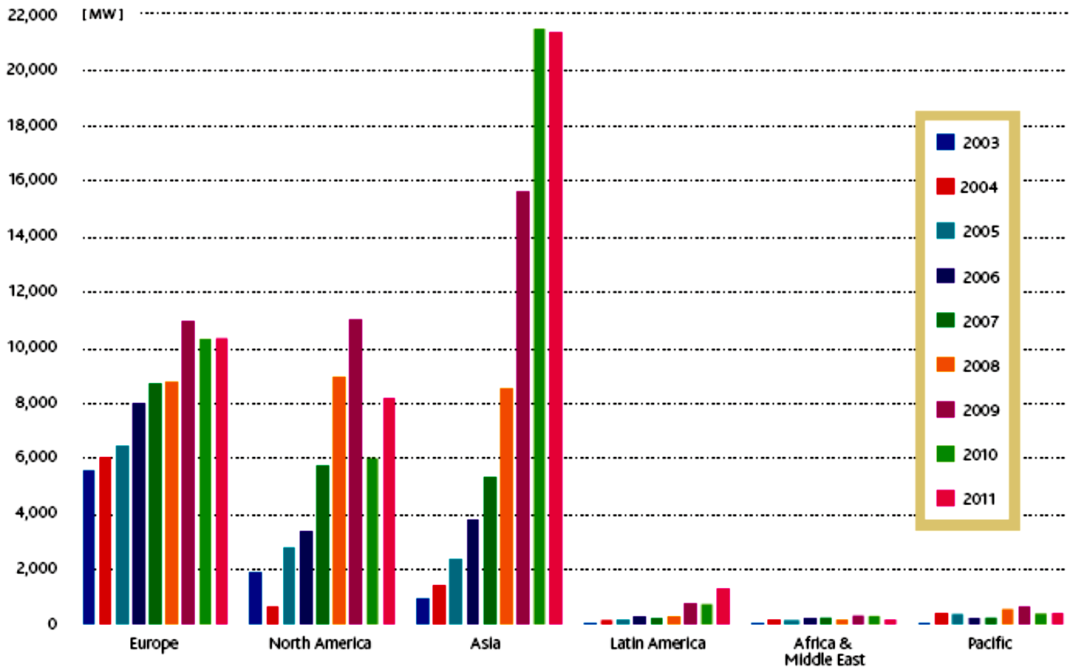

Figure 1.5.Annual Installed Capacity by Region [5]

The modern wind turbines can be classified with respect to the axis of rotation; horizontal axis and vertical axis wind turbines (HAWT and VAWTs, respectively). HAWTs are more commonly in use and their technological development, together with the financial investments, is more sophisticated. However, the interest in VAWTs is growing and important studies are being done on that subject. The VAWTs consist of three main shapes; Savonius Rotor, Darrieus Rotor and H-Rotor. The Darrieus Rotor and H-Rotor are lift type, which means that the rotation occurs due to lift force, whereas Savonius Rotor is drag type, which means the rotation occurs due to the drag force created by the wind. Those rotor concepts with a vertical axis of rotation are shown in Figure 1.6 and the detailed information about them can be found in the study of Eriksson et al. [8].

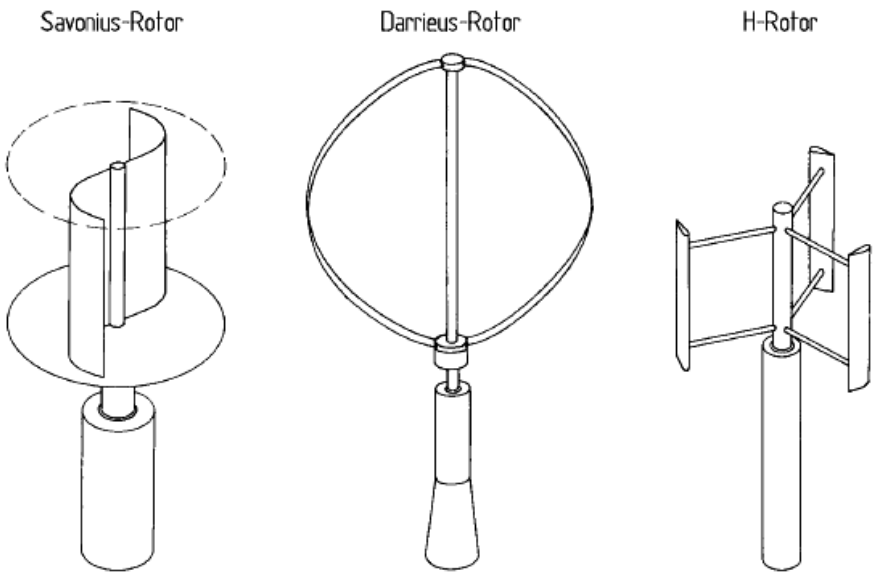

Figure 1.6.Rotor Concepts with a Vertical Axis of Rotation [2]

Also, the HAWTs may be defined by considering the position of the rotor with respect to wind direction; downwind and upwind turbines. The rotors of upwind turbines are placed in front of the rest of the turbine such that the wind strikes the blades first. On the other hand, in downwind turbines the rotors are to meet the wind after the tower and nacelle. Upwind and downwind configurations of horizontal axis wind turbines are described schematically in Figure 1.7.

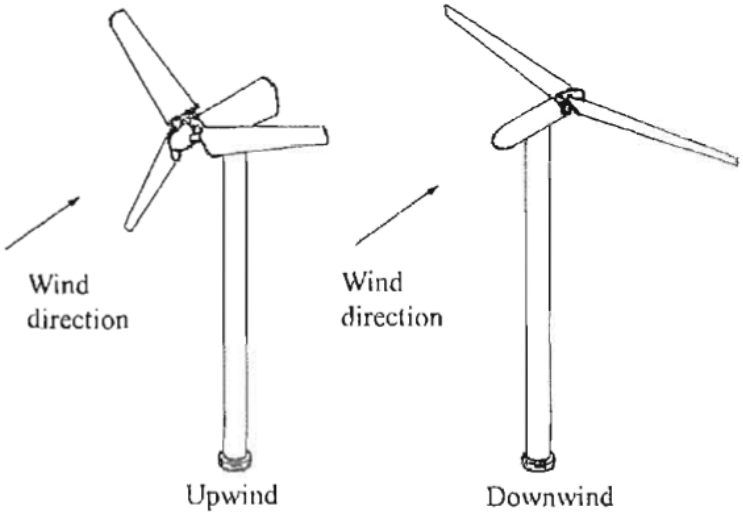

Figure 1.7.HAWT configurations [3]

1.3. Aim and Scope of the Thesis

According to the latest regulation done by Republic of Turkey Energy Market Regulatory Authority, for the wind turbine facilities generating power up to 500 kW getting license is no longer mandatory [6]. Since this arrangement has induced high demand towards small scale wind turbines, the objective of this study is to design and analyze small scale wind turbine blades using computer programs. Namely horizontal axis, 3 bladed wind turbines with a desired output power of 1, 5, 10, 25, 50, 100, 250 and 500 kW have been designed. The design process of a wind turbine blade is actually a multi-disciplinary case which includes many constraints from the prospective of aerodynamics, aeroelasticity, acoustics, etc. [7]. However, it should be noted that, both of the design and analysis process followed in this thesis is based on aerodynamics and basic aeroacoustics.

The process starts with design and analysis of the airfoil which is done by PROFOIL and a user interface for XFOIL called PROFILI, respectively. After obtaining the results from the designed airfoil such as its maximum lift to drag ratio point, they are put as inputs to a program developed using modified blade element momentum theory on MATLAB®. The program is designed to read the airfoil data and rotor characteristics such as number of blades, desired radius and tip speed ratio, etc. together with the average speed of incoming wind velocity and give the geometric characteristics of the blade such as chord and twist distribution and the expected coefficient of power as outputs. Those geometrical data of the blade are then inputted to CFD software called NUMECA which gives the probable power output of the design. The schematic view of the followed process of the design and analysis is given in Figure 1.8.

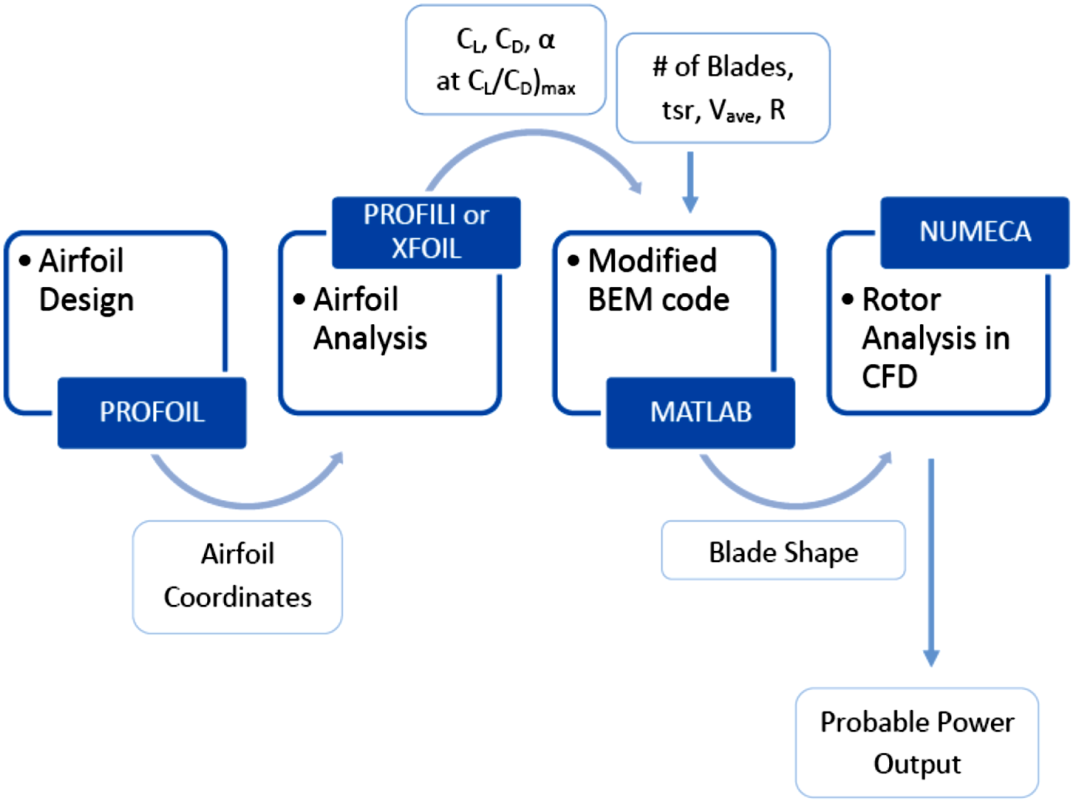

Figure 1.8.Design and Analysis Process Followed

Note that, after obtaining the power output from the CFD analysis, it can be decided to modify the blade and the process may start again from the beginning which is the airfoil creation.

In this chapter of the thesis, together with the content and objective of this study, a general overview of the usage of wind power throughout the history and its transformation to the electricity production has been given. Some of the innovative designs and understandings have been emphasized. Also, worldwide prospect of wind energy usage has been stressed in order to see the importance of wind energy business.

'In Chapter 2', more detailed information about horizontal axis wind turbines (HAWTs) is given. The subsystems of a HAWT (i.e. the rotor, power-train, nacelle and tower) together with the control mechanisms are discussed.

'In Chapter 3', the wind turbine aerodynamics is explained in a very detailed manner consisting of basic 1-D Momentum Theory, General Momentum Theory, Blade Element Theory and Blade Element Momentum (BEM) Theory.

'*In Chapter 4*', a detailed literature survey is presented. The studies about airfoil design and the blade design studies are summarized.

'In Chapter 5', design and analysis methodology of wind turbines blades that is used in this thesis is discussed in three parts; airfoil design and analysis, blade design and rotor analysis. The theories and the methodologies followed are expressed with the brief explanations of the software used.

'*In Chapter 6',* the aerodynamic design and analysis procedure of 1, 5, 100 and 250 kW turbine rotors are given. The results are presented and related statements are made.

'In Chapter 7', all the information is summed up and the study is concluded.

CHAPTER 2

HORIZONTAL AXIS WIND TURBINE CHARACTERISTICS

In this chapter, the subsystems of the horizontal axis wind turbines will be explained. Firstly, the rotor will be described and then, power-train, nacelle, tower and foundation which can be seen in Figure 2.1.

2.1. Subsystems of Horizontal Axis Wind Turbines (HAWTs)

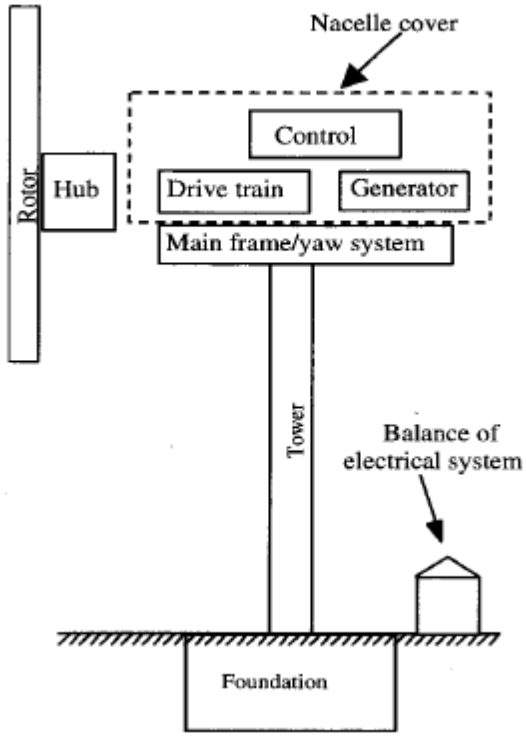

Figure 2.1.Main components of a horizontal axis wind turbine [3]

2.1.1. Rotor Subsystem

The rotor subsystem of a wind turbine is considered to be the most important part of a wind turbine in terms of performance and cost criterion and it consists of two parts: hub and blades. One bladed rotor designs is not practical since a counter-weight is required to balance the structural and aerodynamic forces. Two bladed designs are only 2 or 3% less efficient compared to three bladed systems [20] and therefore preferable conceiving manufacturing costs. However, since less bladed rotors needs to have higher rotational speed in order to produce same amount of power, that leads to emission of higher levels of noise and higher maintenance costs. The forces are more evenly balanced in three bladed rotors and for many, it is aesthetically more pleasing since image corrosion is another obstacle especially for the wind turbines closer to the urban areas.

Classifications of the hubs used in horizontal axis wind turbine may be the rigid hub and teetered hub. Rigid hub is the configuration in which the blades are connected to the hub with bolts and hub is connected to shaft, rigidly. For instance, in two bladed designs, teetered hub is considered to be more convenient since rigid hub transmits the dynamic loads directly to the shaft. However, in teetered connections, it is possible to balance the structural loads with aerodynamic loads.

The main material of the blades has been wood for the historical wind turbines. Although wood and wood laminate are still in use, there are other methods more common today such as glass reinforced plastic (GRP), carbon fiber reinforced plastic (CFRP), steel and aluminum. For very small wind turbines, less than 5 m diameter, the selection of the material is done due to its production efficiency. On the other hand, for larger blades, mostly GRP is used [20].

2.1.2. Power-Train Subsystem

A power train subsystem consists of main shaft, couplings, gearbox, brakes, and generator which are required to transmit mechanical power into electrical power. Main shaft is the primary shaft that transfers the torque produced by the rotor to rest of the drive train. Couplings are the elements that are used to connect the shafts and they are responsible from the transfer of torque from the main shaft to the second one. The

gearbox, which is one of the heaviest and most expensive equipment in the nacelle, is used to increase the speed transmitted from the shafts to the level that the generator can operate. Breaks are the elements that simply prevent the rotors from turning when the wind turbine is out of operation. Lastly, all grid connected turbines include an alternating current (AC) generator in order to complete the transmission of mechanical energy into electricity. The generators are mainly divided into two parts; an alternator or synchronous generator which operates at the same frequency with the network and an induction or asynchronous generator which operates at higher frequencies than the network.

2.1.3. The Nacelle Structure Subsystem

The nacelle structure is the path to transfer the loads from main shaft to the tower. Nacelle cover is mainly the protection for the mechanical and electrical components from weather conditions such as rain, snow or ice. They are normally made of light materials such as fiberglass in order not to put extra weight load to the tower and a sample nacelle can be examined from Figure 2.2.

Figure 2.2.Typical nacelle cover. Reproduced by permission of Nordex AG [3]

2.1.4. The Tower Subsystem and Foundation

Towers are the high structures to keep the rotors and the nacelle up in the air. Their height should be at least the length of the radius of the rotor and also some ground clearance should be left. The tower height is considered to be a minimum of 24 m in order to catch higher speed flows and avoid atmospheric boundary layer together with the intense turbulence effects [3]. According to the height of the selected tower, the foundation should be constructed to stabilize the whole system.

CHAPTER 3

HORIZONTAL AXIS WIND TURBINE AERODYNAMICS

In this chapter, airfoil and rotor aerodynamics of wind turbines will be discussed. In rotor aerodynamics, together with the Betz limit concept, 1-D momentum theory, general momentum theory, blade element theory and blade element momentum theory (BEM) will be explained, briefly.

3.1. Aerodynamics of Airfoils

Airfoils are the parts that generate the aerodynamic forces on a wind turbine blade and the power output is directly related to the airfoil characteristics.

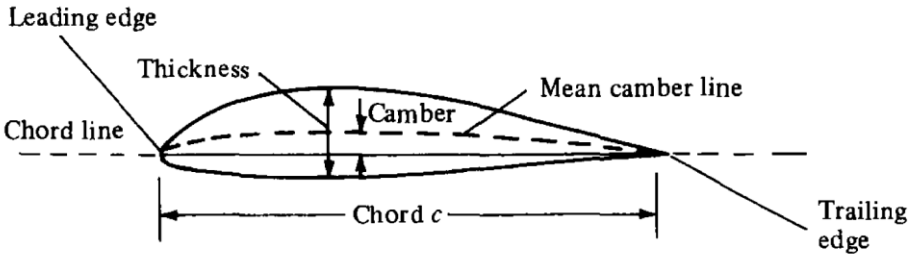

Figure 3.1.Airfoil nomenclature [21]

The aerodynamic properties of an airfoil are characterized by its geometry and the dimensions define that geometry is mostly given in terms of chordlength. Two important examples are thickness and camber distributions. They are commonly given as maximum thickness and maximum camber divided by chord length, i.e. thickness to chord ratio and camber to chord ratio. According to the coordinates on the airfoil that those two dimensions are at maximum, the airfoil families are created so that they can be used together on a wind turbine blade.

The flow over an airfoil causes many forces to be created and distributed over its surface and where the geometry is convex; those forces congregate and lower the

pressure. Therefore, the upper side of an airfoil is called a “suction side”. On the contrary, when geometry is concave; the forces scatter and cause the pressure to increase. Thus, the lower side of an airfoil is called “pressure side”. The components of the net force created are called lift and drag and their conventional directions are given in Figure 3.2 together with the moment created.

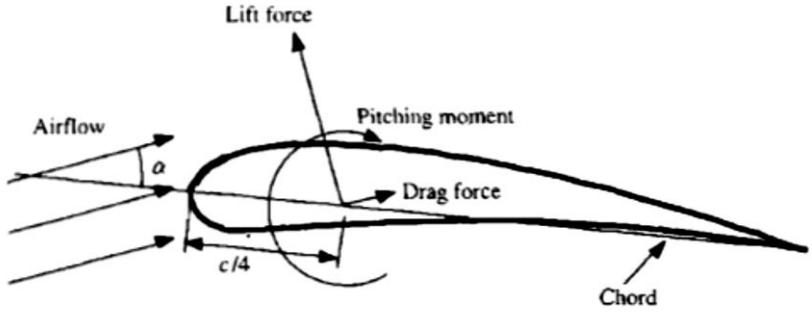

Figure 3.2.Drag and lift forces on stationary airfoil; α, angle of attack; c, chord [3]

To analyze the fluid flow over an airfoil, non-dimensional parameters are used. And the most important parameter that determines the characteristics of a fluid flow is the Reynolds number, Re, and it is defined as;

$$Re = \frac{inertial\ force}{viscous\ force} = \frac{\rho U l}{\mu} \tag{3.1}$$

In Equation 3.1, ρ is the fluid density, μ is the fluid viscosity, U is the flow velocity and l is the length scale of the flow, corresponding to the root chord length of a wind turbine blade.

The other dimensionless parameters that plays an important role in analyzing the flow over an airfoil is the lift and drag coefficients which are given in Equations 3.2 and 3.3.

$$C_l = \frac{lift\ force}{dynamic\ force} = \frac{L}{\frac{1}{2}\rho U^2 c} \tag{3.2}$$

$$C_d = \frac{drag\ force}{dynamic\ force} = \frac{D}{\frac{1}{2}\rho U^2 c} \tag{3.3}$$

where, c is the chordlength of the airfoil, L and D are the lift and drag forces, respectively.

The lift and drag forces of an airfoil changes with angle of attack and this change varies with the Reynolds number. A typical lift coefficient variation with angle of attack for a non-symmetric airfoil is given in Figure 3.3.

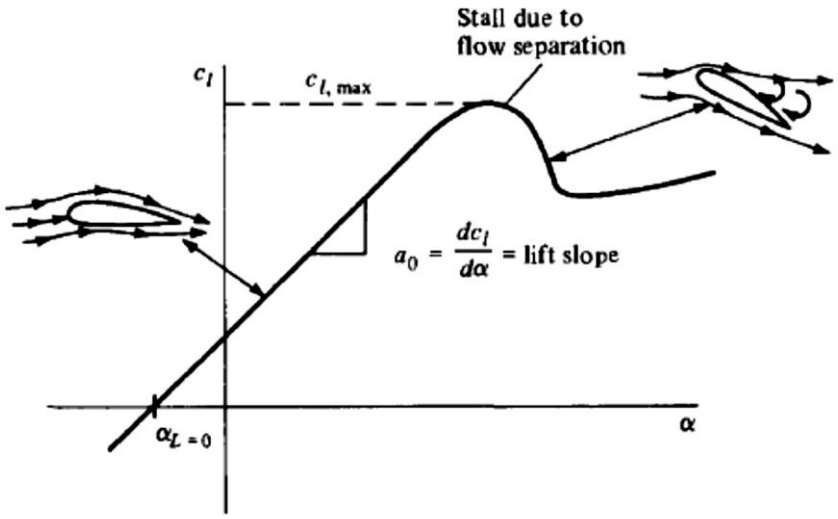

Figure 3.3.Schematic of lift coefficient variation with angle of attack for an airfoil [21]

Since the operating Re range for an aircraft is very high comparing to the wind turbines, the airfoil selection or design should be made according to that. Also, in air vehicles, the variation of angle of attack is quite limited whereas the rotors face the wind from many directions during rotation. Therefore, the concerns about the variations of lift and drag coefficients with respect to angle of attack is also different and should be kept in mind.

3.2. Rotor Aerodynamics

3.2.1. Actuator Disk Concept and Betz Limit

1-D momentum theory is based on linear momentum theory and the actuator disk model is used in which the wind turbine is taken as an actuator disk i.e. infinite number of blades. The flow around the actuator disk is taken to be homogenous, incompressible and steady. Also, the thrust is taken to be uniformly distributed over the disk area and the velocity through the disk is taken to be constant. A schematic of the control volume assigned in that theory is shown in Figure 3.4.

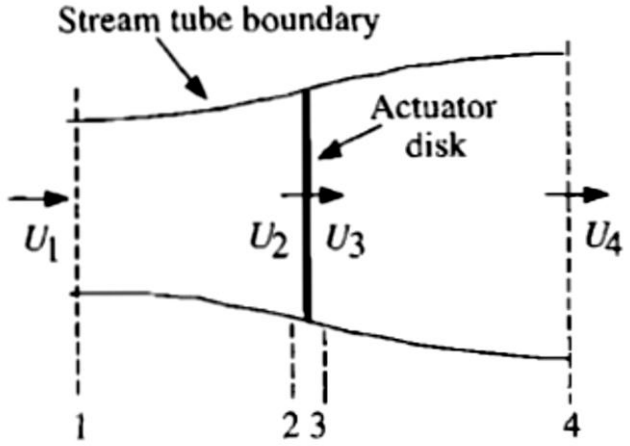

Figure 3.4.Actuator disk model of a wind turbine where U is the mean air velocity [3]

Conservation of linear momentum in that control volume gives;

$$T = (\rho A_1 U_1)U_1 - (\rho A_4 U_4)U_4 \tag{3.4}$$

Equation 3.4 combined with conservation of mass yields to Equation 3.5.

$$T = \rho A_2 U_2 (U_1 - U_4) \tag{3.5}$$

From conservation of energy principle or Bernoulli's Equation, Equations 3.6 and 3.7 can be obtained.

$$p_1 + \frac{1}{2}\rho {U_1}^2 = p_2 + \frac{1}{2}\rho {U_2}^2 \tag{3.6}$$

$$p_3 + \frac{1}{2}\rho {U_3}^2 = p_4 + \frac{1}{2}\rho {U_4}^2 \tag{3.7}$$

The net force on the actuator disk is;

$$T = A_2(p_2 - p_3) \tag{3.8}$$

If $(P_2 - P_3)$ is solved by using Equations 3.6 and 3.7 with the assumption of $U_2 = U_3$ and then substituted into Equation 3.8;

$$T = \frac{1}{2}\rho A_2({U_1}^2 - {U_4}^2) \tag{3.9}$$

Equating the thrust,T, values in Equation 3.5 and 3.8,

$$U_2 = \frac{U_1 + U_4}{2} \tag{3.10}$$

Axial induction factor,a, may be defined as the fractional decrease between the free stream velocity and the rotor plane [3];

$$a = \frac{U_1 - U_2}{U_1} \tag{3.11}$$

Power output of the control volume may be formulated as;

$$P = T \cdot U_2 \tag{3.12}$$

With the definitions above, Equation 3.12 becomes;

$$P = \frac{1}{2}\rho A U^3 4a(1-a)^2 \tag{3.13}$$

where $A_2 = A$and $U_2 = U$.

The potential power in the wind may be described as;

$$P_{wind} = \frac{1}{2}\rho A U^3 \tag{3.14}$$

Therefore, the coefficient of power is identified as;

$$Cp = \frac{P}{\frac{1}{2}\rho A U^3} = 4a(1-a)^2 \tag{3.15}$$

Maximizing power coefficient by equating its derivative to zero gives $a = {}^1/_3$ and Cp becomes;

$$Cp = \frac{16}{27} = 0.5926 \tag{3.16}$$

Which represents the maximum gain from the power of the wind and it is called the Betz limit. It is the theoretically maximum coefficient that can be achieved in any wind turbine rotor design. The wake rotation, finite number of blades, tip losses and non-zero aerodynamic drag are some of the factors that yield to decrease that value.

The thrust coefficient is described as;

$$C_T = \frac{T}{\frac{1}{2}\rho A U^2} = 4a(1-a) \tag{3.17}$$

A graph of the power and thrust coefficients for an ideal Betz turbine and the non-dimensionalized downstream wind speed are illustrated in Figure 3.5.

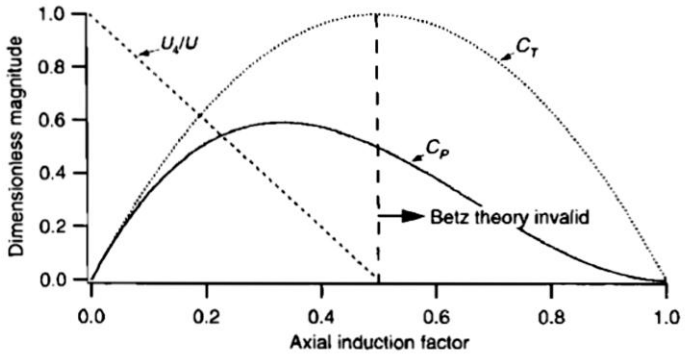

Figure 3.5.Operating parameters for Betz turbine [3]

3.2.2. Momentum Theory

Different than the actuator disk concept, momentum theory considers the angular momentum created by the rotating actuator disk which is called torque. The flow behind the rotor is also taken rotational in the opposite direction of the rotor which is called the wake rotation. The control volume of the theory and some of the boundary conditions may be listed as;

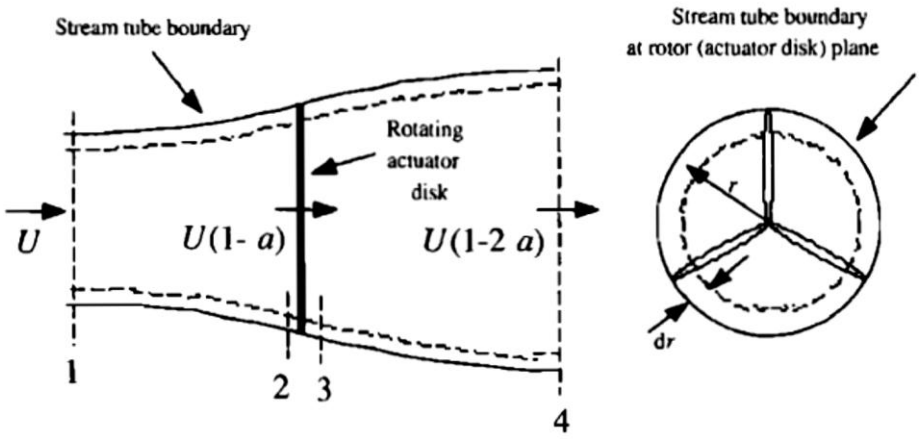

Figure 3.6.Considered geometry in the angular momentum theory [3]

$$p_1 = p_4 = p_\infty \tag{3.18}$$

$$U_1 = U \tag{3.19}$$

$$U_2 = U_3 = U(1-a) \tag{3.20}$$

$$U_4 = U(1-2a) \tag{3.21}$$

where p_∞ is the free stream pressure.

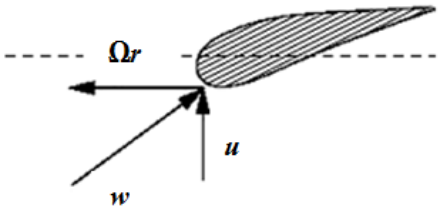

Figure 3.7.Velocity triangle in the upstream. *u*; upstream velocity, Ω*r*; local rotational velocity, *w*; relative velocity

Although, the linear velocities are taken to be equal across the disk, the angular velocity of the air relative to the blade increases from Ω to Ω+ω where ω is angular velocity imparted to the flow stream and it called as angular induced velocity. Therefore, the Bernoulli Equation along the disk, using axial velocities becomes;

$$p_2 + \frac{1}{2}\rho\Omega^2 r^2 = p_3 + \frac{1}{2}\rho(\Omega + \omega)^2 r^2 \tag{3.22}$$

And the pressure difference may be written as;

$$p_2 - p_3 = \rho\left(\Omega + \frac{1}{2}\omega\right)\omega r^2 \tag{3.23}$$

Thrust on an annular element, dT can be described by using Equation 3.23 as;

$$dT = (p_2 - p_3)dA = \left[\rho\left(\Omega + \frac{1}{2}\omega\right)\omega r^2\right] 2\pi r dr \tag{3.24}$$

The angular induction factor is defined as;

$$a' = \frac{\omega}{2\Omega} \tag{3.25}$$

Then using the angular induction factor definition, Equation 3.24 becomes;

$$dT = \rho\Omega^2 r^2 [4a'(1 + a')]\pi r dr \tag{3.26}$$

The derivative of Equation 3.9 gives the thrust on annular element and combining with Equation 3.11, Equation 3.27 can be obtained as;

$$dT = \rho u^2 [4a(1 - a)]\pi r dr \tag{3.27}$$

Equating the thrust expressions in terms of angular and axial inductions, i.e. Equations 3.26 and 3.27 yields;

$$\frac{a(1 - a)}{a'(1 + a')} = \frac{\Omega^2 r^2}{U^2} = {\lambda_r}^2 \tag{3.28}$$

where $\lambda_r = {\Omega r}/{u}$ is local tip speed ratio and $\lambda = {\Omega R}/{u}$ is overall tip speed ratio. Their ratio then becomes;

$$\lambda_r = \frac{r}{R}\lambda \tag{3.29}$$

The conservation of angular momentum gives;

$$dQ = d\dot{m}(\omega r)r \tag{3.30}$$

where $\dot{m} = \rho u_2 2\pi r dr$ and $u_2 = u(1-a)$. Combining with Equation 3.25;

$$dQ = \rho U \Omega r[4a'(1-a)]\pi r^2 dr \tag{3.31}$$

The differential power may be defined as;

$$dP = \Omega dQ \tag{3.32}$$

Combining with Equation 3.31, 3.28, 3.29 and the induction factors;

$$dP = \frac{1}{2}\rho U A^3 \left[\frac{8}{\lambda^2}a'(1-a){\lambda_r}^3 d\lambda_r\right] \tag{3.33}$$

which is a function of axial and angular induction factors and local and overall tip speed ratios.

With this power expression, Equation 3.15 becomes;

$$Cp = \frac{8}{\lambda^2}\int_0^{\lambda} a'(1-a){\lambda_r}^3 d\lambda_r \tag{3.34}$$

3.2.3. Blade Element Theory

In blade element theory, the blade is divided into N elements or sections and it is assumed that there are no aerodynamic interactions between the elements. The schematic of a blade element is given in Figure 3.8 where R is the blade length and r is the local radius.

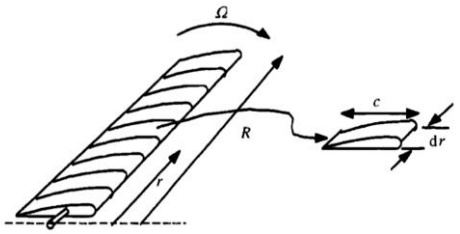

Figure 3.8.Schematic of a blade element [3]

In order to analyze a wind turbine blade using that theory, the aerodynamic characteristics of the airfoil needs to be known beforehand. The control volume that is used to derive the set of equations is given in Figure 3.9.

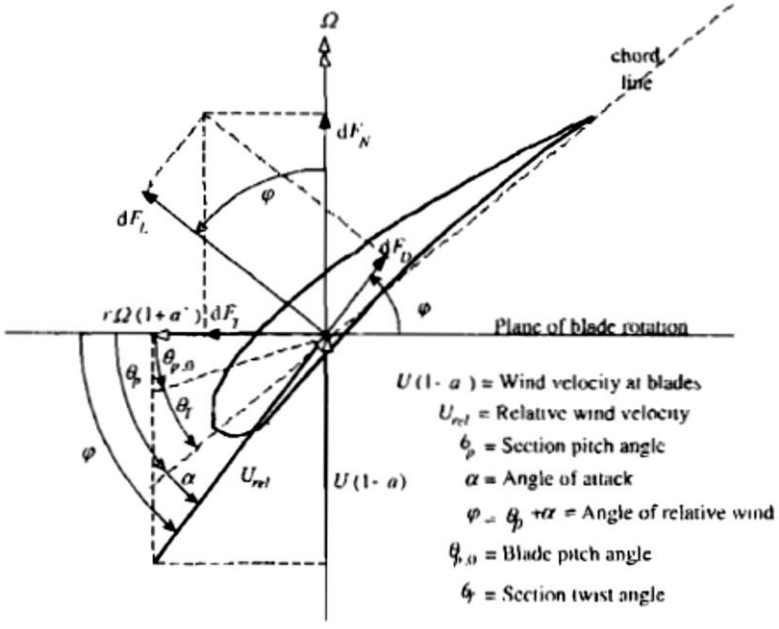

Figure 3.9.Blade geometry for analysis of a horizontal axis wind turbine [3]

From the figure it can be interpreted that;

$$U_{rel} = w_2 = \frac{U(1-a)}{sin\varphi} \tag{3.35}$$

$$dL = \frac{1}{2}\rho {w_2}^2 c_L c dr \tag{3.36}$$

$$dD = \frac{1}{2}\rho {w_2}^2 c_D c dr \tag{3.37}$$

$$dF_N = dL \cdot cos\varphi + dD \cdot sin\varphi \tag{3.38}$$

$$dF_T = dL \cdot sin\varphi - dD \cdot cos\varphi \tag{3.39}$$

Note that F_N is the force acting normal and F_T is the force acting through the tangential direction to the plane of rotation.

If the force has B number of blades, using equation 3.36 and 3.37, the total normal force on the section at r becomes;

$$dF_N = B\frac{1}{2}\rho {w_2}^2 (c_L cos\varphi + c_D sin\varphi) c dr \tag{3.40}$$

And the differential torque due to F_T at spanwise location r;

$$dQ = B \cdot dF_T \cdot r \tag{3.41}$$

$$dQ = B\frac{1}{2}\rho {w_2}^2 (c_L sin\varphi - c_D cos\varphi) \cdot c \cdot r dr \tag{3.42}$$

The local solidity is defined as;

$$\sigma' = \frac{Bc}{2\pi r} \tag{3.43}$$

3.2.4. Blade Element Momentum Theory

Blade element momentum theory, as the name implies, is the combination of blade element and momentum theory. The forces and moments derived from both theories are equalized to each other.

By equating torque equations; i.e. Equations 3.31 and 3.42 and neglecting drag losses gives;

$$\frac{a'}{1-a} = \frac{\sigma' c_L}{4\lambda_r sin\varphi} \tag{3.44}$$

And by equating normal force equations, i.e. Equations 3.27 and 3.40;

$$\frac{a}{1-a} = \frac{\sigma' c_L cos\varphi}{4sin^2\varphi} \tag{3.45}$$

Solving Equations 3.44 and 3.45 together for axial and angular induction factor yields;

$$a = \frac{1}{1 + \frac{4sin^2\varphi}{\sigma' c_L cos\varphi}} \tag{3.46}$$

$$a' = \frac{1}{\frac{4cos\varphi}{\sigma' c_L} - 1} \tag{3.47}$$

CHAPTER 4

LITERATURE SURVEY

In this chapter, the studies about aerodynamic design of airfoil and blades mainly for small wind turbine applications are presented. Since wind turbine technology is relatively new and growing rapidly, recent researches have been the focus point.

4.1. Airfoil Design Studies

There are many studies done in terms of airfoil design. However, designing an airfoil for a wind turbine is quite different than aircrafts or air vehicles in general in terms of performance considerations and corresponding design parameters and therefore the academic studies that can be reached are limited.

First study is an example of combination method, meaning that the designed airfoil is a combination of two different airfoils and more advanced than both of them in terms of aerodynamic performance. Wata et al. [9] selected the combination of SG6043 and Eppler 422 and the created geometry is shown in Figure 4.1 where x/c states the x coordinates over chord and y/c states y coordinates over chord.

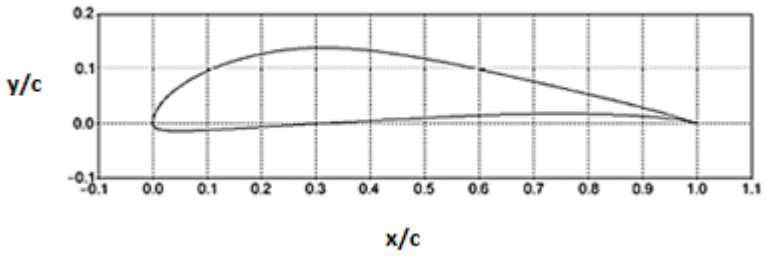

Figure 4.1.The geometry of the new airfoil designed by Wata et al. [9]

Lift to drag ratio of the created geometry, which is one of the most important criteria that defines the performance of a wind turbine blade profile was not calculated numerically, namely in XFOIL but experimentally the results are presented as;

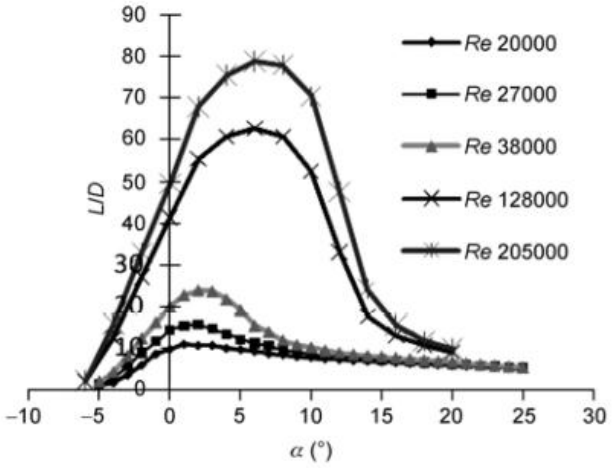

Figure 4.2.L/D ratio vs. angle of attack of the combined airfoil. [9]

The combined airfoil has maximum lift to drag ratio at angle of attack of 8^o which may be used as design angle of attack for the blade. It has been concluded that the performance results obtained numerically and experimentally show good agreement with each other especially in terms of lift coefficient distribution. However, it was not specified in which position of the blade the airfoil is most suitable and flow field around the combined airfoil needs to be further investigated.

Another trend in designing an airfoil is to use inverse design methods which are the methods in order to design airfoil profiles by inputting the desired flow field around it. In the study of Henriques et al. [10] an iterative use of analysis code has been considered instead of directly gaining the geometry of the airfoil with the help of an immediate problem formulation making.

The design methodology of this research is based on cascade Panel Method with a blade camberline modification algorithm. And the typical control volume in order to solve momentum balance equations is;

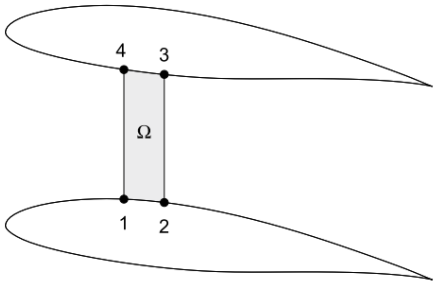

Figure 4.3.Typical control volume used for tangential momentum balance in a cascade of blades. [10]

The algorithm has been started with an initial geometry and then converged in 8 iterations which mean almost constant difference in upper and lower pressure distributions is achieved. The resulting airfoil is named T.Urban 10/193 and its manufactured section in order to measure its performance criterion experimentally is shown in Figure 4.4.

Figure 4.4.The wind tunnel model of the T.Urban 10/193 blade section [10]

The algorithm and calculation method of the profile is computationally expensive though straightforward. However, the viscosity effects and the separation characteristics of the leading and trailing edge regions, namely before 20% and after 80% of the chord needs to be further investigated.

As opposed to the inverse-design techniques, another method to design airfoils is direct method. In research of Fuglsang et al. [11], a direct design method has been obtained by using optimization algorithms with design objectives and design points together with the airfoil analysis code XFOIL. Three airfoil families corresponding to different turbine working conditions have been generated and the numerical results are achieved using CFD code Ellipsys2D and test results are obtained from VELUX wind tunnel which is of the closed return type with an open test section having a cross section of 7.5 x 7.5 m and a length of 10.5 m. The design parameters of airfoil family A-1 with numerical predictions and the wind tunnel results (in parenthesis) are presented in Table 4.1.

Table 4.1.The Risø-A1 design parameters and wind tunnel results at Re = 1.6 x10^6 [11]

	x/c at max t/c	y/c at T.E.	Re·10^6	α_0	max c_l	design α	design c_l	max c_l / c_d
Risø-A1-18	0.336	0.025	3.0	-3.6(-3.8)	1.53 (1.43)	6.0 (7.5)	1.15 (1.22)	167 (107)
Risø-A1-21	0.298	0.005	3.0	-3.3(-3.3)	1.45 (1.38)	7.0 (6.3)	1.15 (1.10)	161 (96)
Risø-A1-24	0.302	0.01	2.75	-3.4(-3.3)	1.48 (1.36)	7.0 (6.5)	1.19 (1.15)	157 (91)
Risø-A1-27	0.303	0.01	2.75	-3.2	1.44	7.0	1.15	N/A
Risø-A1-30	0.3	0.01	2.5	-2.7	1.35	7.0	1.05	N/A
Risø-A1-33	0.304	0.01	2.5	-1.6	1.2	7.0	0.93	N/A

The second airfoil family designed with the same method is Risø-P family which has been designated to replace A-1 family for pitch – controlled wind turbines. The parameters of that family were represented in the same trend as;

Table 4.2.The Risø-P design parameters [11]

	x/c at max t/c	y/c at T.E.	Re·10^6	α_0	max c_l	design α	design c_l	max c_l / c_d
Risø-P-15	0.328	0.0010	3.0	-3.5	1.49	6.0	1.12	173
Risø-P-18	0.328	0.0014	3.0	-3.7	1.50	6.0	1.15	170
Risø-P-21	0.323	0.01	3.0	-3.5	1.48	6.0	1.4	159
Risø-P24	0.320	0.01	2.75	-3.7	1.48	6.0	1.17	156

It is indicated in the study that Risø-P family has not been tested and thus, the wind tunnel measurements of the specified parameters were not available.

The last airfoil family included in that paper is called Risø-B1 and they are designed for the conditions of rotors at size larger than 1MW. The design parameters for that family are indicated as;

Table 4.3.The Risø-B1 design parameters and wind tunnel results at Re = 1.6x10^6 [11]

	x/c at max t/c	y/c at T.E.	Re·10^6	α_0	max c_l	design α	design c_l	max c_l / c_d
Risø-B1-15	0.278	0.006	6.0	-4.1	1.92	6.0	1.21	157
Risø-B1-18	0.279	0.004	6.0	-4.0(-3.4)	1.87 (1.64)	6.0 (6.5)	1.19 (1.16)	166 (100)
Risø-B1-21	0.278	0.005	6.0	-3.6	1.83	6.0	1.16	139
Risø-B1-24	0.270	0.007	6.0	-3.1(-2.3)	1.79 (1.62)	6.0 (7.0)	1.15 (1.10)	120 (73)
Risø-B1-30	0.270	0.01	6.0	-2.1	1.61	5.0	0.90	N/A
Risø-B1-36	0.270	0.012	6.0	-1.3	1.15	5.0	0.90	N/A

It was concluded that, the design procedure is validated through the consistency of test results and expected values of the design objectives. However, it was added that

the profiles are over-sensitive to roughness and this drawback is to be improved in further studies for all of the airfoil families mentioned in the study.

Another example of the usage of optimization techniques in airfoil design may be the study done by Singh et al. [12]. In that research, XFOIL code has been used to design and optimize the airfoil sections. Firstly, many of the existing low Re airfoils have been simulated and their performance has been evaluated. Ten airfoils (A1-10) were chosen since they have the most suitable combination of maximum lift coefficient and L/D ratio. Then, they are far optimized geometrically in order to achieve higher c_L and L/D namely their nose radius has been changed together with the thickness and then it is seen that nose radius has no important role in the change of the performance criterion mentioned above. The below table shows the values of c_L and L/D corresponding to the modified trailing edge thickness;

Table 4.4.Optimum lift coefficients and L/D ratios at minimum and maximum Reynolds numbers of 55,000 and 148,000 respectively for different airfoils [12]

Airfoil	Optimum C_L range		L/D range		α range	
	Re min	Re max	Re min	Re max	Re min	Re max
A3 (3%)	1.91	1.97	39.5	65.24	8	8
A3 (4%)	1.94	2	38.31	61.85	8	8
A3 (5%)	1.97	2.03	37.62	58.63	8	8
A3 (2%)	1.85	1.93	38.3	68.69	8	8
A3 (1%)	1.78	1.88	37.8	72	8	8
A4 (1%)	1.65	2.19	41.08	55.95	4	10
A3 (s1210)	1.78	1.86	33.9	59.4	10	10
A4 (s1223)	1.7	2.2	32.5	50	6	12
A4 (2%)	1.72	2.22	40.87	54.49	4	10
A4 (3%)	1.77	2.27	40.12	52.8	4	10
A5 (s1221)	1.4	1.9	24.7	60.2	8	12
A9 (FX 63-137)	1.6	1.7	32	54.8	10	10
A7 (E210)	1.3	1.4	25.8	64.4	12	10
A1 (ah93w145)	1.2	1.43	16.4	65.3	13	10

Due to its performance ranges in terms of Re, A3 (3%) airfoil has been chosen which has an overall increase of 6.11% and 3.41% in C_L and 16.53% and 9.83% increase in L/D ratios at Re 55,000 and 148,000 respectively compared to the baseline airfoil of A3. The new airfoil is named as ‘AirFish’, AF300, and owing to its thick

trailing edge; it has the both structural and aerodynamic advantages such as strength and stall delay.

Then AF300 has been compared with the commercial airfoils that are used in wind turbine industry especially for the small wind turbines and the resulting values of performance parameters are listed in the table below.

Table 4.5.Optimum lift coefficients and L/D ratios at minimum at Reynolds of 100,000 for different airfoils [12]

Airfoil	Optimum C_L and L/D ratio			Maximum L/D ratio		Maximum C_L	
	C_L	L/D ratio	α (^{o})	L/D ratio	α (^{o})	C_{Lmax}	α stall (^{o})
AF300	1.95	54	8	39.5	8	8	8
s1210	1.89	59.56	9	38.31	8	8	8
s1223	1.99	46.29	8	37.62	4	8	8
FX63-137	1.62	61.61	8	61.61	8	8	8
s1221	1.84	44.35	12	47.78	4	8	8
SH3055	1.7	45.57	11.45	46.84	10.32	4	10
SG6043	1.41	61.43	8	63.84	6	10	10
Aquila	1.35	50.04	10	53.14	8	6	12
E387	1.18	54.53	8	54.53	8	4	10

Since the flow around AF300 stays attached even in low Reynolds number and its thickened area supports the structure of the rotor, it is concluded that AF300 may be preferable around the near-root region of the blade.

Even though the performance of AF300 at low Reynolds number is desirable, there exist other profiles which can meet similar expectations by having thinner trailing edge where a thick trailing edge is proven to be one of the main sources of airfoil self-noise. Especially for small wind turbines which are mainly operating around urban areas, the noise is one of the biggest concerns that need to be avoided.

4.2. Wind Turbine Blade Design Studies

Although several design methods can be found in the literature, the parameters chosen and the final geometry of the wind turbine blade is mostly hidden because of commercial concerns. In this part, the most prominent design methodologies together with the results obtained will be presented.

First study is the design done by Ameku et al. [13] which is the design of 3 kW wind turbine with thin airfoil blades. In this research "7 arcs airfoil" is created and then analyzed by XFOIL code. New airfoil has 11% camber at 0.35 chord and 8.5% thickness at 0.1 chord.

Specifications of the wind turbine generator may be tabulated as shown below.

Table 4.6.Design parameters of 3kW, thin bladed wind turbine [13]

Type	Horizontal. up-wind	
No. of blades	3	
Yaw control	Free yaw	
Design	Tip speed ratio	3
	Output	2.5 kW at 160 rpm
	Wind speed	11 m/s
Generator capacity	3 kW	

where the profile of the blade will be used as;

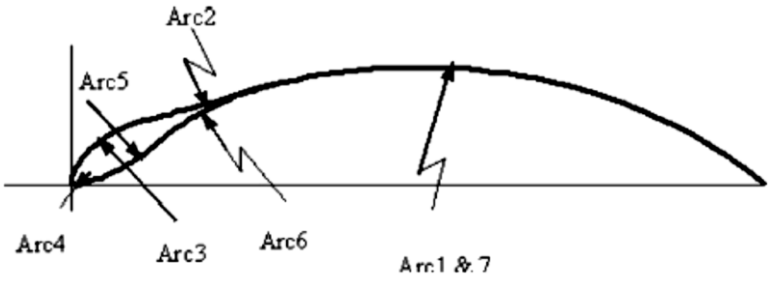

Figure 4.5.The wind tunnel model of the T.Urban 10/193 blade section [13]

The design and analysis of the blade is done using BEM method which was described in detail in Chapter 3 and theoretical and numerical designs have been combined with experimental measurements in the end. The most important calculation in terms of the considerations of this study is that the 7 arc thin airfoil blade has 1105W generator output and its coefficient of performance (Cp) is 0.14 which is quite low.

The other study that BEM theory is used to design and analyze is done by Dong et al. [14]. In that paper, BEM theory is modified by including the tip and drag losses and together with the corrections in chord and twist corrections due to both practical and aerodynamic reasons. 2MW horizontal axis wind turbine (HAWT) is designed as an example application of the method. The design parameters are listed in Table 4.7.

Table 4.7.Design parameters of 2MW wind turbine [14]

Rated power (MW)	2
Number of Blades	3
Rated Incoming wind speed (m/s)	13.2
Design Cp	0.29
Rotor Diameter (m)	80
Rotor Hub Diameter (m)	2.4
Design max. Rotational Speed (rpm)	18.62
Tip speed ratio	7

For different sections of the blade, varying airfoils have been chosen and they may be listed as;

Table 4.8.Airfoils chosen in 2MW wind turbine [14]

Airfoil	t/c (%)	Lift Coeff.	Attack angle. α (^{o})	L/D	Radial Position (%)
AH 93-W-300	29.98	1.207	7	112.8	38
AH 93-W-257	25.67	1.2427	7	157	48
FFA-W3-211	21.11	1.5264	7.5	157	62
AH 93-W-174	17.43	1.265	7	194.6	76
AH 93-W-145	14.48	1.2122	6.5	186	97

After analyzing the performance, the results have been corrected due to the possible problems may be encountered during manufacturing process. The comparison of the chord and twist distributions before and after the correction is shown below.

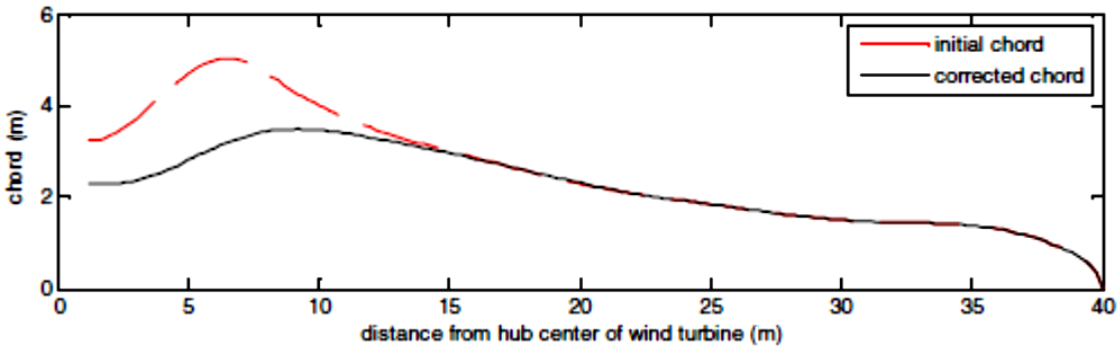

Figure 4.6.The comparison of initial chord distribution and corrected chord distribution for the 2MW wind turbine example [14]

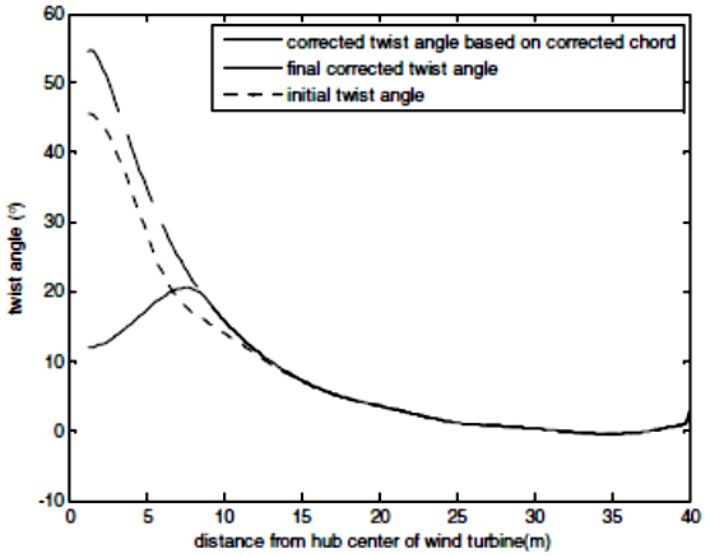

Figure 4.7.The comparison of initial and corrected twist angle distributions for the 2MW wind turbine example [14]

The method used in that study is compared with GH Bladed software simulation and the coefficient of power comparison gives;

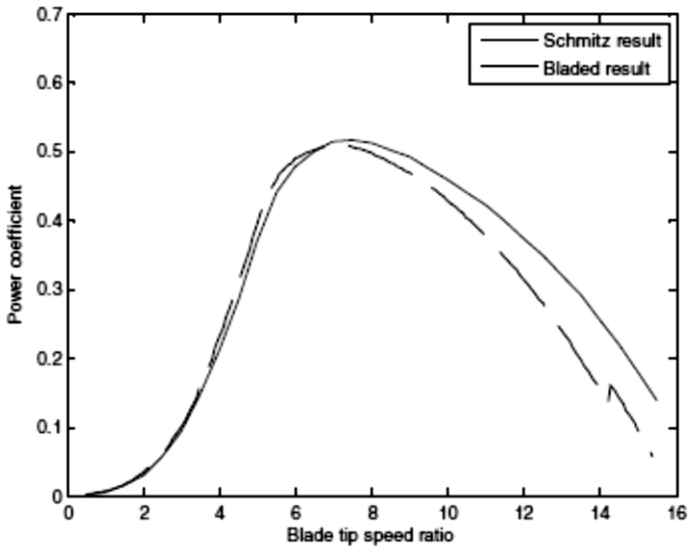

Figure 4.8.Power coefficient calculation results for 2MW wind turbine example [14]

The difference between the results is due to hub losses and different calculation methods mostly.

The method used in this paper seems quite practical in terms of manufacturing considerations and not much expensive computationally. However, the comparison between GH Bladed Software simulations show that the results are not in a very good

agreement and the method should be improved. Also, in terms of analyzing the blade, a proper CFD Simulation with indicated boundary conditions should have been used. Even though, the importance of airfoil choice has been emphasized still not a case specific airfoil family is designed.

Similar to airfoil design processes, in wind turbine blade design the optimization tools are widely used. The design parameters and objectives are varying for each case and first example of this trend is the study done by Hu et al. [15]. The study is focused on a design method that includes multiple design parameters with minimum cost / maximum power output design objective. Taguchi method is a quality control approach and it differs from the classical ones by the ability of introducing a loss function for the product which fails at its designed performance level.

While calculating the blade performance, classical blade element momentum theory with the tip losses and wake rotation is considered.

As the design profile, NACA 23018 is chosen and the design variables are listed in the table below.

Table 4.9.Design variables used in Taguchi method [15]

	Design Variable	Unit	Level 1	Level 2	Level3	Noise Tolerances
A	Blade chord length (root)	m	0.5	0.7	0.9	±0.005
B	Twist angle for element 1	deg	8	12	46	±1
C	Twist angle for element 2	deg	4	6	8	±0.5
D	Twist angle for element 3	deg	2	3	4	±0.25
E	Twist angle for element 4	deg	0	1	2	±0.125
G	Number of blade	#	2	3	4	N/A
H	Rotational speed	rpm	75	125	175	±5
I	Pitch angle	deg	0	3	6	±1
J	Rotor radius	m	4	4.25	4.5	±0.005
K	Hub Radius	m	0.5	0.75	1	±0.005

The levels of the profiles namely “Level 1”, “Level 2” and “Level3” in Table 4.9 are specified as;

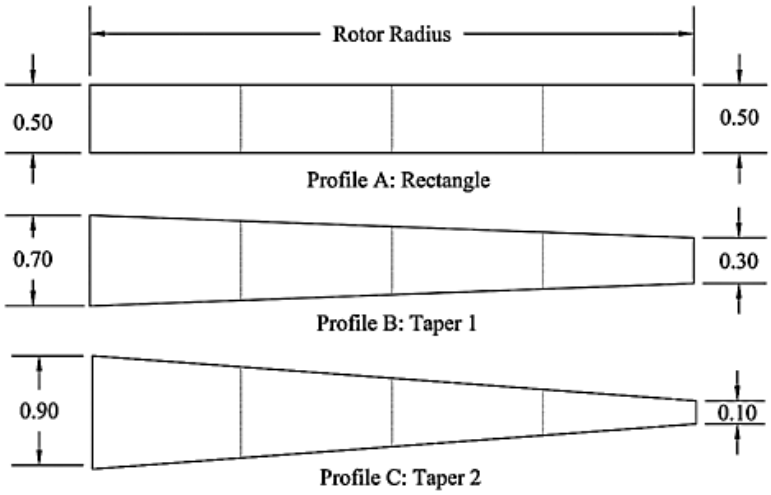

Figure 4.9.Three different levels of shape profiles [15]

Combination of Figure 4.9 means that the blade chord length defined in Table 4.9 is for the root and the rest of the blade is configured so that the chord distribution is linear.

The study has included the structural and economic considerations into the optimization process by defining them as a part of the objective function also. However, for more complicated designs such as, non-uniform chord and twist distributions and more aerodynamic shaped airfoils, the numerical process may be too costly and hard to converge.

Another usage of optimization tools is seen in the research of Benini et al. [16]. In that study, the multi-objective optimization method has been constructed to design stall regulated horizontal axis wind turbines. The objectives of this optimization code are to maximize the annual energy production (AEP) density and minimize the cost of energy (COE). Their mathematical explanations are given in Equations 4.1 and 4.2.

$$f_1(x) = AEP/R^2 \tag{4.1}$$

$$f_2(x) = \frac{TC + BOS}{AEP} FCR + O\&M \tag{4.2}$$

Where TC corresponds to the turbine cost which is directly related with the blade weight, BOS is the balance of station which is proportional to turbine rated

power, FCR is the fixed charge rate and O & M represents the cost for operation and maintenance.

Other than that, the researchers modeled the flow around the wind turbines in order to predict its performance in a rather classical way. The modified blade element theory (BET) theory is used in which Prandtl tip-loss model is included. Figures 4.10 and 4.11 describe the considered control volume and the velocity triangle, respectively.

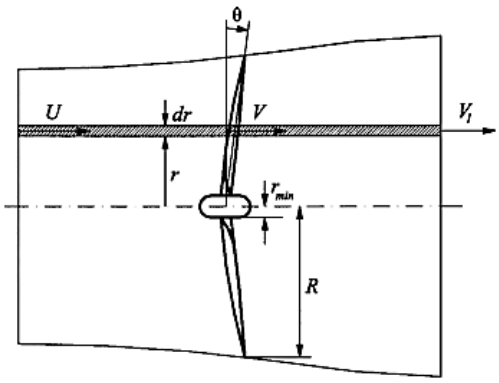

Figure 4.10.Control volume considered [16]

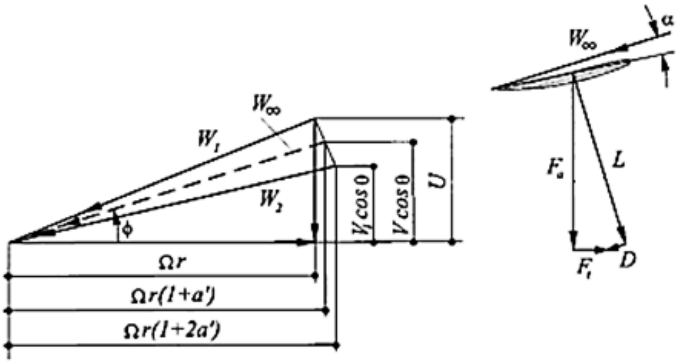

Figure 4.11.Velocity triangle [16]

In order the program to achieve its objectives, the constraints are defined as the following; tip speed ΩR, 40 m/s < ΩR < 80 m/s which is the case in practice for similar range of wind turbines in terms of power output, hub/Tip ratio, $\nu = r_{min}/R$ which is an important parameter especially in terms of stall aerodynamics of the root section and the boundaries of this parameter are inputted as 0.005< ν <0.2.

The chord (c/R) and twist distribution (Υ_c) along the blade is given as a Bezier curve.

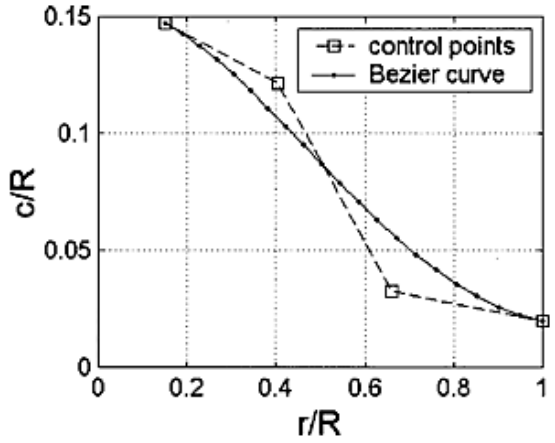

Figure 4.12.Chord distribution [16]

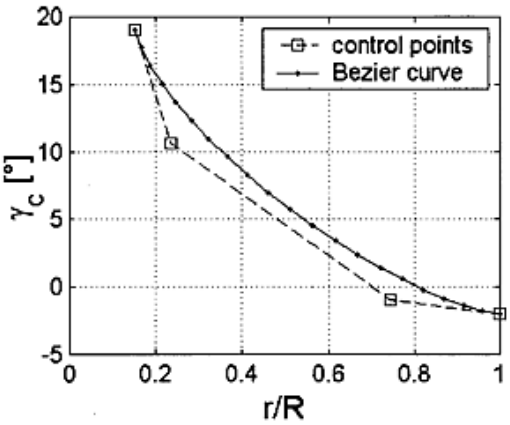

Figure 4.13.Twist distribution [16]

Also, the airfoils chosen for root, primary and tip sections are given as; NACA 63-2-21, NACA 63-2-18 and NACA 63-2-15 respectively. Their performance has been taken into account using experimental data and those data are obtained at Reynolds number of $3x10^6$. In addition to that, rated power of turbine is fixed, cut in wind speed is taken to be 3 m/s and cut out wind speed is 25 m/s. The axial induction factor, a, must not exceed 0.5 in any element of the blade. Shell thickness must not be greater than half of blade profile thickness at any element. In order to calculate shell thickness, the Figure 4.14 may be used.

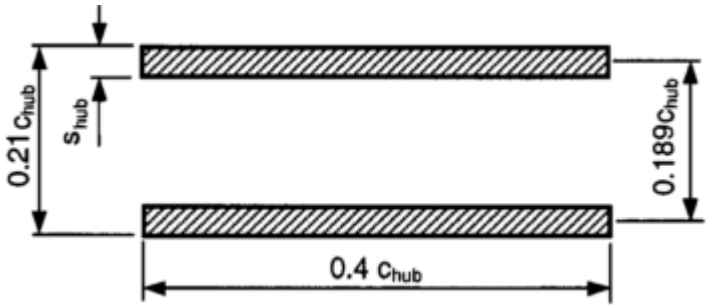

Figure 4.14.Shell thickness calculation [16]

This multi-objective design problem has been solved using evolutionary algorithm which is an algorithm that is inspired from "natural evolution" process and the scheme below demonstrates the process.

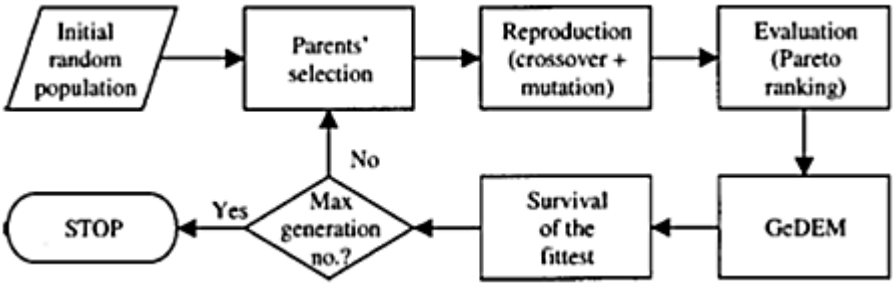

Figure 4.15.Scheme of the multi-objective evolutionary algorithm used in the study [16]

After applying this algorithm, the results obtained is listed in comparison with the commercial turbines. From those results, it can be understood that except for the tip speed, ΩR; the blade radius, annual energy production (AEP) and blade weight is quite similar with the commercial turbines. The difference made by the cost optimization part is, however, more clear. In summary, in this paper, authors present a multi-objective optimization of horizontal axis wind turbines. The evolutionary algorithm is used, basically and while evaluating the performance of the airfoils, blade element theory (BET) is used. Since, the airfoil data taken is valid for constant and relatively high Reynolds numbers, the solution process may have some errors in terms of aerodynamic performance and the process may result in having very low accuracy in low Reynolds number airfoil calculations or in general optimization of small scale wind turbines.

A similar but more practical solution for designing rotors is explained by Maalawi et al. [17]. In that research, a mathematical optimization method is also used. The equations solved were dimensionless. The design parameters selected include

number of blades, airfoil selection and blade root offset from hub center. A computer program is developed according to that algorithm.

The chord and twist distributions are constructed as;

$$\text{Chord distribution; } C = a_c + b_c x \tag{4.3}$$

$$\text{Twist distribution; } \theta_0 = a_\theta (1 - e^{b_\theta x}) \tag{4.4}$$

where a_c and b_c are the constants specified for the chord and a_θ and b_θ are the constants specified for twist distributions.

Using the flowcharts provided in the study, the optimum coefficients of chord and twist distributions are calculated for NACA series airfoils, namely; 23012, 23015, 23018, 23021 and the resulting analysis of the blades designed is given as power curves (Cp vs. tip speed ratio) in Figure 4.16.

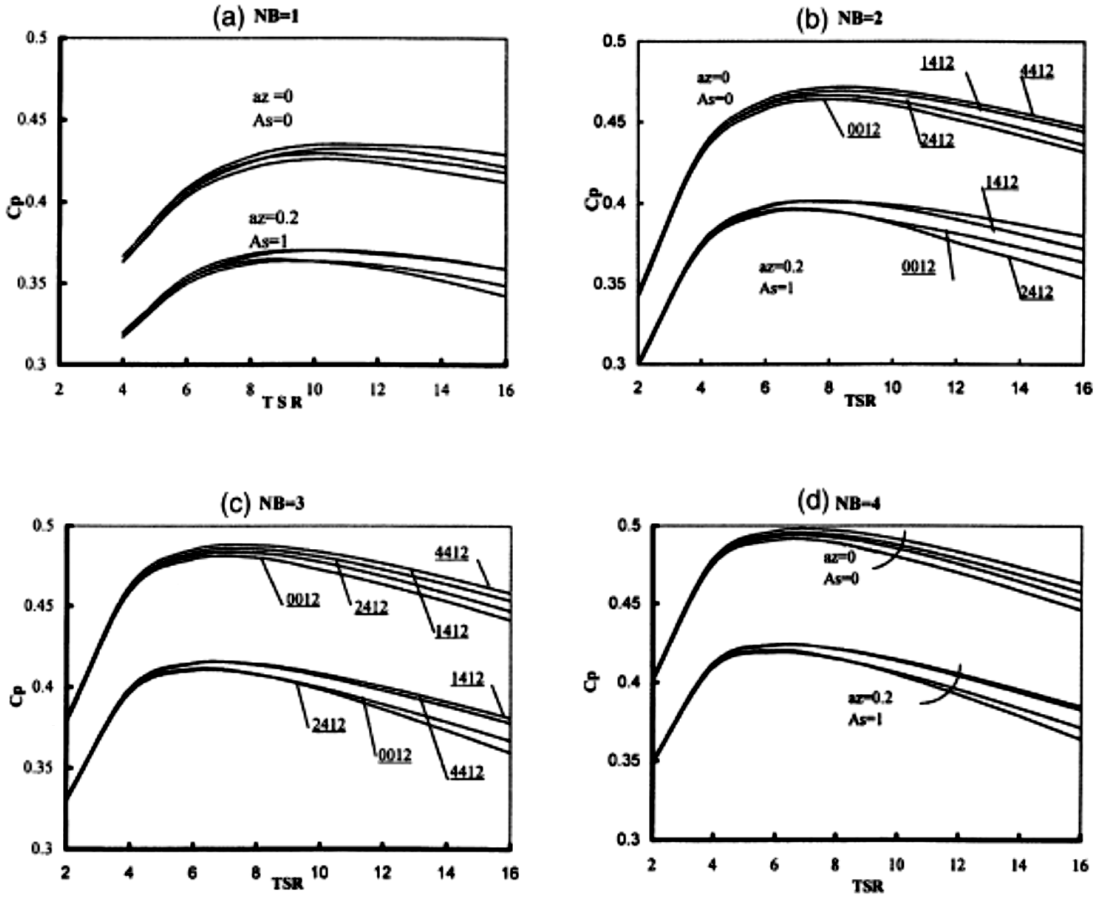

Figure 4.16.Power coefficient for different blades (NACA four-digit airfoils) [17]

There are also iterative approaches that use theoretical studies to obtain numerical results either in terms of design or analysis of wind turbine blades. One of the examples of that trend is the project of Vitale et al. [18] in which a commercial code called “Zeus Diseñador” is explained. It uses iterative algorithm and specified for low-powered horizontal axis wind turbines. The inputs for the code are desired rotor efficiency, incoming wind speed, number of blades, desired rated rotor power, and the ratio between internal and tip radius. Also, the selected airfoil profiles are read by the program. Then, using these values torque and power are calculated using classical BEM theory.

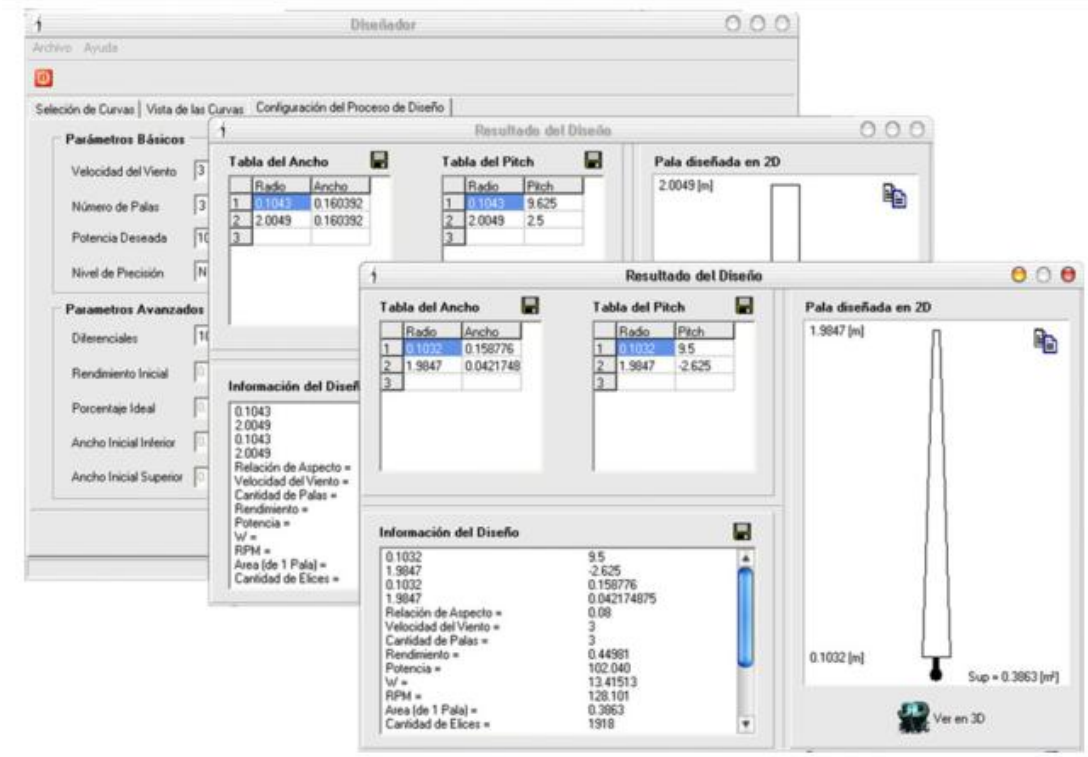

Figure 4.17.User interface of “Zeus Diseñador” [18]

Even though this program provides “user-friendly” interfaces and good visualization of the results, mathematically and physically the theory behind the code is rather deficient. The losses are not included and the approximations that the method uses have not been clearly indicated. Also, the validations of the code have been explained superficially.

Finally, as in the airfoil design case, the inverse methodologies are also applicable to wind turbine blade design. In the studies of Battisti et al. [19], geometry of the blade is determined by describing a design objective. Classical BEM theory is not

used and instead of using the velocity distributions, vortex distributions with appropriate boundary conditions are inputted to the meridional flow analysis of axial turbomachinery. In the wake, radial pressure gradient is considered.

The inverse design procedure is given as;

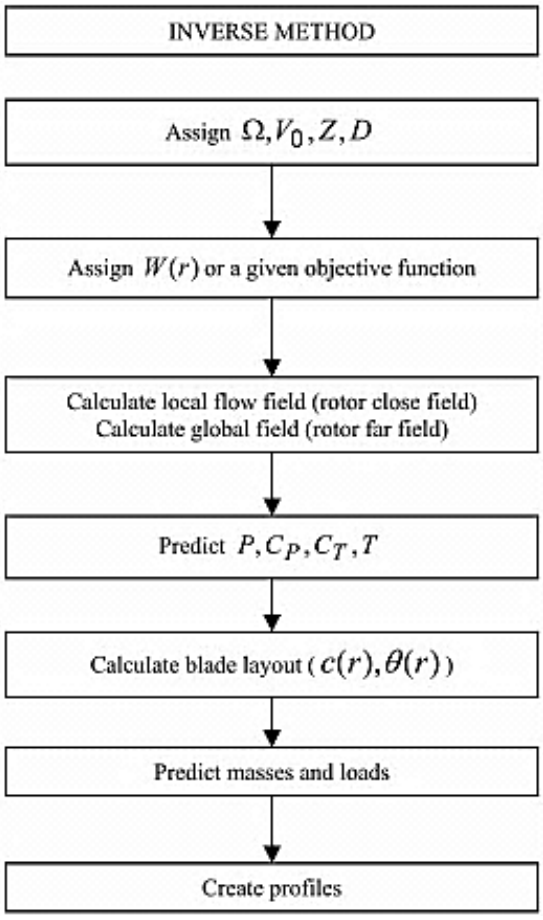

Figure 4.18.The inverse design procedure [19]

When solving for the geometry, actual disk theory (1D momentum theory) is modified and the flow field is discretized into 4 sections; section 0 for upstream; 1 and 2 for rotor's near flow field, upstream and downstream respectively; and section 3 is for downstream. The representation of the annular stream tube is given in Figure 4.19.

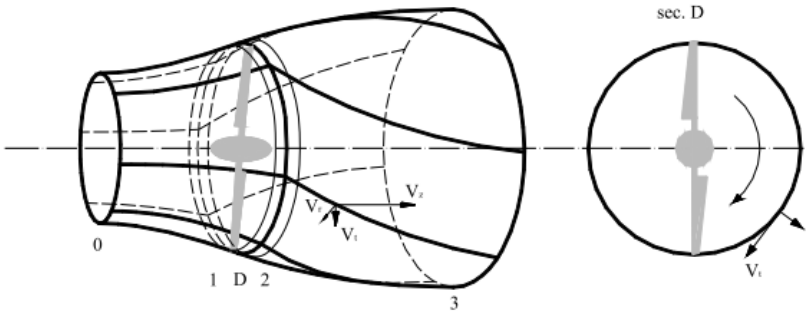

Figure 4.19.The control volume of the inverse design procedure [19]

The equations are listed for the sections visualized in Figure 4.18 and they are inputted in MATLAB. The code is validated using a real case, GAIA wind turbine and the dimensions of the real turbine and output of the chord was fairly consistent.

To summarize, this method has used axial turbomachinery stage design approach with wake rotation included. It is able to show reliable flow fields and realistic blade geometry. However, the case-based design of airfoil geometry, which has been proved to be critical for wind turbines, and also, the method, is lack the ability of taking radial velocity component and tip loss factor into consideration.

CHAPTER 5

DESIGN AND ANALYSIS METHODOLOGY

In this chapter, the methodology of design and analysis process will be explained. Firstly, the airfoil design technique including the software used will be described in detail. Secondly, the blade design procedure together with the constructed computer code will be mentioned and it will be validated using MIE wind turbine designed in Risø Laboratories. Finally, the analysis process and used CFD code with the equations and boundary conditions will be clarified.

5.1. Airfoil Design and Analysis

5.1.1. Airfoil Design

In the design of airfoil, the PROFOIL code, which has an inverse approach to airfoil design, has been used. This method is especially developed for low speed airfoil design which is the case in small scale wind turbines. In inverse airfoil design methodologies, as mentioned in Chapter 2, first, the desired velocity profile around the airfoil is determined and from that, the airfoil geometry is designated. A typical inverse airfoil design methodology is shown in Figure 5.1 [22], [23].

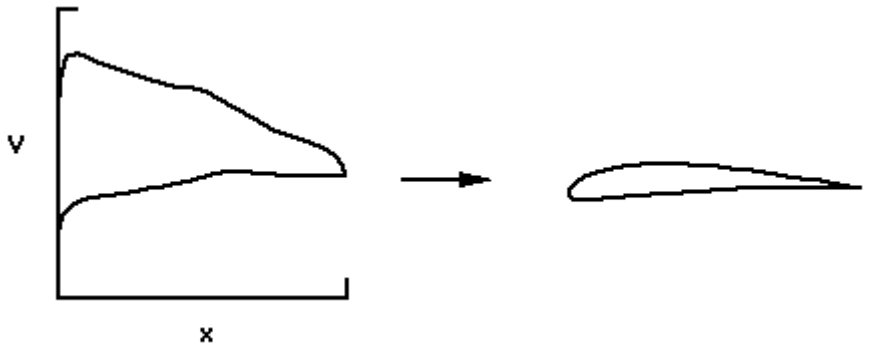

Figure 5.1.Inverse airfoil design methodology

The method depends on conformal mapping and Jukowski airfoil problem is the simplest procedure of conformal mapping that can be applied to airfoil design. The geometry is fixed and the mathematical transformation is changed to obtain different airfoils. This change in transformation is not done by the user explicitly, instead the parameters that define the velocity distribution around the airfoil determines the change. Therefore, the conformal mapping method forms a bridge to allow the designer to specify the velocity distribution.

Another aspect of the method is that "multipoint" design can be performed. Multipoint design corresponds to the generation of more than one design point in which many performance criteria are required. Since, in wind turbine operation, a high range of angles of attack is swept, the performance needs to be optimized for more than one condition. Therefore a multipoint design is necessary and PROFOIL has the capability to do it [23].

In this study, PROFOIL is used with four design segments and a circle mapping to an airfoil as in Kutta - Jukowski transformation [21]. The mapping methodology and design segments can be seen in Figure 4.2.

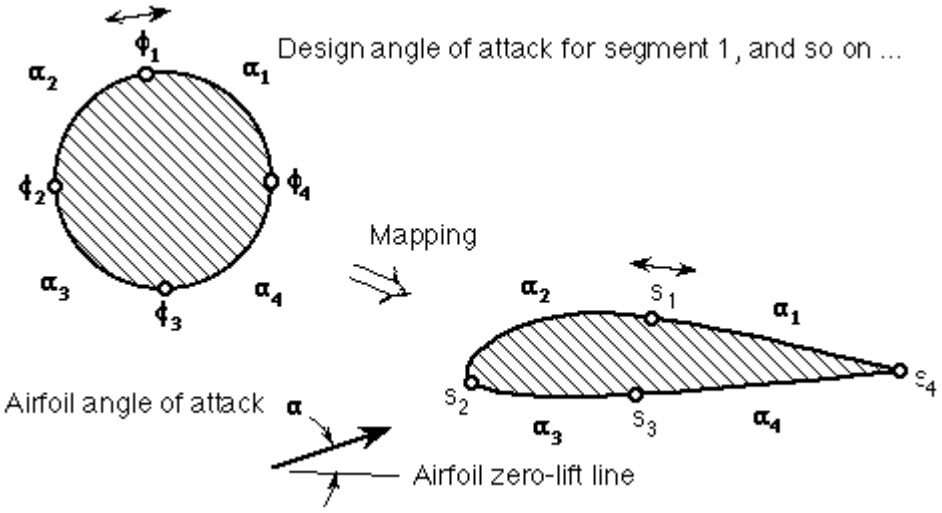

Figure 5.2.Mapping circle to an airfoil with four design segments

Each segment is associated with a design angle of attack which means that the velocity profile on that segment will be constant when the airfoil operates at that specified angle of attack. It is also noted that, the design angle of attack is referenced not to the airfoil chord line but to airfoil zero-lift line. Thus, the specified angle of

attack may also mean a specified lift coefficient where the lift coefficient of the airfoil referenced to zero lift line approximately given as;

$$c_L = 2\pi\alpha \tag{5.1}$$

where α corresponds to a user-specified angle of attack.

In Figure 5.2, segments 1 and 4 are called the recovery regions; the velocity distributions are not constant when the airfoil operates at the corresponding design angles of attack. Moreover, the angles of attack in these regions have little effect on the velocity distributions. In the recovery part, the recovery velocity distributions are determined by the method so that the airfoil closes at the trailing edge. This is a requirement of the method. In fact, any inverse method must allow for some degrees of freedom in the velocity distribution so that (1) the airfoil trailing edge closes and (2) the airfoil velocity distribution is consistent with the freestream [22]. In order to control the velocity distributions over the recovery regions, PROFOIL includes two more design parameters, pitching moment C_M and trailing edge closure parameter KS. C_M defines the camber or aft loading where KS determines the relative thickness of the trailing edge. Since in small scale wind turbines, noise emission is one of the most important concerns and one of its main sources is a blunt trailing edge, while designing an airfoil in PROFILI, KS parameter should be kept as small as possible in order to avoid high sound pressure levels, for instance.

5.1.2. Airfoil Analysis

After the velocity profiles corresponding to a certain desired power output are inputted PROFOIL, the airfoil geometry is obtained. That geometry of airfoil is analyzed using 2D airfoil analysis tool XFOIL [24] and a user interface software PROFILI has been used. XFOIL is especially validated for low Reynolds numbers which is the case of this study. The agreement between XFOIL and experimental results for a designed airfoil AF300 by Singh et al. [12] can be seen in Figure 5.3. The validation is done under the Reynolds numbers between 128,000 and 205,000.

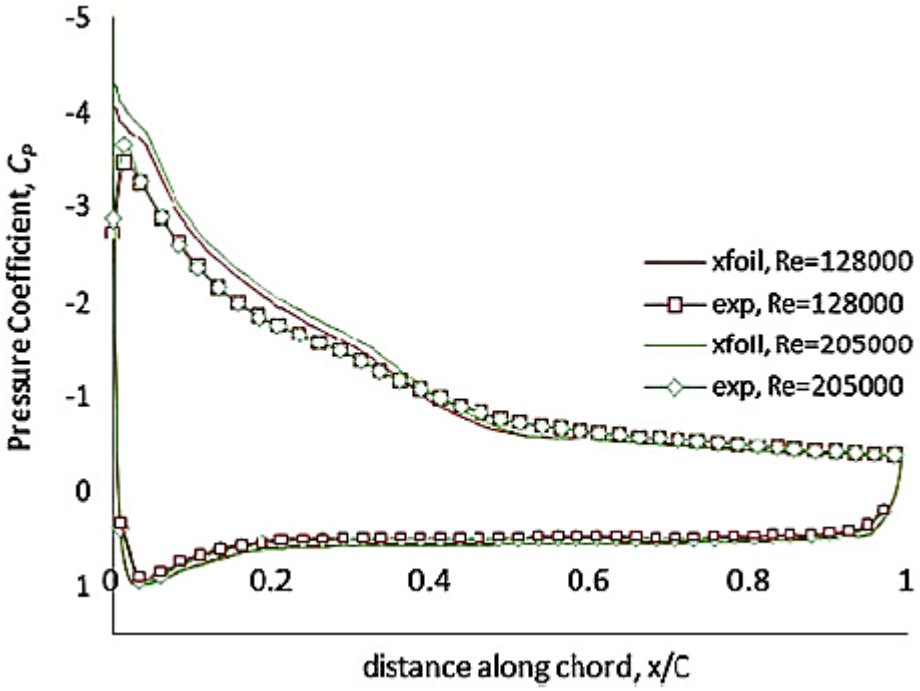

Figure 5.3.Validation of XFOIL for AF300 at Re=128,000 and Re=205,000 [12]

For higher ranges of Reynolds number, the validation examples may be found in the studies of Hoogendoorn et al. [25].

5.2. Blade Design

This process aims to determine the basic aerodynamic performance characteristics of the wind turbine blade. Firstly, the basic parameters needs to be defined, namely the desired power output at a particular wind velocity. In this study, as incoming velocity profile, the former research done around the campus area of Izmir Institute of Technology, IZTECH, by Ünveren et al. will be considered. The mean wind speed map of the campus area is presented as;

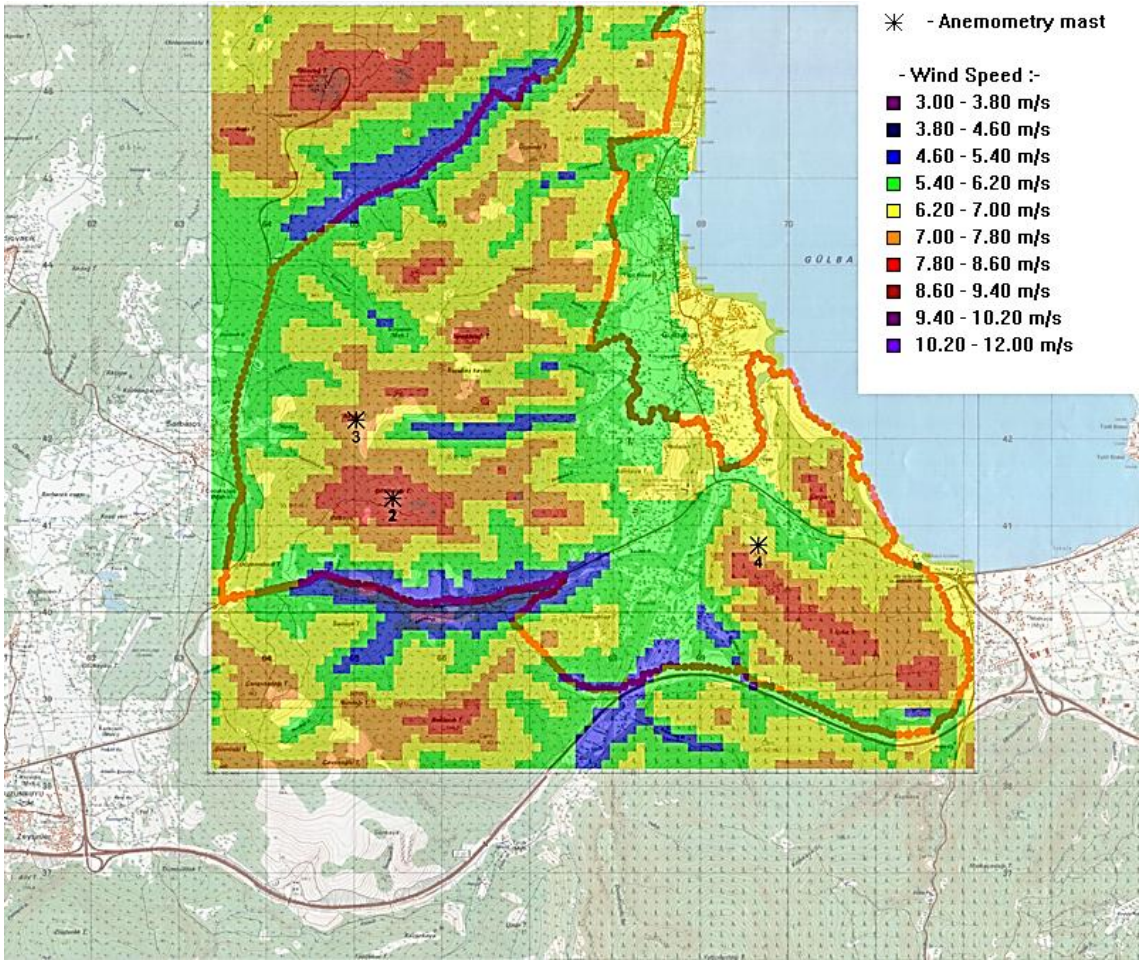

Figure 5.4.Mean wind speed map of IZTECH campus area [26]

The hub height of the constructed masts is presented as 50 m in that study and it has been taken into account throughout the design process.

After the decision of the power output, the radius of the blade is estimated using the general power output expression in Equation 5.2.

$$P = Cp\frac{1}{2}\rho\pi R^2 U^3 \tag{5.2}$$

In Equation 5.2, Cp is the power coefficient, ρ is the density of the flow, i.e. air density at the specified altitude and temperature and U is the incoming freestream velocity, i.e. mean wind speed. Substituting all the values of those parameters, Equation 5.2 can be solved for radius R. In order to achieve the desired power output with minimum blade length at a certain wind speed c_P is taken to be the Betz limit; 0.5926 in

all designs which is the theoretical maximum coefficient of performance, as mentioned in Chapter 4.

Depending on the type of application, a tip speed ratio, λ, was chosen. Conventionally, for electric power generation, it is between 4< λ <10 [3]. In order to decide that parameter, the research done by Bak et al. in which the selection of the tip speed ratio is directly related to the aerodynamic performance of the selected or designed airfoil [27] is used for all the applications.

Another input parameter for the blade geometry design is the airfoil empirical curves. $c_{l_{design}}$, $c_{d_{design}}$ and α_{design} should be chosen such that $^{c_{l_{design}}}/_{c_{d_{design}}}$ is at a maximum for each section of the blade. The c_l vs α, c_d vs α and $^{c_l}/_{c_d}$ vs α plots of the designed airfoil for that specific power output is obtained using PROFILI and then the values at where $^{c_l}/_{c_d}$ is maximum are taken as design values.

For each design, the blade is divided into 10 elements in spanwise direction. Therefore, where *r* is the local radius and *N* defines the number of division, Table 5.1 indicates the number of the section corresponding to the spanwise position.

Table 5.1.Number of sections and corresponding spanwise positions

Section #	1	2	3	4	5	6	7	8	9	10	11
r/R	0.0	0.1	0.2	0.3	0.4	0.5	0.6	0.7	0.8	0.9	1.0

In this study, the geometry of the blade is design based on the Blade Element Momentum Theory (BEM) including wake rotation mentioned in Chapter 4. However, there will be an addition of tip loss factor to BEM theory and a correction factor F is introduced. This factor is a function of the number of blades, *B*, the angle of relative wind, *φ*, and the position of the section along spanwise direction, *r/R*. based on Prandtl's method it can be described as;

$$F = \frac{2}{\pi} cos^{-1}\left[exp\left(-\left\{\frac{(^{B}/_{2})[1-(^{r}/_{R})]}{(^{r}/_{R})sin\varphi}\right\}\right)\right] \tag{5.3}$$

And the angle of relative wind, φ, also using the definition of local tip speed ratio, may be written as;

$$tan\varphi = \frac{U(1-a)}{\Omega r(1+a')} = \frac{(1-a)}{(1+a')\lambda_r} \tag{5.4}$$

The twist angle of the blade is expressed as;

$$\theta_T = \theta_P - \theta_{P,0} \tag{5.5}$$

where θ_P is the blade pitch angle and $\theta_{P,0}$ is the blade pitch angle at the tip such that $\theta_{P,0}$ corresponds to the position of the blade and θ_P changes if $\theta_{P,0}$ changes. Section pitch angle is also the difference between the relative angle of the wind and angle of attack, as shown in Equation 5.6.

$$\varphi = \theta_P + \alpha \tag{5.6}$$

Since the blade is discretized into 10 elements, now the geometrical parameters need to be defined locally. For instance, local chord, *c*, is given as;

$$c = \frac{8\pi r}{Bc_l}\left(\frac{sin\varphi}{3\lambda_r}\right) \tag{5.7}$$

And the solidity, which physically compares the blade with a solid disk, is locally defined as;

$$\sigma' = s = \frac{B \cdot c}{2\pi r} \tag{5.8}$$

And the thrust coefficient;

$$c_T = \frac{\sigma'(1-a)^2(c_l \cdot cos\varphi + c_d \cdot sin\varphi)}{sin^2\varphi} \tag{5.9}$$

Due to its small run time and theoretically strong and valid aerodynamic background, these equations are solved using an iterative approach to obtain optimum chord and twist distribution that maximizes the coefficient of power is used. Another application can be investigated in the study of Rajakumar et al. [28]. In order to start the iteration, initial guesses of angle of relative wind and axial and induction factors are needed. The angle of relative wind is initialized by;

$$\varphi_1 = \frac{2}{3} tan^{-1}\left(\frac{1}{\lambda_r}\right) \tag{5.10}$$

And for axial induction factor;

$$a_1 = \frac{1}{\left[1 + \frac{4sin^2(\varphi_1)}{\sigma'_1 \cdot c_l \cdot cos(\varphi_1)}\right]} \tag{5.11}$$

And for angular induction factor;

$$a'_1 = \frac{1 - 3a_1}{4a_1 - 1} \tag{5.12}$$

If c_T is greater than 0.96 then the blade is overloaded and Glauert correction is applied [29]. According to that theory, when c_T > 0.96;

$$a = \frac{1}{F}(0.143 + \sqrt{0.0203 - 0.6427(0.889 - c_T)} \tag{5.13}$$

If c_T < 0.96 is the case;

$$a = \frac{1}{\left[1 + \frac{4 \cdot F \cdot sin^2(\varphi)}{\sigma' \cdot c_l \cdot cos(\varphi)}\right]} \tag{5.14}$$

Using the value of axial induction, angular induction factor becomes as shown in Equation 5.15.

$$a' = \frac{1}{\frac{4Fcos\varphi}{\sigma' c_l} - 1} \tag{5.15}$$

If a and a' converges within the specified criteria where in this study the convergence criteria for both design and analysis of the rotor is taken to be 10^{-9}, the program may continue to calculate the coefficient of power or performance. It is indicated as;

$$Cp = \frac{8}{\lambda N} \sum_{i=1}^{N} F_i sin^2\varphi_i (cos\varphi_i - \lambda_r sin\varphi_i)(sin\varphi_i + \lambda_r cos\varphi_i)\left[1 - \left(\frac{c_d}{c_l}\right) cot\varphi_i\right] \tag{5.16}$$

Using the expressions from Equation 5.3 to Equation 5.16, an iterative MATLAB code has been produced and it is given in APPENDIX A.1. The classical BEM theory is modified using Prandtl's tip loss correction and Glauert's correction. The code gives the optimum chord and twist distribution corresponding to the inputs shown in Figure 5.5.

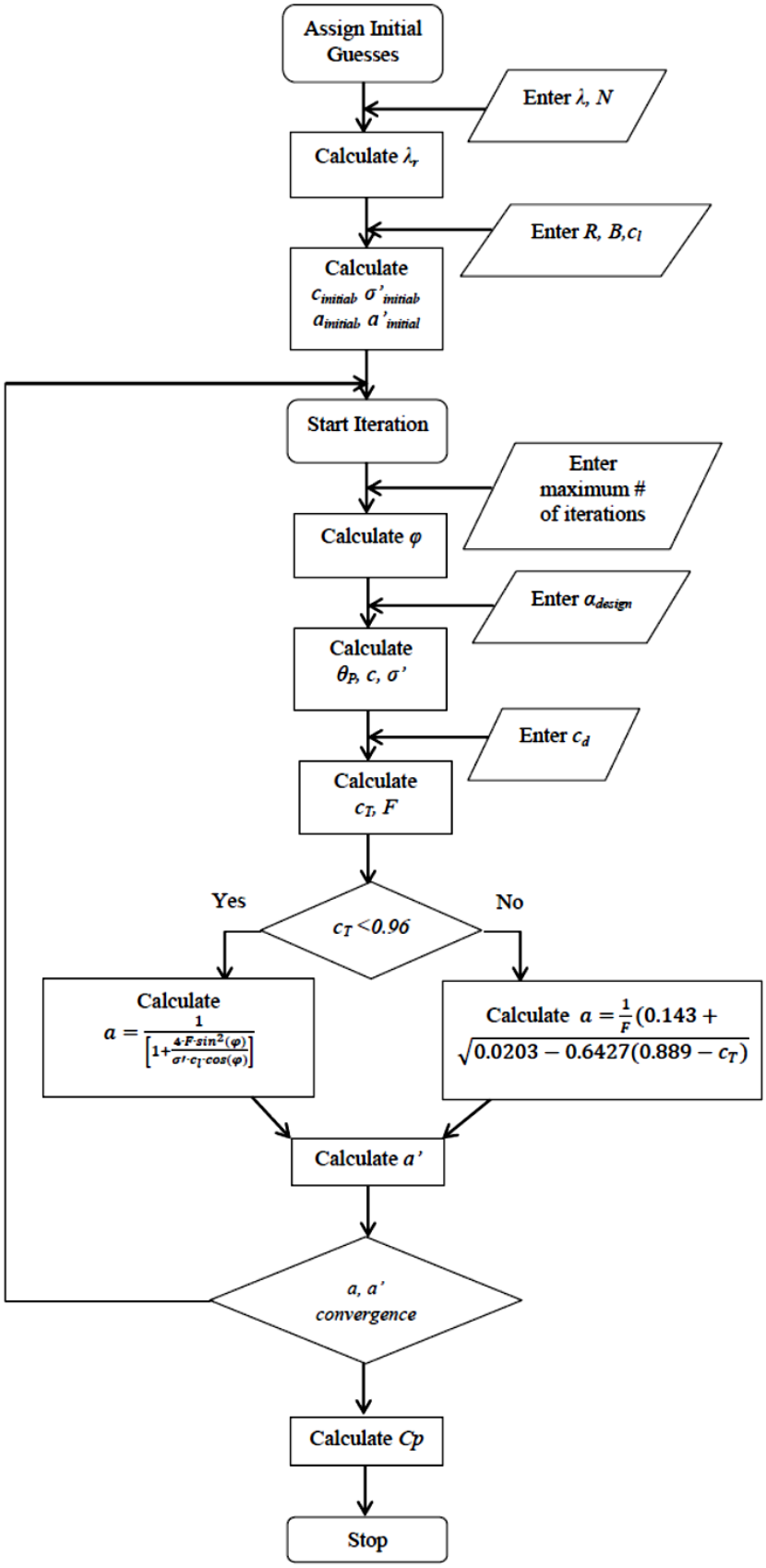

Figure 5.5.Flowchart of the optimization procedure

5.2.1. Validation of Modified BEM Code

The constructed iterative blade design code is validated in order to understand the capability and the limits of the theory. Validation is performed for the 8 kW output MIE wind turbine which have experimental results presented in Reference [22].

In the analysis, the aerodynamic performance parameters of the chosen airfoils in MIE wind turbine will be inputted to the constructed program and resulted chord distributions will be compared with the experimental results. The main characteristics of MIE turbine is tabulated in Table 5.2.

Table 5.2.Basic machine parameters of MIE wind turbine

Design Variable	Unit	Value
Number of blades	#	3
Rotor diameter	m	10
Root extension	m	0.433
Rotational speed	rpm	90
Hub Height	m	13.3
Cut-in wind speed	m/s	3
Cut-out wind speed	m/s	12
Rated Power	kW	8

Also, the tip speed ratio, λ, is calculated using rotational speed and design wind speed which is taken as 5.5 m/s. Using those data and additional values in Table 5.2, the chord distribution obtained from the modified BEM code for that configuration is presented in Figure 5.6.

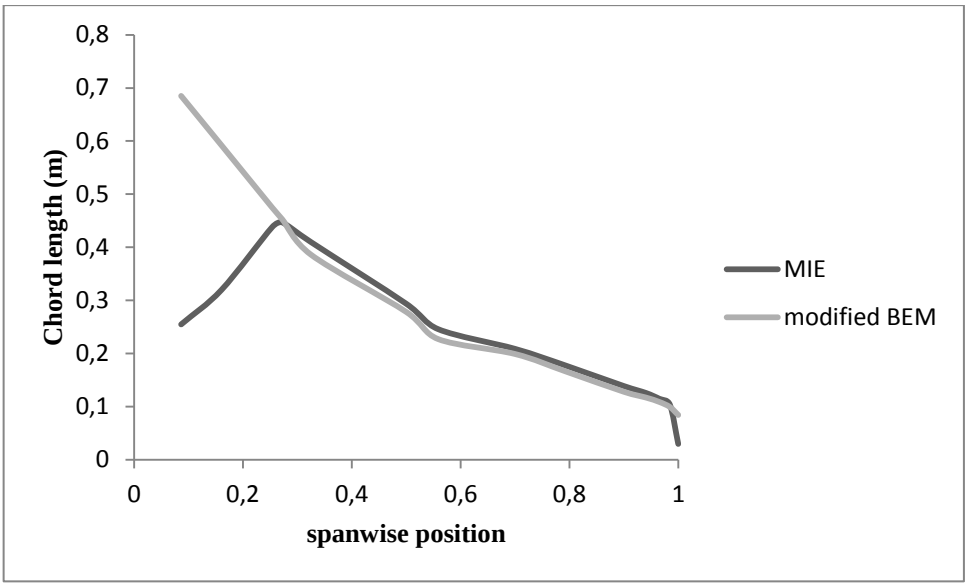

Figure 5.6.Comparison of chord distributions between MIE turbine and modified BEM theory output

It can be interpreted from Figure 5.6 that except for the sections near hub and tip, the program is capable of producing geometrical specifications that can be accepted. It should be noted that, near hub and tip, structural and dynamic loads are major concerns and for that reason, those sections are designed specifically. In MIE turbine, for instance, the first three design sections near the hub are made of cylindrical like geometries instead of airfoils exactly where the BEM code seems to fail. Other than those areas, the agreement seems satisfactory. The maximum percentage error between the chord values is 7.7 % whereas the minimum is 1.3 %. The data list of this analogy is given in APPENDIX B.

Since twist distribution of MIE turbine is selected concerning other parameters rather than aerodynamic efficiency, it was not found appropriate to compare the values in terms of validation.

5.3. Rotor Analysis

Rotor analysis is done using Numeca software developed by Numeca International. Numeca provides a series of integrated mesh-solver-analysis packages; FINE™/Turbo, FINE™/Open, and FINE™/Design3D. FINE™/Turbo and the integrated meshing tool Autogrid5™ which is a fully automatic mesh generator for

blade geometries is used in this study. Comparing to the other commercial CFD programs in the market, Numeca gives solution out in quite a small amount of time such that, according to the developer, a full second-order accurate solution can be completed in less than 30 minutes on a quadcore PC for 1 million mesh points with the implemented CPU Booster [31].

The numerical analysis of the wind turbine blade starts with the geometrical modeling which is done in the AutoBlade™ module of FINE™/Turbo. The data files of the airfoil coordinates are implemented together with the chord and twist distributions obtained from the BEM code. After the geometry is constructed, it is exported as geomturbo file in order to start the meshing process in Autogrid5™. Geomturbo file is then imported to Autogrid5™ and the meshing parameters are given considering the rotational speed, far field domain, desired mesh intensity along spanwise and chordwise directions, etc. After the geometry is discretized, the solution process begins in Euranus module in FINE™/Turbo.

The governing equations solved in Euranus are expressed in the relative frame of reference for the absolute velocity components where for wind turbine and propeller problems, the formulation based on relative velocities has the disadvantage that the far field relative velocity can reach high values. This induces an excess of artificial dissipation leading to a non-physical rotational flow in the far field region, this dissipation being based on the computed variables [31].

The governing equations in Cartesian coordinates can be expressed as;

$$\frac{\partial}{\partial t}\vec{U} + \nabla\vec{F}_I + \nabla\vec{F}_V = \vec{Q} \tag{5.17}$$

where $\vec{U}$ is the vector of conservative variables (mass, momentum and energy).

$$\vec{U} = \begin{bmatrix} \rho \\ \rho\vec{v} \\ \rho E \end{bmatrix} \tag{5.18}$$

$\vec{F}_I$ and $\vec{F}_V$ are respectively the inviscid and viscous flux vectors.

$$\vec{F}_{I_i} = \begin{bmatrix} \rho v_i \\ \rho v_1 v_i + \rho \delta_{1i} \\ \rho v_2 v_i + \rho \delta_{2i} \\ \rho v_3 v_i + \rho \delta_{3i} \\ (\rho E + p) v_i \end{bmatrix} \tag{5.19}$$

$$-\vec{F}_{V_i} = \begin{bmatrix} 0 \\ \tau_{i1} \\ \tau_{i2} \\ \tau_{i3} \\ q_i + v_j \tau_{ij} \end{bmatrix} \tag{5.20}$$

where τ represent the stress and q define the heat flux components.

And Q contain the source terms.

$$\vec{Q} = \begin{bmatrix} 0 \\ \rho \overrightarrow{f_e} \\ W_f \end{bmatrix} \tag{5.21}$$

With $\overrightarrow{f_e}$ corresponds to the effects of external forces W_f is the work performed by those external forces such that $W_f = \rho \overrightarrow{f_e} \cdot \vec{v}$. Other source terms are possible also, like gravity, depending on the chosen functionalities.

Using the turbulence modeling, the Navier-Stokes' equations are modified according to the rotating frame of reference for the absolute velocity. Together with the Boussinesq's approximation, where parameters with a bar above indicates the average velocities, the Navier-Stokes' equations become;

$$-\overline{\rho v_i v_j} = \mu_t \left[\frac{\partial v_i}{\partial x_i} + \frac{\partial v_j}{\partial x_i} - \frac{2}{3} \left(\overrightarrow{\nabla \tilde{v}} \right) \delta_{ij} \right] - \frac{2}{3} \rho k \delta_{ij} \tag{5.22}$$

where v_i and x_i are the components of absolute velocity, $\tilde{v}$ is turbulent working variable and $\mu_t = \frac{\nu_t}{\rho}$ where ν_t is the turbulent viscosity and its description depends on the turbulence model.

Throughout this study, for all the wind turbine blades analysis, one equation Spalart- Allmaras model is used [32]. This model acts like a bridge between algebraic models and 2-equation models like k-ε and its main advantage over the algebraic models is that, the turbulent eddy viscosity field is always continuous and capable of treating more complex flows. Spalart-Allmaras is also advantageous towards the k-ε model in terms of robustness and usage of lower additional CPU and Memory. This practicality was the main reason that this model is used in the analysis process since the results of this process is used to improve the geometrical model of the blade.

The principle of this turbulence model is based on the implementation of an additional transport equation for the eddy viscosity. The equation contains an advective, a diffusive and a source term and is exerted in a non-conservative manner. The implementation is based on the papers of Spalart and Allmaras [32] with the improvements described in Ashford and Powell [33] in order to avoid negative values for the production term. The mathematical explanation of Spalart-Allmaras model may be described as;

$$\nu_t = \tilde{\nu} f_{v1} \tag{5.23}$$

where $\tilde{\nu}$ is the turbulent working variable and f_{v1} is a function defines as;

$$f_{v1} = \frac{\chi^3}{\chi^3 + c_{v1}} \tag{5.24}$$

With χ being ratio between working variable, $\tilde{\nu}$ and molecular viscosity, ν.

$$\chi = \frac{\tilde{\nu}}{\nu} \tag{5.25}$$

The turbulent working variable needs to obey the transport equation;

$$\frac{\partial \tilde{\nu}}{\partial t} + \vec{V} \cdot \nabla \tilde{\nu} = \frac{1}{\sigma} \{\nabla \cdot [(\nu + (1 + c_{b2})\tilde{\nu}) \nabla \tilde{\nu}] - c_{b2} \tilde{\nu} \nabla \tilde{\nu}\} + Q \tag{5.26}$$

where $\vec{V}$ is the velocity vector, Q is the source term and σ and c_{b2} are constants. The source term includes a production and destruction parts dependent on the working variable, such as;

$$Q = \tilde{\nu}P(\tilde{\nu}) - \tilde{\nu}D(\tilde{\nu}) \tag{5.27}$$

$$\tilde{\nu}P(\tilde{\nu}) = c_{b1}\check{S}\tilde{\nu} \tag{5.28}$$

$$\tilde{\nu}D(\tilde{\nu}) = c_{w1}f_w\left(\frac{\tilde{\nu}}{d}\right)^2 \tag{5.29}$$

The product term, P is constructed as;

$$\check{S} = Sf_{v3} + \frac{\tilde{\nu}}{\kappa^2 d^2}f_{v2} \tag{5.30}$$

$$f_{v2} = \frac{1}{(1+\frac{\chi}{c_{v2}})^3} \tag{5.31}$$

$$f_{v3} = \frac{(1+\chi f_{v1})(1-f_{v2})}{\chi} \tag{5.32}$$

where d is the distance to the closest wall and S the magnitude of vorticity. Also, in Equation 5.29, f_w term is described in Equation 5.33;

$$f_w = g\left(\frac{1+{c_{w3}}^6}{g^6{c_{w3}}^6}\right)^{\frac{1}{6}} \tag{5.33}$$

where

$$g = r + c_{w2}(r^6 - r) \tag{5.34}$$

and

$$r = \frac{\tilde{\nu}}{\check{S}\kappa^2 d^2} \tag{5.35}$$

The constants in the model may be listed as;

$$c_{w1} = \frac{c_{b1}}{\kappa^2} + \frac{1 + c_{b2}}{\sigma} \tag{5.36}$$

With $c_{w2} = 0.3,\ \ c_{w3} = 2,\ \ c_{v1} = 7.1,\ \ c_{v2} = 5,\ \ c_{b1} = 0.1355,\ \ c_{b2} = 0.622,$ $\kappa = 0.41, \sigma = 2/3.$

In order to solve Equation 5.26, appropriate boundary conditions are needed. Firstly, on solid wall, $\tilde{\nu} = 0$. Along the inflow boundaries the value of ν_t is specified where $\tilde{\nu}$ is obtained using a Newton-Raphson procedure and solving Equation 5.23, and along the outflow boundaries it is extrapolated from the interior values.

In the software, the Spalart-Allmaras modeled turbulence characteristics are inputted in both initial and boundary conditions sections as turbulent viscosity. In Numeca, Spalart-Allmaras turbulent kinematic viscosity, ν_t may be modeled for turbomachinery as;

$$1 < \frac{\nu_t}{\nu} < 5 \tag{5.37}$$

Since the design area of the turbines is IZTECH campus, according to Reference [26], turbulence intensity, T_u is given as 0.9 where it changes between the limit $0 < T_u < 1$. Since it is the only turbulence characteristics we know about the incoming wind, an analogy was made and ν_t/ν was chosen to be 4 for all the geometries. Thus, ν_t corresponds to approximately 7.056 x 10^{-5} m^2/s.

After constructing the set of equations and boundary conditions specified for the design, a numerical model should be implemented in order to obtain a solution. In Numeca, to define numerical parameters of the computation, the Numerical Model page is used, Figure 5.7. It has several aspects of computation, such as; CFL number, multigrid and preconditioning parameters. CFL (Courant-Friedrich-Levy) a number that globally scales the time-step sizes used for the time-marching scheme of the flow solver. A higher value of the CFL number results in a faster convergence, but will lead to divergence if the stability limit is exceeded [31]. It is set to 3 as default, however, in order to get consistent results, CFL number is taken to be 2 for all analysis. After CFL number is assigned, the multigrid parameters are to be defined. The first one is 'Grid

levels: current/coarsest' and it indicates for each of i, j and k directions the currently selected grid level and the number of the coarsest grid level available in the corresponding direction. The second one of the multigrid parameters that allows to define for each of i, j and k directions the 'Current grid level'. The grid levels and their corresponding number of points are given in Table 5.3.

Table 5.3.Current grid levels in Numeca, FINE™/Turbo [31]

Grid level	Number of points	
0 0 0	17*33*33	(18513 points)
1 1 1	9*17*17	(2601 points)
2 2 2	5*9*9	(405 points)
3 3 3	3*5*5	(75 points)
4 4 4	2*3*3	(18 points)
4 5 5	2*2*2	(8 points)

Using the values represented in Table 5.3, 'Current grid level' is set to be 1 1 1 so that a detailed solution may be obtained without being computationally expensive.

At low Mach number values, the time marching algorithms designed for compressible flows show lack of efficiency and therefore a low speed preconditioner has been developed in order to achieve fast convergence and more accurate solutions when the Mach number is very low as in the case of this study. Mach number M is defined as;

$$M = \frac{V}{a} \tag{5.38}$$

where V is the velocity of the source with respect to the medium and a is the speed of sound in that medium. Numeca has two types of preconditioning parameters when low speed flow is studied: Hakimi and Merkle. Due to its robustness and accuracy, Merkle parameter was chosen [34].

After all the sections were filled, the numerical solution page in Numeca FINE™/Turbo is presented in Figure 5.7.

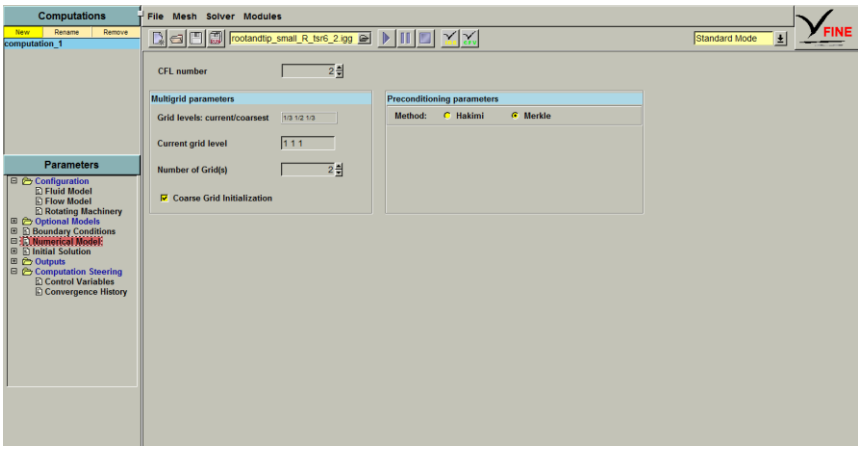

Figure 5.7.Numerical model interface of Numeca FINE™/Turbo

As initial solution, the free stream pressure and temperatures have been inputted as constant values together with the design velocity of the rotor, as can be seen in Figure 5.8. Note that, the atmospheric pressure is taken to be 1 atm and the temperature to be 20^{o}C.

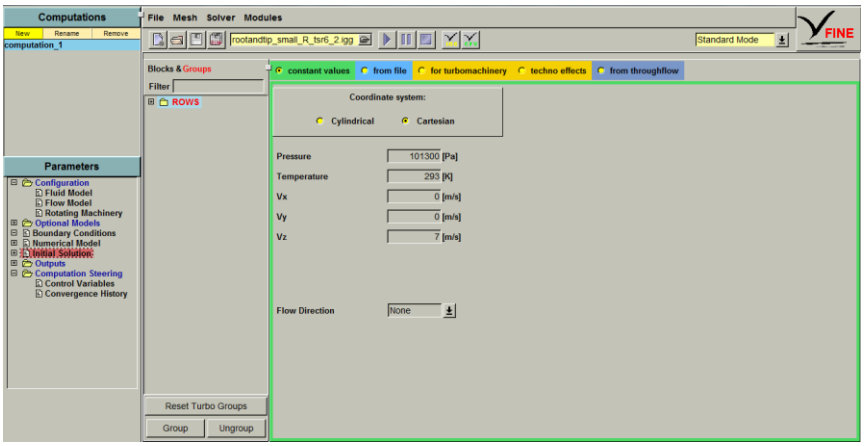

Figure 5.8.Initial solution interface of Numeca FINE™/Turbo

In the ‘Outputs’ section of Numeca the incoming and relative velocities are selected in order to visualize the velocity triangle onto the blade to blade cross section.

Under ‘Computation Steering’, in ‘Control Variables’ section, it is possible to designate the convergence criteria, maximum number of iterations and the expert functions. Except for the ‘IVELSY’ function, all the parameters were left in their default values, which can be examined in detail in Reference [31]. By setting the IVELSY function equal to zero, the mathematical solution is expressed in the relative frame of reference for the absolute velocity components, which has been modeled above. In ‘Convergence History’ section, it is possible to monitor the global residuals

together with the change in the defined output parameters with respect to the number of iterations. Throughout this study, the convergence on torque is followed and the change in the axial thrust was observed.

CHAPTER 6

RESULTS AND DISCUSSION

In this chapter, the designed geometries will be presented together with the performance analysis done using CFD code, Numeca FINE™/Turbo and the results will be discussed. Starting from the airfoil analysis, all the choices and decisions made will be justified and their capability to meet the expectations will be investigated.

6.1. 1 kW Horizontal Axis Wind Turbine Generator

6.1.1. Airfoil Design

In terms of selection or design of an airfoil, the wind turbine blade may be divided up to four main sections; inboard (near hub region), mid-span (*r/R=0.5* approximately), semi-span (*r/R=0.7* approximately) and tip (*r/R=0.9* approximately). For inboard and mid-span sections, the considerations are a mixture of structural and aerodynamic requirements whereas semi-span and tip design understanding in aerodynamics point of view is more dominant.

The airfoil characteristics of a wind turbine should demonstrate; a high lift to drag ratio in order to obtain a high power coefficient or maximize the annual energy production and a moderate high design lift coefficient to reduce the blade area since according to the modified blade element theory applied, chord is inversely proportional to the design lift coefficient. Also, low roughness sensitivity is demanded with respect to maximum *L/D* ratio in order the design to be able to tolerate production imperfections especially around the leading edge area. Finally, high operational angle of attacks, in other words, delayed stall and flow separation is desired.

Those demands lead to a design which follows a procedure of limiting the thickness of upper surface of the airfoil to decrease upper surface velocities. For the lower surface, an S-shape tail or an under camber tail is preferred in order to obtain sufficient lift. Also, it should be noted that, the location of maximum thickness in

combination with nose radius are the main parameters that define lift to drag ratio and roughness sensitivity [35].

As mentioned in Chapter 5, airfoils have been designed using the inverse-design method, PROFOIL and its interface of design page can be seen in Figure 6.1.

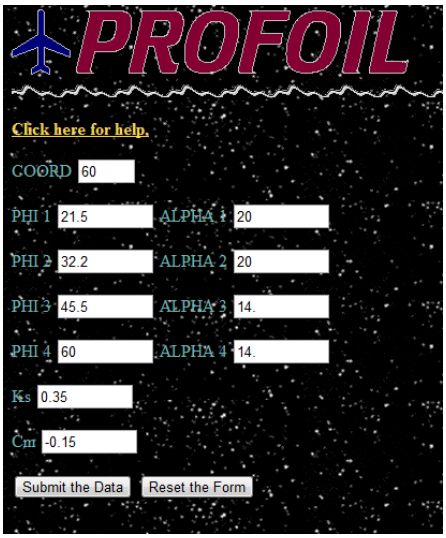

Figure 6.1.PROFOIL design page (default values)

PHI 1, 2, 3 and *4* corresponds to the locations of the design points on the surface of the airfoil and *ALPHA 1, 2, 3* and *4* are the design angle of attacks for each segment at which the velocity profile is constant. Also, Ks is the trailing edge closure parameter and C_M is the pitching moment.

For the design of 1 kW HAWT generator, the chosen PROFOIL input parameters are listed in Table 6.1.

Table 6.1.PROFOIL input parameters for 1 kW wind turbine generator airfoil

Parameters	Values
PHI 1	21.5
PHI 2	32.2
PHI 3	40
PHI 4	60
ALPHA 1 (deg)	8
ALPHA 2 (deg)	10
ALPHA 3 (deg)	-10
ALPHA 4 (deg)	14
Ks	0.15
Cm	-0.15

As can be seen from Table 6.1, *PHI 1, 2* and *4* was left at their default values, where *PHI 3* has been reduced to take the design point on the lower surface of the airfoil slightly forward, i.e. closer to the leading edge so that S-shape can be achieved easily. *ALPHA 1, 2, 3* and *4* are selected in such a way that the formed profile would be thick enough to fulfill the structural requirements together with the carved tail to meet the aerodynamic expectations.

The output of airfoil of PROFOIL for those given parameters was named as "tfprofoil_nt2" and its geometrical shape is given in Figure 6.2 where its coordinates are presented in APPENDIX C.1. The maximum thickness to chord ratio of tfprofoil_nt2 is 19.95% at 19.8% of the chord and it maximum camber is 2.85% at 60% of the chord.

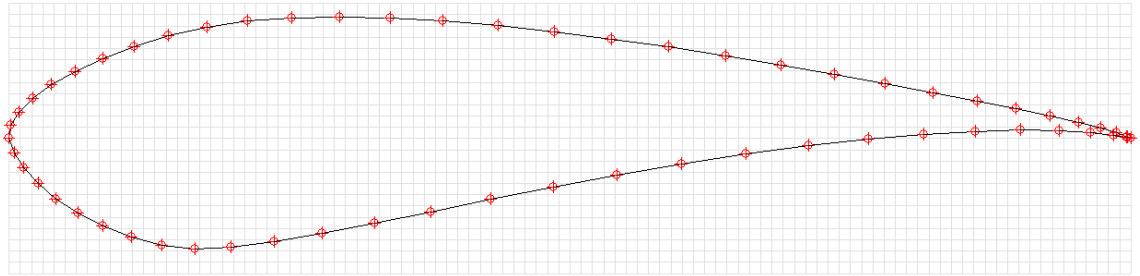

Figure 6.2.Geometry of tfprofoil_nt2

The profile is then analyzed using XFOIL through its interface PROFILI and its performance parameters obtained at *Re = 250000* are presented in Table 6.2.

Table 6.2.Performance parameters of tfprofoil_nt2 obtained using XFOIL

$(c_L/c_D)_{max}$	68.5215
c_L	1.4321
c_D	0.0209
c_M	-0.0845
α (deg)	10.5

6.1.2. Blade Design

The blade design process starts with the assignment of design wind speed. Then, using Equation 5.2, together with the rated power and Betz limit, the rotor radius may be obtained. Note that, using Reference [26] and Figure 5.4, design wind speed was

chosen to be 7 m/s. Also, according to Bak et al. [27], tip speed ratio λ is chosen to be 6 since design (c_L/c_D) is sligthy greater than 50 and the diameter of the rotor is around 1.75 m. Knowing that $\lambda = {\Omega R}/{u}$, the corresponding rotational speed becomes 23.56 rad/s or 225 rpm. Basic design parameters of 1 kW wind turbine generator are presented in Table 6.3.

Table 6.3.Basic design parameters of 1 kW wind turbine

Design Variable	Unit	Value
Number of blades	-	3
Rotor radius	m	1.78
Root extension	m	0.29
Tip speed ratio	-	6
Rotational speed	rpm	225
Design wind speed	m/s	7
Rated Power	kW	1

Those parameters are then inserted to MATLAB code of modified BEM theory together with the airfoil performance results in Table 6.2, so that the optimum chord and twist distributions and coefficient of performance Cp may be obtained. The results of the code are listed with respect to the spanwise directions in Table 6.4.

Table 6.4.Chord and twist distributions and Cp results of 1 kW wind turbine generator using modified BEM code

Section	r/R	chord (m)	twist (deg)	Cp
1	0.0	0.2875	24.4112	0
2	0.1	0.2627	21.7706	0.1204
3	0.2	0.2379	19.1259	0.1483
4	0.3	0.1842	12.8121	0.2384
5	0.4	0.1469	8.7164	0.3232
6	0.5	0.1212	5.9779	0.4039
7	0.6	0.1027	4.0471	0.4807
8	0.7	0.0886	2.6189	0.5511
9	0.8	0.0769	1.5157	0.6027
10	0.9	0.0643	0.6337	0.5786
11	1.0	0.0550	0.0000	0.3060

Modifying Equation 5.16 and applying for the discretization shown in Table 6.4;

$$Cp = \frac{8}{\lambda N} \sum_{i=1}^{N} Cp_i \tag{6.1}$$

Since the blade is divided into 10 elements $N = 10$; and $\lambda = 6$, $Cp = 0.5004$ may be obtained. Note that, this value of Cp will be compared with the results to be obtained using CFD.

6.1.3. Blade Analysis

As mentioned previously, the CFD analysis of the blade will be done using Numeca and the process starts with the construction of the geometry. To do that, AutoBlade™ module which can be examined in Figures 6.3 and 6.4 is used.

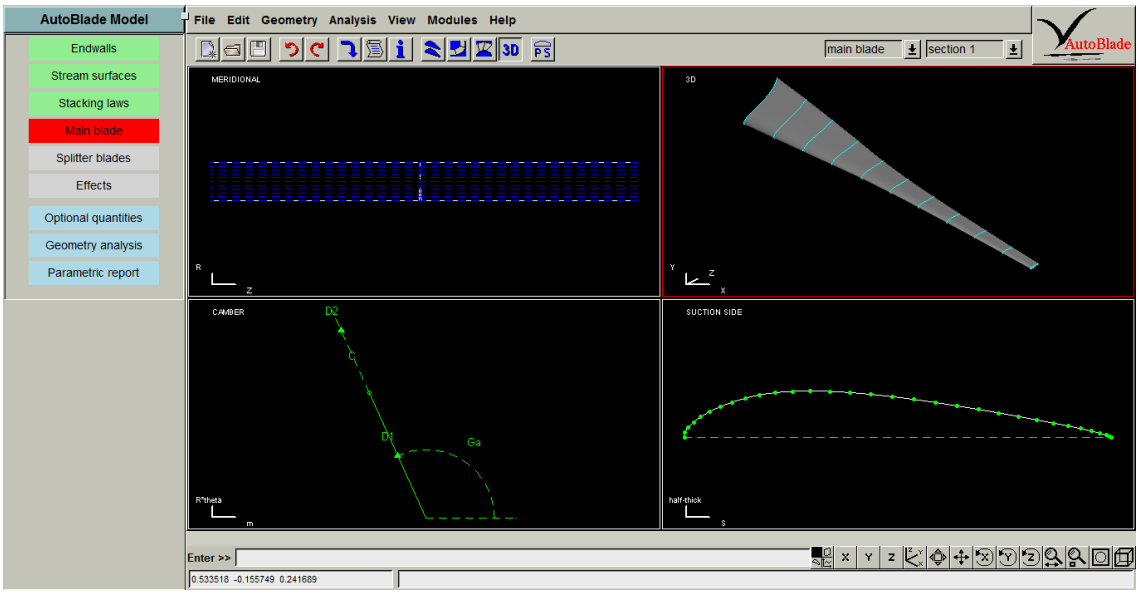

Figure 6.3.Geometry of 1 kW wind turbine blade, AutoBlade™

In Figure 6.3, the upper left corner describes the far-field boundaries, in other words, upstream and downstream regions around the blade; upper right corner is the 3D view of the blade; lower left corner describes the camber specifications and from the lower right corner, suction or pressure side of the airfoil used in the specified section may be investigated. In Figure 6.4, 3D view of the rotor without the hub is presented.

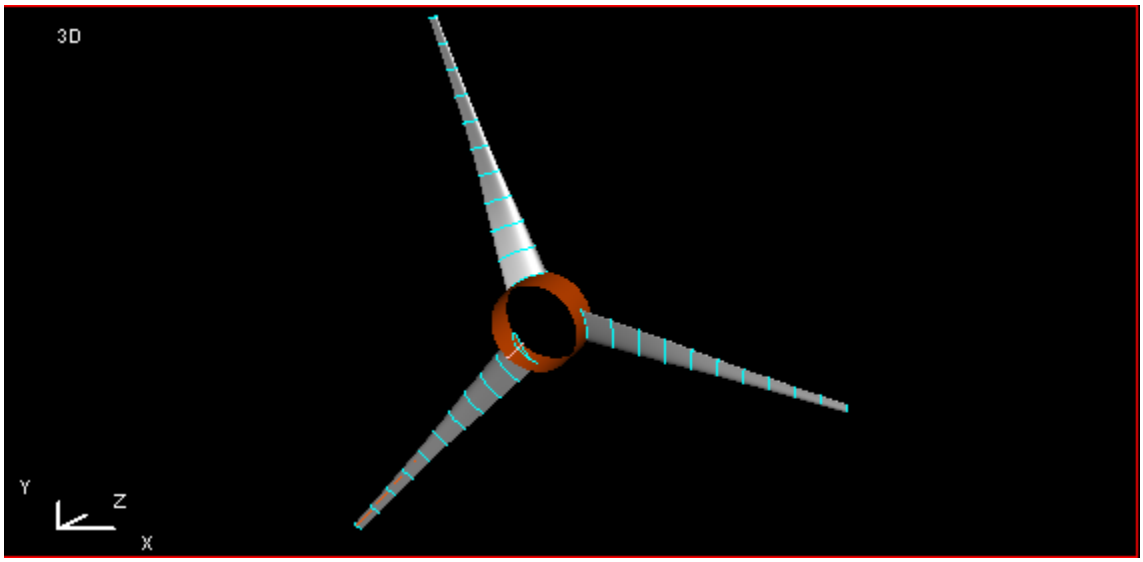

Figure 6.4.Geometry of 1 kW wind turbine rotor, AutoBladeTM

Discretization of 3D domain is done using the AutoGrid5^{TM} module of Numeca. AutoGrid5^{TM} includes meshing parameters specified for wind turbine applications; therefore it is accepted to be as semi-automatic process. Those parameters specified may be listed as; rotational speed in terms of revolutions per minute, inputted as 225; far-field domain that is desired to be meshed, taken to be 6 times of the blade length both upstream and downstream; lastly, the density of the grids along blade, chosen in such a way that spanwise expansion ratio is around 1.3. The 3D and blade to blade mesh distribution around 1 kW turbine blade may be seen in Figures 6.5 and 6.6, respectively.

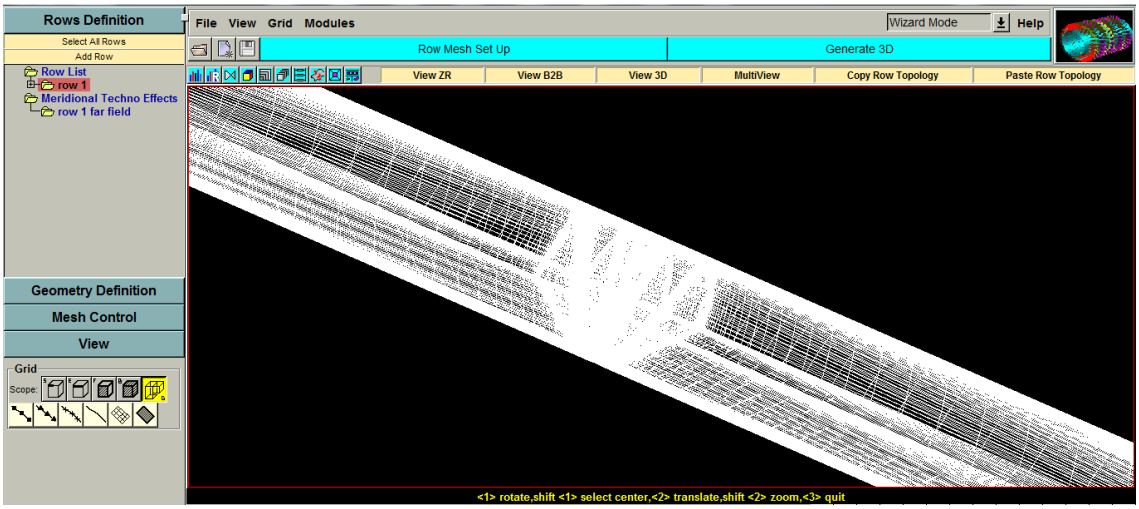

Figure 6.5.3D mesh distribution of 1 kW wind turbine blade, AutoGrid5TM

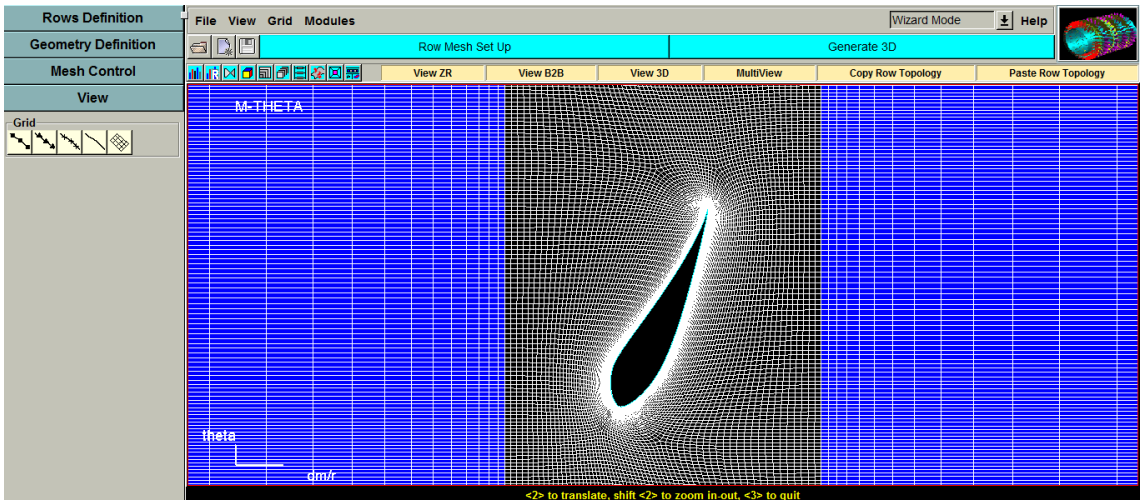

Figure 6.6.Blade to Blade (2D) mesh distribution of 1 kW wind turbine blade, AutoGrid5TM

Also, in Table 6.5, the mesh quality report for 1 kW wind turbine blade discretization is presented in which also the number of grid points can be observed.

Table 6.5.Grid quality report of 1 kW wind turbine blade

Number of Points	1,597,167
Minimal Skewness Angle (deg)	3.354
Maximal Skewness Angle (deg)	90
Average Skewness Angle (deg)	78.211
Minimal Spanwise Skewness Angle (deg)	165.346
Maximal Spanwise Skewness Angle (deg)	180
Average Spanwise Skewness Angle (deg)	179.716
Minimal Spanwise Expansion Ratio	1
Maximal Spanwise Expansion Ratio	1.19725
Average Spanwise Expansion Ratio	1.11274
Minimal Aspect Ratio	1
Maximal Aspect Ratio	13074.2
Average Aspect Ratio	522.675
Minimal Expansion Ratio	1
Maximal Expansion Ratio	1.872
Average Expansion Ratio	1.40001

The grid quality of discretization has vital importance in convergence and the accuracy of solutions. The Skewness angle, also called orthogonality, in Table 6.4 is the measure of the minimum angle between the edges of the element. According to Hildebrandt et al. the limit of minimum orthogonality is 20^{o}, maximum expansion ratio

in all direction is 2 and maximum aspect ratio is 5000 [36].In theory, orthogonality and aspect ratio seems to be violated. However, it can be interpreted from Figure 6.7 that, only 0.0042% of the cells have Skewness angle less than 18^{o} and 0.0746% have aspect ratios higher than 5000 which is the least important quality criterion. This grid may not be ideal but considering the challenging application and the considerable computational increase in computational costs required to improve the grid, the grid is deemed adequate.

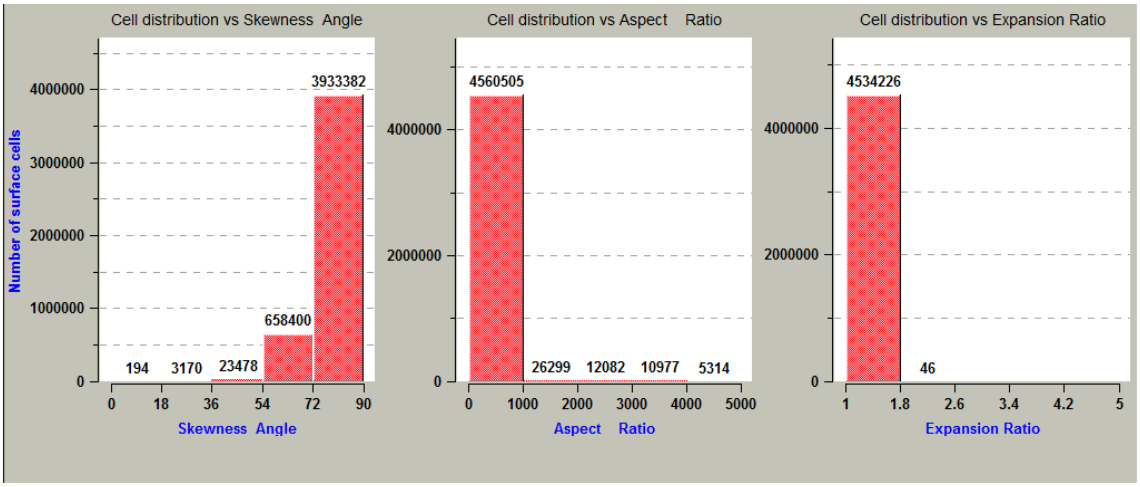

Figure 6.7.Grid quality report of 1 kW wind turbine blade, AutoGrid5^{TM}

Following the completion of discretization, the solution process which is performed using FINE™/Turbo module may be started. In FINE™/Turbo, the fluid is taken as air, flow is considered to be steady, low speed i.e. Mach number < 0.3 and mathematically modeled as turbulent Navier-Stokes with turbulence model of Spalart-Allmaras. The external boundary conditions of static pressure, static temperature, velocity components along x, y and z directions and turbulent viscosity terms have been inputted as 101300 Pa or 1 atm, 293 K or 20^{o}C, $V_x = V_y = 0$ where $V_z = 7$ m/s and $\nu_t = 7.056 \times 10^{-5}$ m^2/s as indicated in Chapter 5, respectively. In initial solution segment, pressure, temperature and velocity component values have been taken as identical with the external boundary conditions. Number of iterations was taken as 20000 in order to observe full convergence and the program was started to run. After 2000 iterations, the program converges and the resulting global residual and the behavior of torque output value is bestowed in Figure 6.8 and 6.9, respectively.

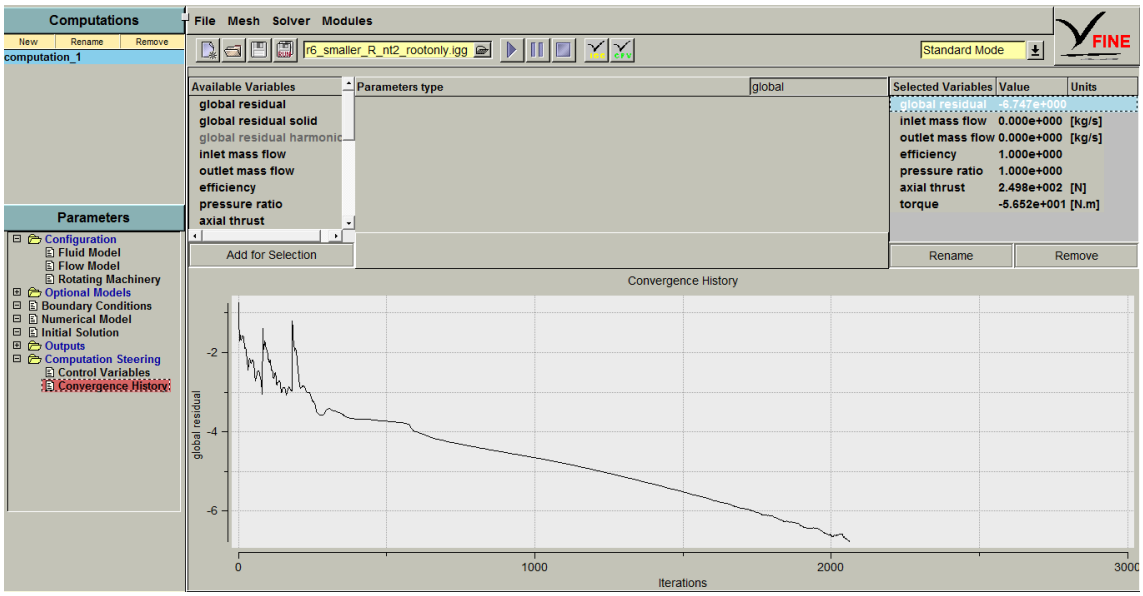

Figure 6.8.Global residual of 1 kW wind turbine rotor, FINE™/Turbo

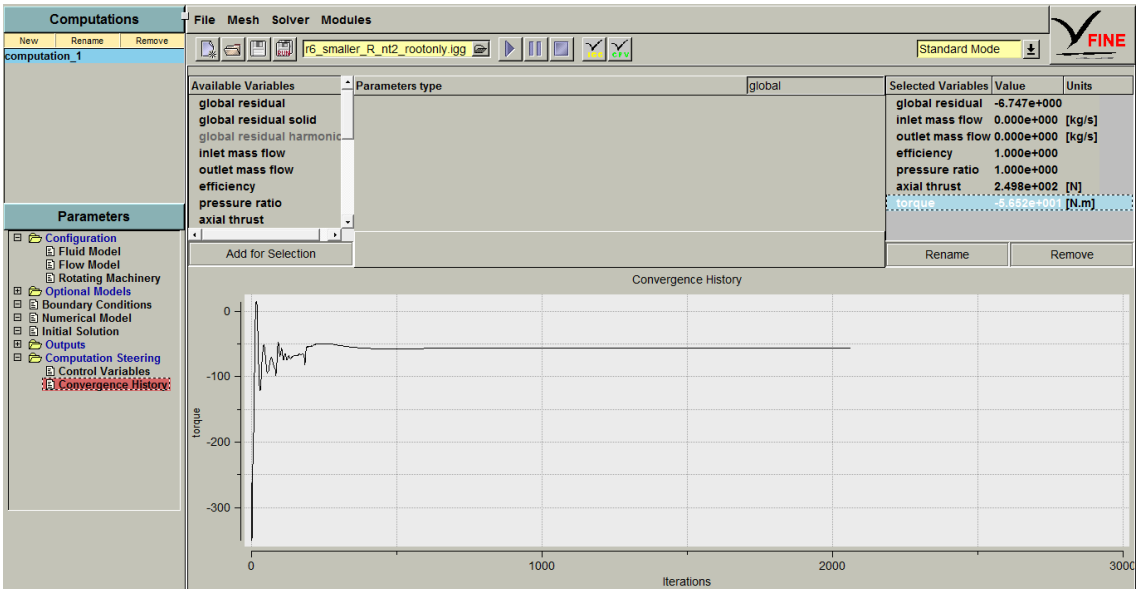

Figure 6.9.Torque output behavior of 1 kW wind turbine rotor, FINE™/Turbo

It can be seen from Figure 6.9 that, torque produced by designed 1 kW wind turbine rotor is 56.52 Nm which corresponds to the power production of 0.959 kW using Equation 3.32 and transmission and gear box efficiencies taken to be 0.9 and 0.8 respectively since the generator may not be fully capable of reaching to higher rpm values at which this turbine operates [3]. With the help of Equation 3.15, coefficient of performance *Cp* may be calculated for that design and it is found as 0.4593 which has a

deviation of 8 % with respect to the value obtained from modified BEM code probably caused by high amount of mechanical losses taken into consideration.

The velocity triangle obtained for the design around the cross-section taken at half span is presented in Figure 6.10.

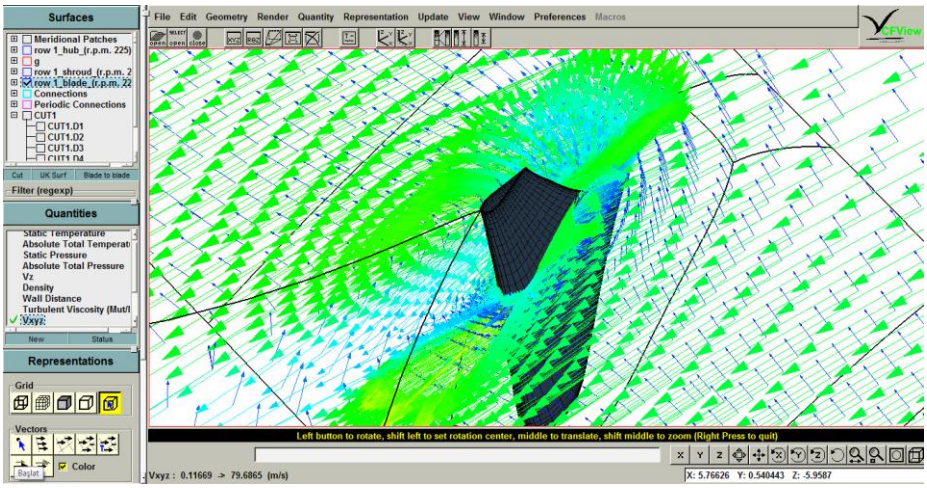

Figure 6.10.Velocity triangle formed around 1 kW wind turbine blade, CFView™

In Figure 6.10, the blue arrows define the incoming velocity striking through the pressure side of the blade whereas the green arrows represent the relative velocity formed by the vectoral summation of incoming velocity and angular velocity.

The total pressure distribution along the blade is shown in Figure 6.11.

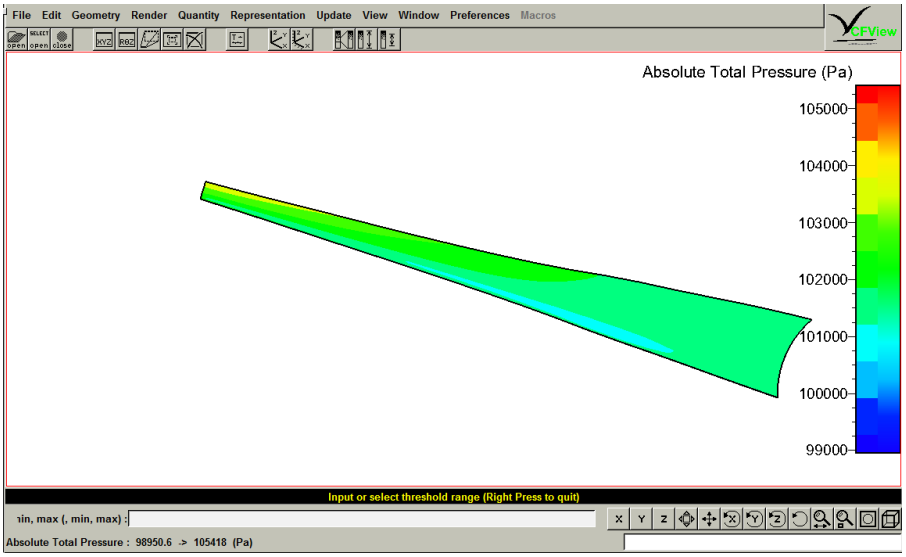

Figure 6.11.Total pressure distribution along pressure side of 1 kW wind turbine blade, CFView™

It can be seen from Figure 6.11 that the total pressure along the blade is distributed in such a way that trailing edge is more pressurized than the leading edge and the tip region of the blade is under a lot of pressure forces compared to the hub region. Therefore, in total, suction side trailing edge around tip region is the most critical area in terms of pressure loads. However, for that particular design, the pressure loads are to be concerned since the highest pressure value recorded is slightly above 1 atm.

When analyzing the rotor for different wind speed values, it was seen that the solution diverges for 3 and 12 m/s. this may verify that, those values may be taken to be cut-in and cut-out wind speeds where wind turbine stops operating. The operational power curve i.e. including electrical and mechanical braking for 1 kW wind turbine generator design is given in Figure 6.12.

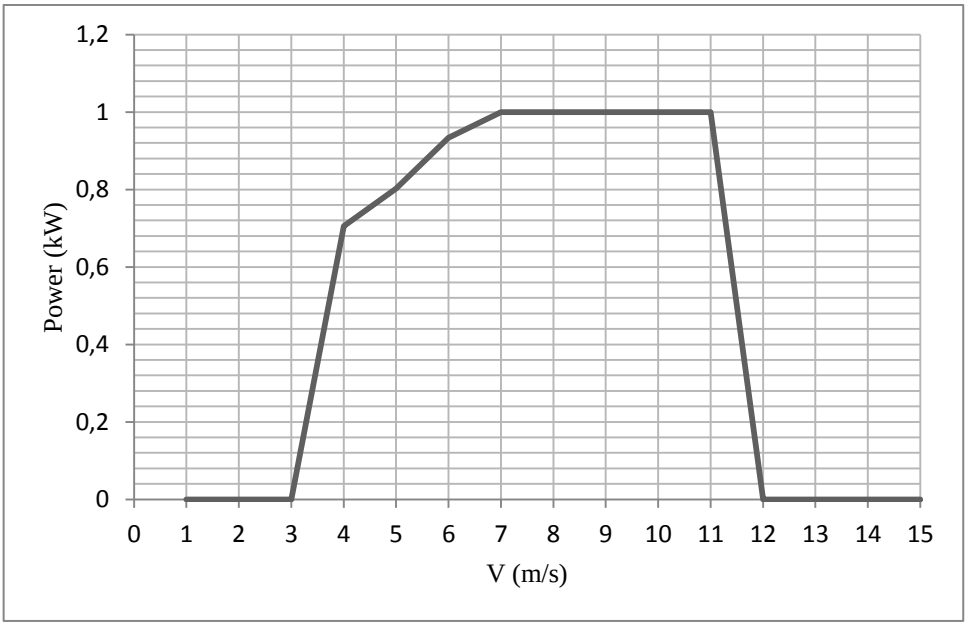

Figure 6.12.Power curve of 1 kW wind turbine

6.2. 5 kW Horizontal Axis Wind Turbine Generator

6.2.1. Airfoil Design

In design of 5 kW wind turbine generator, two design locations have been constituted such that from hub to mid-span and from mid-span to tip. Consequently, two

airfoil profiles have been used in those two separate sections and two geometrically different characteristics have been obtained. As the first part, i.e. near hub region, the same profile in 1 kW generator case, tfprofoil_nt2 has been used. On the other hand, for the section near tip region, the structural constraints lessened and more bold aerodynamic shapes are eligible. Thus, tfprofoil_nt2 has been modified to achieve higher performance, greater lift to drag ratio by decreasing its thickness and it is named as tfprofoil_nt2_tip. The maximum thickness to chord ratio of tfprofoil_nt2_tip is 16% at 20.6% of the chord and it maximum camber is 2.85% at 61.7% of the chord. The comparison between those two profiles may be examined in Figure 6.13.

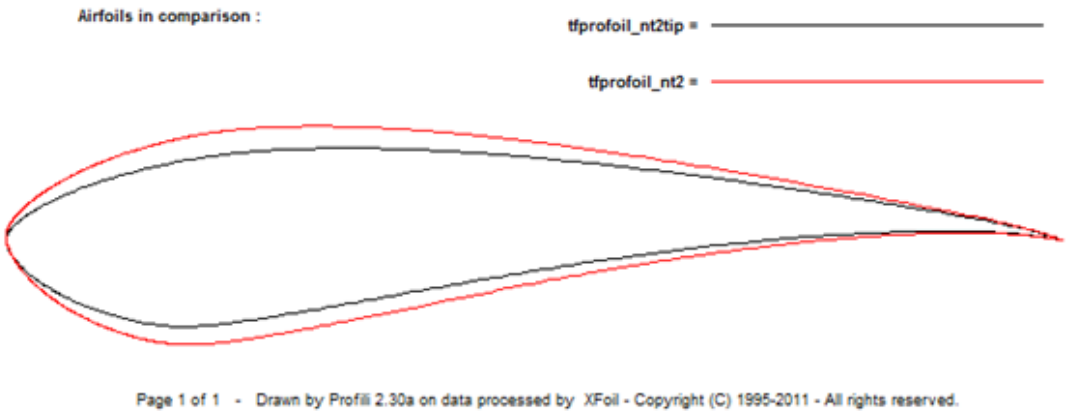

Figure 6.13.Geometrical comparison of tfprofoil_nt2 and tfprofoil_nt2_tip, PROFILI

Since the performance parameters of both of the profiles are needed as inputs to the modified BEM code, tfprofoil_nt2_tip was also analyzed and the resulting values for *Re = 350000* are listed in Table 6.6.

Table 6.6.Performance parameters of tfprofoil_nt2_tip obtained using XFOIL

$(c_L/c_D)_{max}$	77.9655
c_L	1.1305
c_D	0.0145
c_M	-0.114
α (deg)	6.5

6.2.2. Blade Design

The design wind speed for 5 kW wind turbine generator is also chosen using Reference [26] as 7 m/s. Substituting rated power *P = 5 kW* and Betz limit into

Equation 5.2 and solving for *R*, the radius of the blade is found to be 3.6 m. Similarly, tip speed ratio λ was assigned to be 6 according to studies done by Bak et al. [27] and the resulting rotational speed is obtained as 11.67 rad/s or 110 rpm. Basic design parameters of 5 kW wind turbine generator are given in Table 6.7.

Table 6.7.Basic design parameters of 5 kW wind turbine

Design Variable	Unit	Value
Number of blades	-	3
Rotor radius	m	3.6
Root extension	m	0.65
Tip speed ratio	-	6
Rotational speed	rpm	110
Design wind speed	m/s	7
Rated Power	kW	5

The parameters summarized in Table 6.6 are then consigned to the modified BEM code created in MATLAB combined with the performance parameters of the designed airfoils for appropriate sections. The optimum chord and twist distributions and *Cp* attained iteratively are listed in Table 6.8.

Table 6.8.Chord and twist distributions and Cp results of 5 kW wind turbine generator using modified BEM code, MATLAB

Section	r/R	chord (m)	twist (deg)	Cp
1	0.0	0.5663	24.4112	0
2	0.1	0.5237	21.7706	0.1204
3	0.2	0.4811	19.1259	0.1483
4	0.3	0.3725	12.8121	0.2384
5	0.4	0.3206	8.7164	0.3232
6	0.5	0.2901	5.9779	0.4039
7	0.6	0.2712	4.0471	0.4859
8	0.7	0.2523	2.6189	0.5581
9	0.8	0.2190	1.5157	0.6117
10	0.9	0.1832	0.6337	0.5891
11	1.0	0.1604	0.0000	0.3116

Note that, the twist values of 1 kW and 5 kW wind turbine generators are identical since the profiles used and design tip speed ratios are the same. Using Equation 6.1, Cp according to modified BEM code becomes $\mathrm{Cp} = 0.5054$which will be compared with the power output data obtained from CFD analysis.

6.2.3. Blade Analysis

The CFD analysis done by Numeca starts with the application of AutoBlade™ module to construct the geometry gained from the modified BEM code and it can be seen from Figures 6.14 and 6.15. Especially in Figure 6.15, the intensity of twist around hub region can be clearly observed.

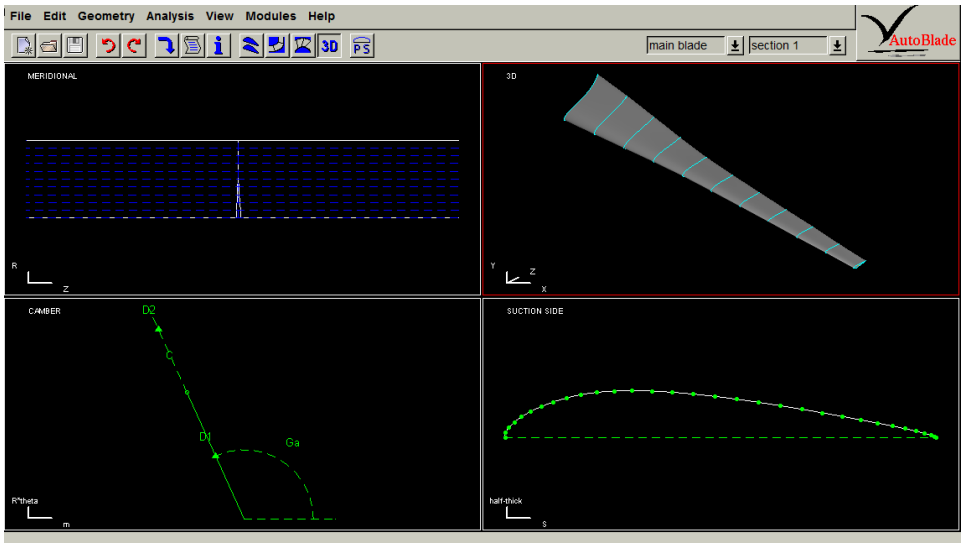

Figure 6.14.Geometry of 5 kW wind turbine blade, AutoBlade™

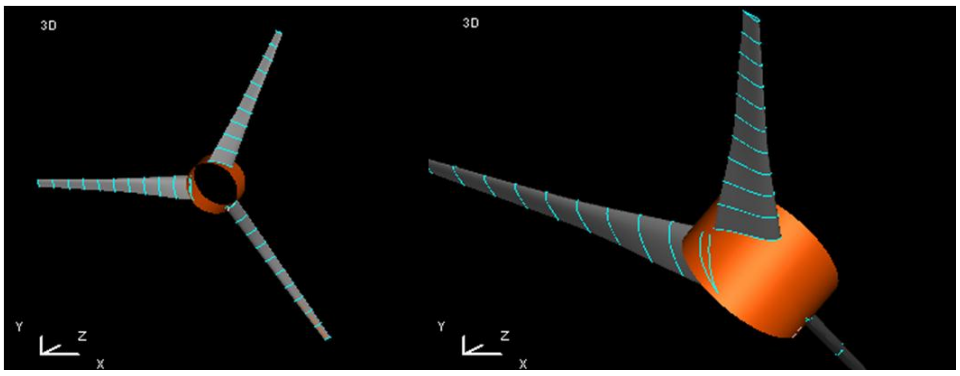

Figure 6.15.Geometry of 5 kW wind turbine rotor, AutoBlade™

As mentioned, discretization of 3D domain is done using the AutoGrid5™ module of Numeca and the meshing was setup as; rotational speed (rpm) inputted as 110; far-field domain that is desired to be meshed, taken to be 5 times of the blade length both upstream and downstream; lastly, the density of the grids along blade,

chosen in such a way that spanwise expansion ratio is around 1.185 in layers and 1.35 in far-field. 3D and blade to blade mesh distribution around 5 kW turbine blade may be seen in Figures 6.16 and 6.17, respectively.

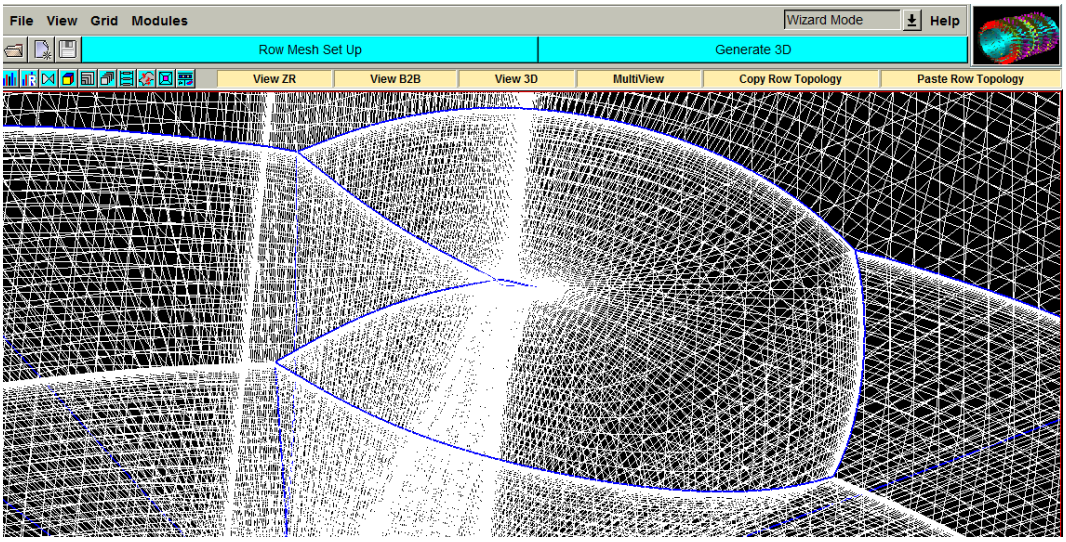

Figure 6.16.3D mesh distribution of 5 kW wind turbine blade, AutoGrid5™

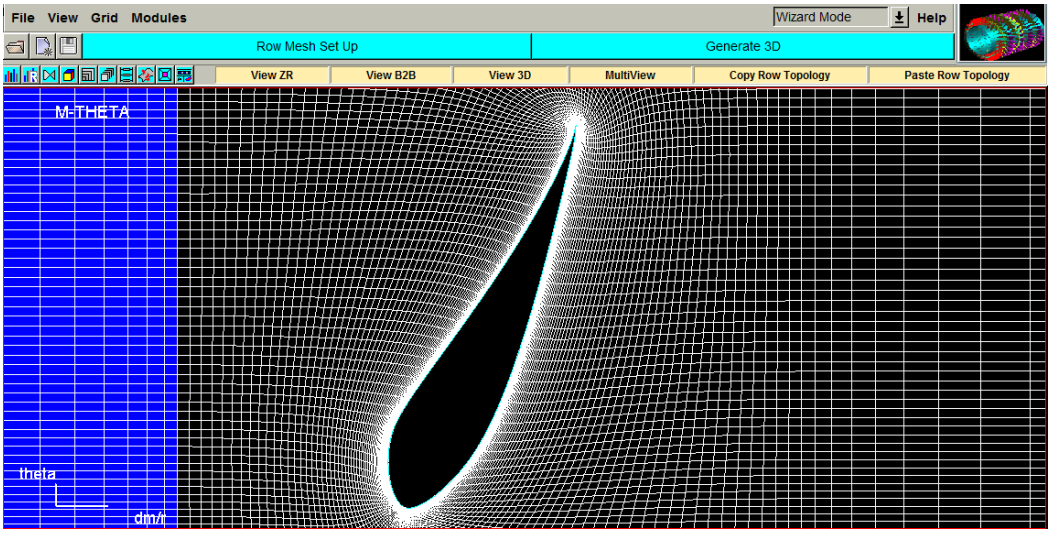

Figure 6.17.Blade to Blade (2D) mesh distribution of 5 kW wind turbine blade, AutoGrid5™

Mesh quality report for 5 kW wind turbine blade discretization is presented in Table 6.9 in which also the number of grids can be observed.

Table 6.9.Grid quality report of 5 kW wind turbine blade

Number of Points	1,772,199
Minimal Skewness Angle (deg)	3.131
Maximal Skewness Angle (deg)	90
Average Skewness Angle (deg)	78.2292
Minimal Spanwise Skewness Angle (deg)	167.249
Maximal Spanwise Skewness Angle (deg)	180
Average Spanwise Skewness Angle (deg)	179.735
Minimal Spanwise Expansion Ratio	1
Maximal Spanwise Expansion Ratio	1.2033
Average Spanwise Expansion Ratio	1.11717
Minimal Aspect Ratio	1
Maximal Aspect Ratio	27673.6
Average Aspect Ratio	519.609
Minimal Expansion Ratio	1
Maximal Expansion Ratio	2.105
Average Expansion Ratio	1.40055

Similar to 1 kW case, while evaluating the grid, studies of Hildebrandt et al. will be taken into consideration as limiting values [36]. According to that, orthogonality and aspect ratio seems to be violated. However, it can be interpreted from Figure 6.18 that, only 0.0059% of the cells have Skewness angle less than 18^{o} and 0.46% have aspect ratios higher than 5000 which is the least important quality criterion. Considering the computational expenses, the discretization was considered to be adequate to converge and give acceptable solutions.

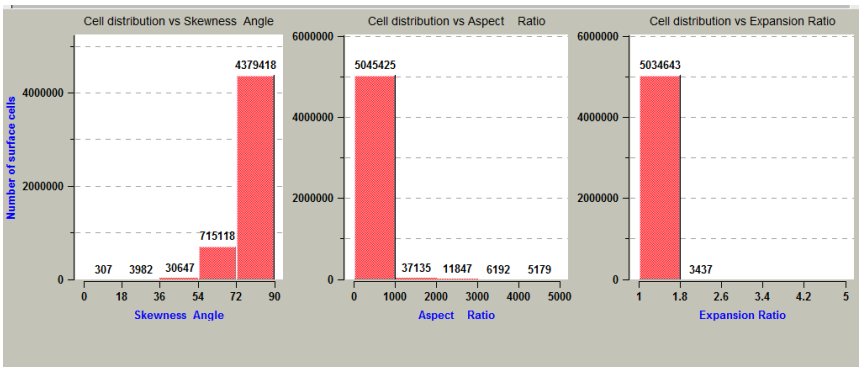

Figure 6.18.Grid quality report of 5 kW wind turbine blade, AutoGrid5™

The solution process in Numeca is performed by FINE™/Turbo module and firstly the fluid flow model needs to be constituted. Similar to the 1 kW case, the fluid is taken as air, flow is considered to be steady, low speed i.e. Mach number < 0.3 and mathematically modeled as turbulent Navier-Stokes with turbulence model of Spalart-

Allmaras. The external boundary conditions of static pressure, static temperature, velocity components along x, y and z directions and turbulent viscosity terms have been inputted as 101300 Pa or 1 atm, 293 K or 20^{o}C, V_x= V_y = 0 where V_z= 7 m/s and ν_t = 7.056x10^{-5} m^2/s, respectively. As initial solution, pressure, temperature and velocity component values have been taken equalto the external boundary conditions. Number of iterations was taken as 20000 and the program was started to run. About 2000 iterations, the convergence criteria were satisfied and the resulting global residual and the behavior of torque output value is shown in Figure 6.19 and 6.20, respectively.

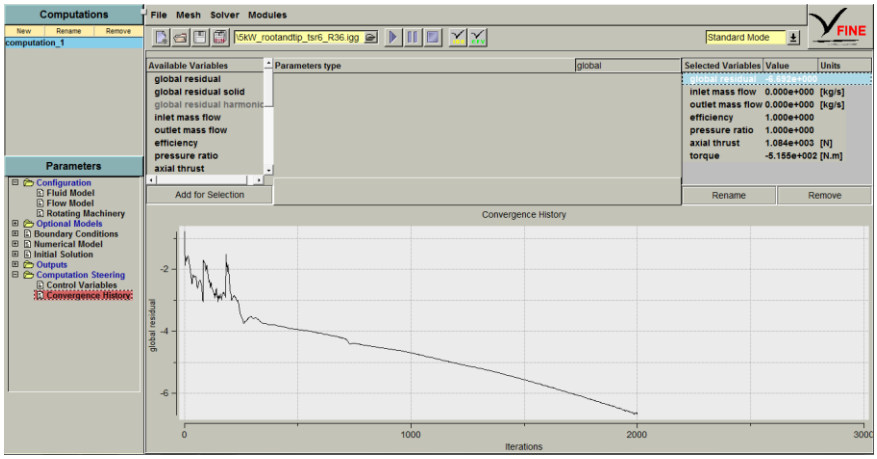

Figure 6.19.Global residual of 5 kW wind turbine rotor, FINE™/Turbo

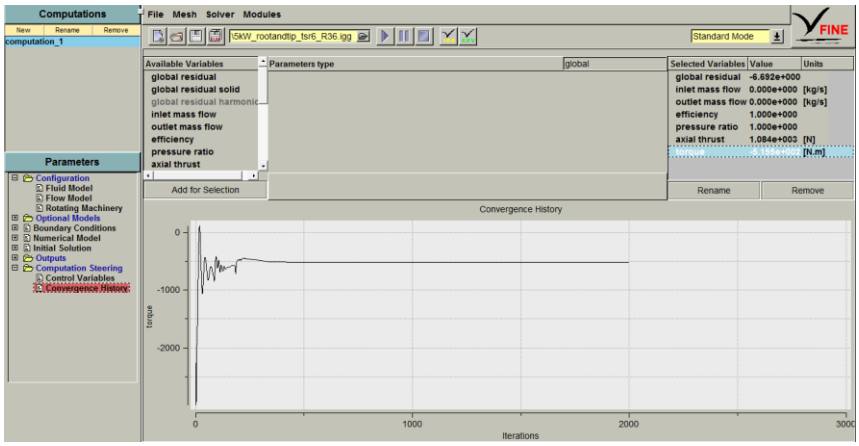

Figure 6.20.Torque output behavior of 5 kW wind turbine rotor, FINE™/Turbo

It can be interpreted from Figure 6.20 that, torque produced by designed 5 kW wind turbine rotor is 515.5 Nm which corresponds to the power production of 4.331 kW using Equation 3.32 and transmission and gear box efficiencies taken to be 0.9 and 0.8 using the similar logic with 1 kW. The coefficient of performance *Cp* is calculated using Equation 3.15 as 0.5072. The values obtained for *Cp* from CFD and modified BEM

codes are in a very good agreement where there is only 0.36 % difference between those values. The velocity triangle obtained for the design around the cross-section taken at half span is presented in Figure 6.9.

The velocity triangle obtained using CFView™ module for the design around the cross-section taken at 0.7 span is presented in Figure 6.21.

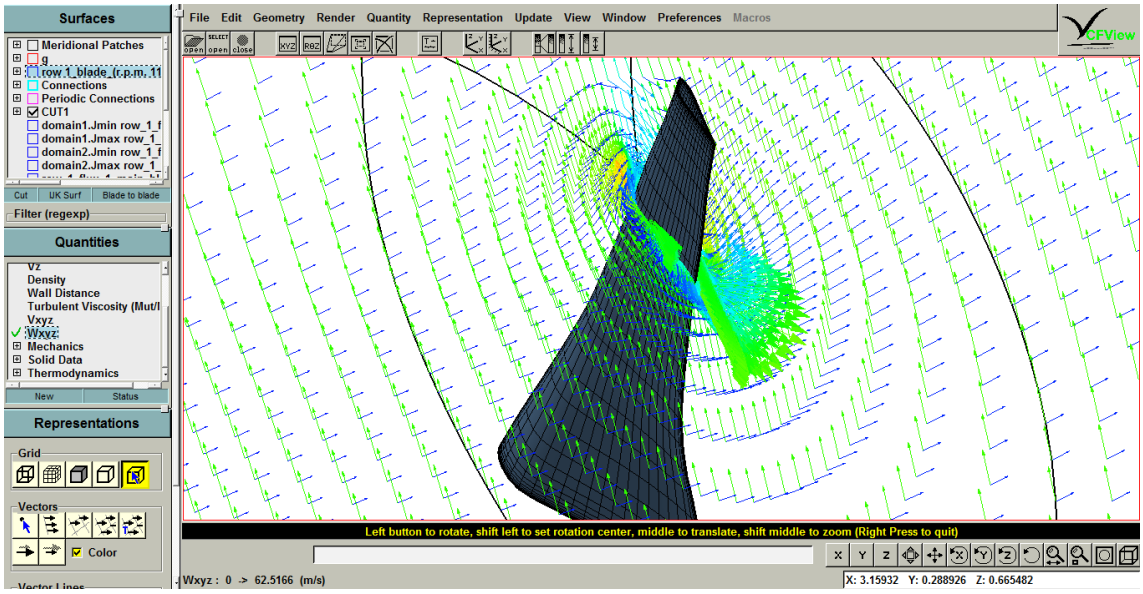

Figure 6.21.Velocity triangle formed around 5 kW wind turbine blade, CFView™

In Figure 6.21, the blue arrows define the incoming velocity striking to the lower side of the blade whereas the green arrows represent the relative velocity formed by the vectoral summation of incoming and angular velocity.

The static pressure distribution along the crass-section taken at 0.7 span is shown in Figure 6.22.

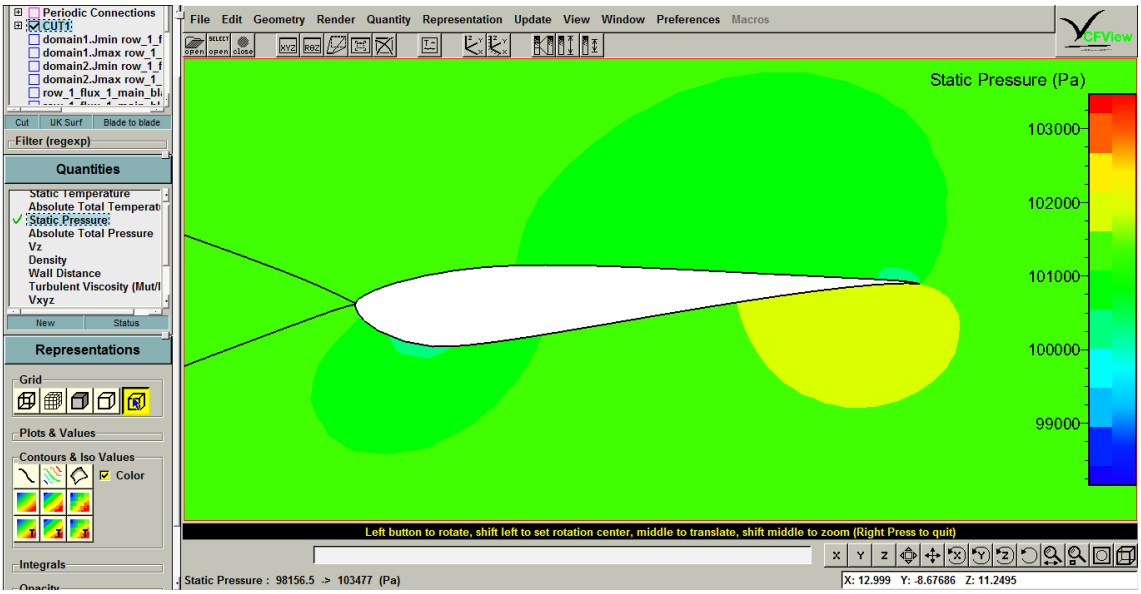

Figure 6.22.Static pressure distribution around 2D cross-section at 0.7 span of 5 kW wind turbine blade, CFView™

It can be seen from Figure 6.19 that, the lower side of the airfoil has higher pressure than the upper side which was expected due to the basic aerodynamic principle of producing lift. Also, the application of pressure boundary condition is clearly viewed since far from the blade the pressure is read to be the atmospheric pressure.

The power curve obtained for pitch controlled 5 kW wind turbine generator is presented in Figure 6.23.

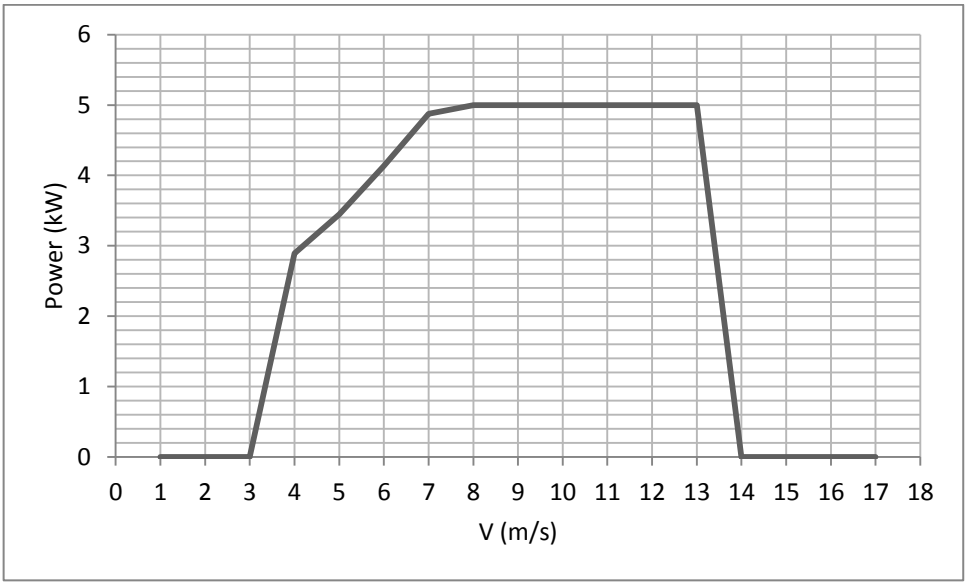

Figure 6.23.Power curve of 5 kW wind turbine

6.3. 10 kW Horizontal Axis Wind Turbine Generator

6.3.1. Airfoil Design

The main aerodynamic and structural principals that have been concerned for the 5 kW design are valid for 10 kW case also. Therefore, similar to the design of 5 kW wind turbine generator, two design locations have been constituted for 10 kW and the same airfoil profiles are used in same regions along the span of the blade.

6.3.2. Blade Design

The design wind speed for 10 kW wind turbine is also chosen using Reference [26] as 7 m/s. Substituting rated power $P = 10\ kW$ and Betz limit into Equation 5.2 and solving for R, the radius of the blade is found to be approximately 5 m. Since the same cross sections are used, tip speed ratio λ was assigned to be 6 according to studies done by Bak et al. [27] and the resulting rotational speed is found to be 8.4 rad/s or 80 rpm. Basic design parameters of 10 kW wind turbine generator are given in Table 6.10.

Table 6.10.Basic design parameters of 10 kW wind turbine

Design Variable	Unit	Value
Number of blades	-	3
Rotor radius	m	5
Root extension	m	0.814
Tip speed ratio	-	6
Rotational speed	rpm	80
Design wind speed	m/s	7
Rated Power	kW	10

The parameters summarized in Table 6.10 are then inserted to the modified BEM code together with the performance parameters of the airfoils. The optimum chord and twist distributions and *Cp* obtained iteratively are listed in Table 6.11.

Table 6.11.Chord and twist distributions and Cp results of 10 kW wind turbine generator using modified BEM code, MATLAB

Section	r/R	chord (m)	twist (deg)	Cp
1	0.0	0.7751	24.4112	0
2	0.1	0.7144	21.7706	0.1204
3	0.2	0.6537	19.1259	0.1491
4	0.3	0.5061	12.8121	0.2432
5	0.4	0.4205	8.7164	0.3263
6	0.5	0.3924	5.9779	0.4087
7	0.6	0.3653	4.0471	0.4859
8	0.7	0.3154	2.6189	0.5581
9	0.8	0.2738	1.5157	0.6117
10	0.9	0.2288	0.6337	0.5891
11	1.0	0.1986	0.0000	0.3116

Since the same tip speed ratio was used, the twist values of 10 kW wind turbine are identical with the previous designs. Using Equation 6.1, Cp according to modified BEM code becomes $Cp = 0.5072$ which will be compared with the power output data obtained from CFD analysis.

6.3.3. Blade Analysis

The geometry created for the blade using AutoBlade™ module of Numeca is then transferred to the Design Modeler segment of ANSYS Fluent to provide different geometrical point of view and it is shown in Figure 6.24.

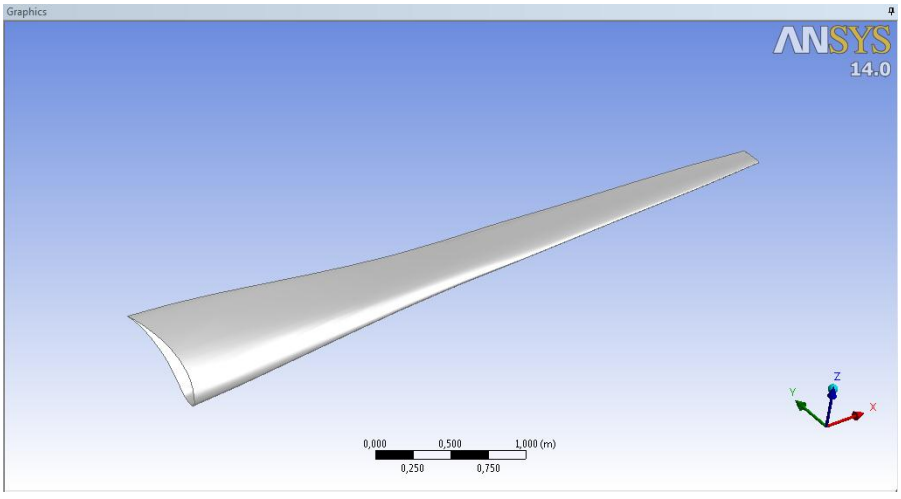

Figure 6.24.Geometry of 10 kW wind turbine blade, ANSYS Design Modeler

Meshing process of that geometry is again performed in AutoGrid5™ module of Numeca. The settings used for that semi-automatic process are; rotational speed is 80 rpm, far-field domains are taken to be 5 times of the blade length both in upstream and downstream, spanwise expansion ratio was adjusted to be 1.25 along the layers and 1.27 for the controls of the far-field. The discretization around the cross section of the blade may be observed in Figure 6.25.

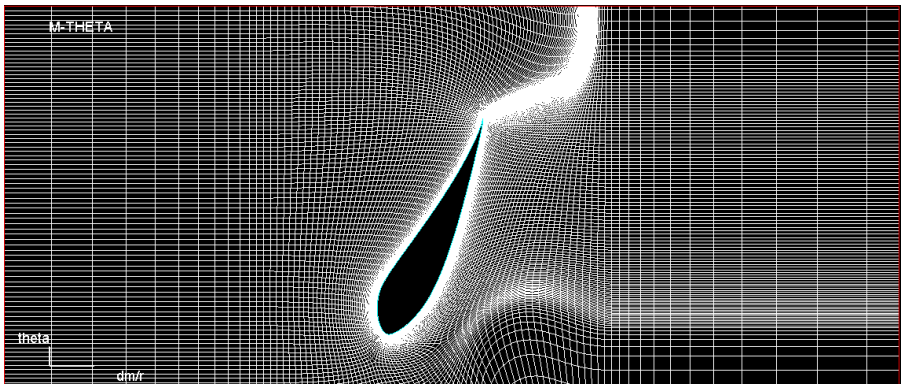

Figure 6.25.Blade to Blade (2D) mesh distribution of 10 kW wind turbine blade, AutoGrid5™

The quality of the mesh distribution for 10 kW wind turbine blade is presented in Table 6.12.

Table 6.12.Grid quality report of 10 kW wind turbine blade

Number of Points	1,509,651
Minimal Skewness Angle (deg)	3.033
Maximal Skewness Angle (deg)	90
Average Skewness Angle (deg)	78.2011
Minimal Spanwise Skewness Angle (deg)	168.915
Maximal Spanwise Skewness Angle (deg)	180
Average Spanwise Skewness Angle (deg)	179.666
Minimal Spanwise Expansion Ratio	1
Maximal Spanwise Expansion Ratio	1.27233
Average Spanwise Expansion Ratio	1.15715
Minimal Aspect Ratio	1
Maximal Aspect Ratio	51341.9
Average Aspect Ratio	523.283
Minimal Expansion Ratio	1
Maximal Expansion Ratio	2.241
Average Expansion Ratio	1.40074

The limiting values have been decided according to the studies of Hildebrandt et al. [36] and orthogonality and aspect ratio seems to be violated. However, it can be interpreted from Figure 6.26 that, only 0.0072% of the cells have Skewness angle less than 18^{o} and 0.63% have aspect ratios higher than 5000 which is the least important quality criterion. Therefore, the discretization was found to be sufficient and no more computation was seen to be required.

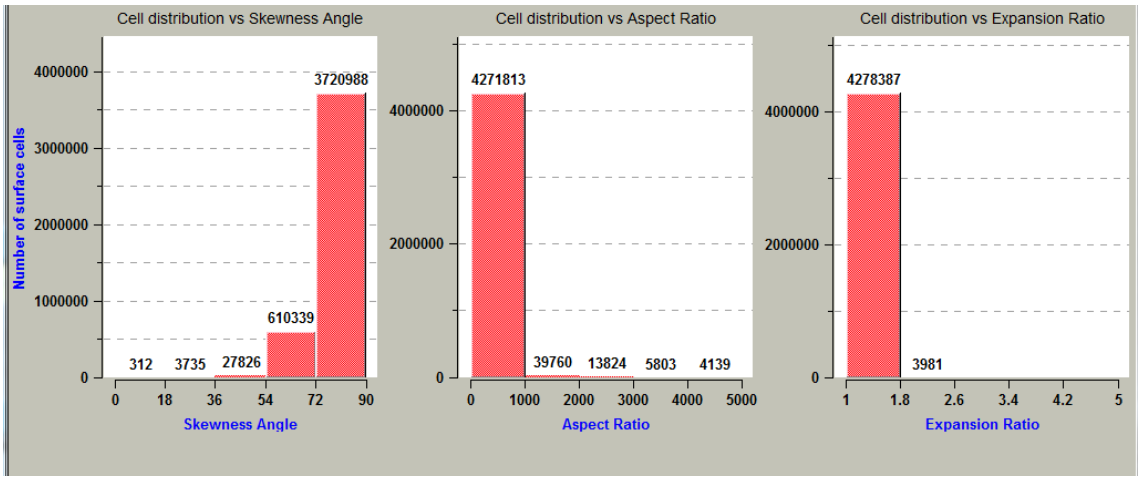

Figure 6.26.Grid quality report of 10 kW wind turbine blade, AutoGrid5™

The solution process performed by FINE™/Turbo starts with the constitution of the fluid flow model and it is taken as air. Also, the flow is considered to be steady, low speed i.e. Mach number < 0.3 and mathematically modeled as turbulent Navier-Stokes with turbulence model of Spalart-Allmaras. The external boundary conditions of static pressure, static temperature, velocity components along x, y and z directions and turbulent viscosity terms have been inputted as 101300 Pa or 1 atm, 293 K or 20^{o}C, V_x= V_y = 0 where V_z= 7 m/s and ν_t = $7.056x10^{-5}$ m^2/s, respectively. As initial solution, pressure, temperature and velocity component values have been taken equal to the external boundary conditions. Number of iterations was taken as 20000 and the program was started to run. After approximately 3000 iterations, the convergence criteria were satisfied and the resulting global residual and the behavior of torque output value is shown in Figure 6.27 and 6.28, respectively.

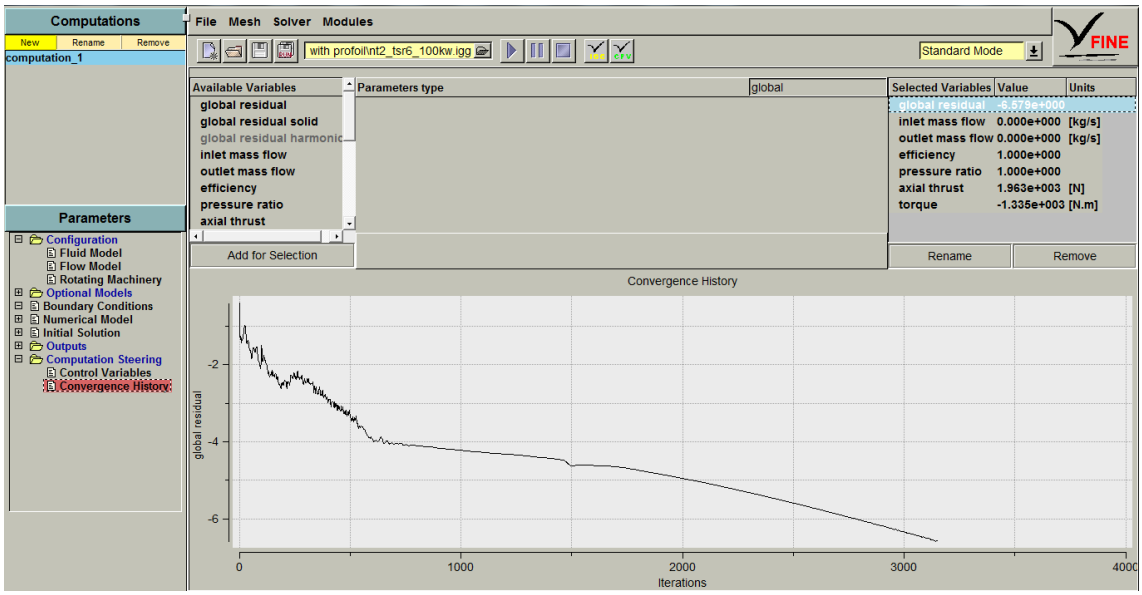

Figure 6.27.Global residual of 10 kW wind turbine rotor, FINE™/Turbo

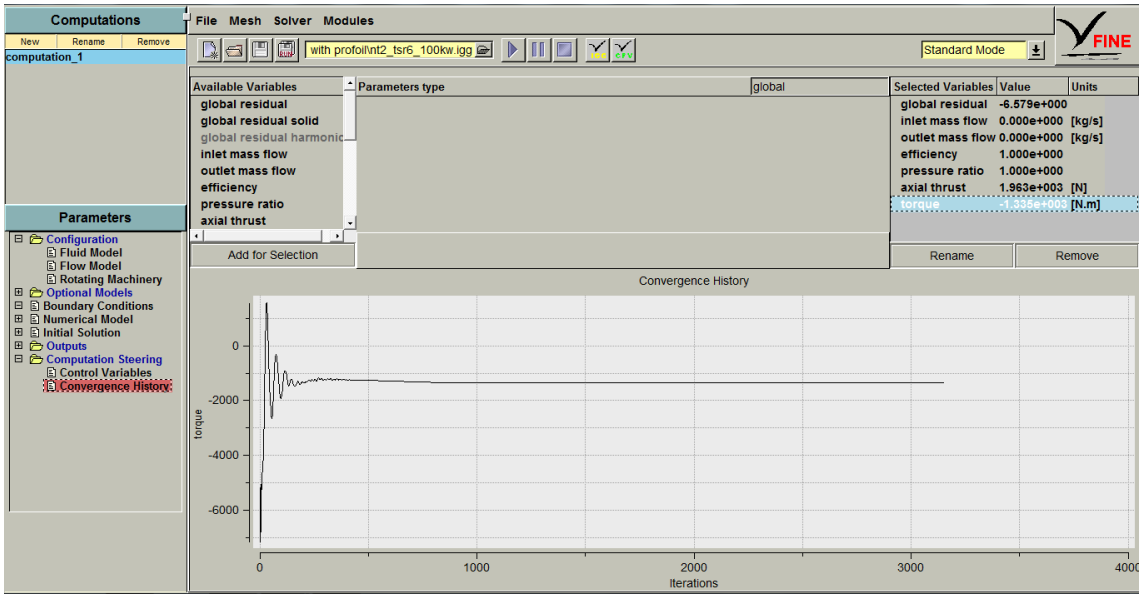

Figure 6.28.Torque output behavior of 10 kW wind turbine rotor, FINE™/Turbo

It can be seen from Figure 6.28 that, torque produced by designed 10 kW wind turbine rotor is 1.335 kNm which corresponds to the power production of 8.074 kW using Equation 3.32 and transmission and gear box efficiencies taken to be 0.9 and 0.8 using the similar logic with the previous designs. The coefficient of performance *Cp* is calculated using Equation 3.15 as 0.4903. The values obtained for *Cp* from CFD and

modified BEM codes are in an acceptable agreement where there is only 3.44 % difference between those values.

The power curve of the designed 10 kW wind turbine rotor which is taken to be pitch-controlled can be seen from Figure 6.29.

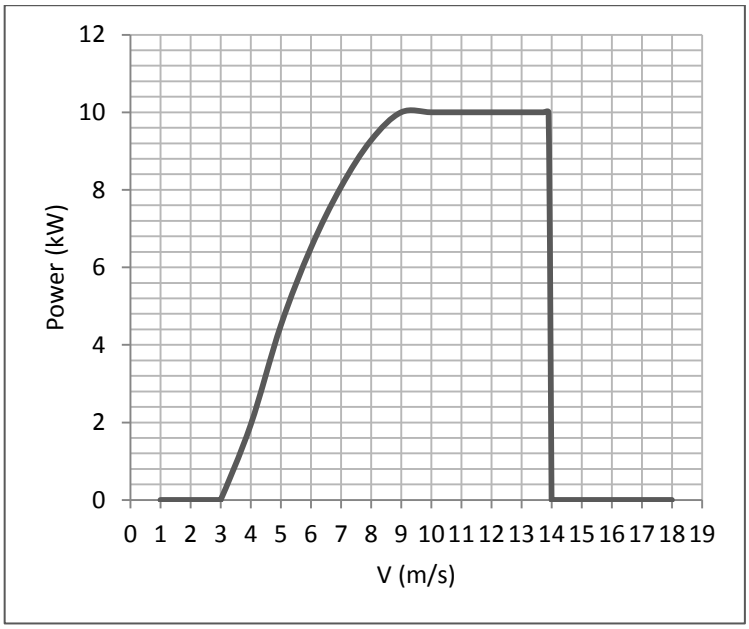

Figure 6.29.Power curve of 10 kW wind turbine

6.4. 25 kW Horizontal Axis Wind Turbine Generator

6.4.1. Airfoil Design

Since 1, 5, 10 and 25 kW wind turbine generators may be considered as the same class under small scale wind turbines, the airfoil sections and the locations of the spanwise design control points were taken to be the same. Thus, also for the blade of 25 kW wind turbine generator; the designed and modified airfoils named tfprofoil_nt2 and tfprofoil_nt2tip will be used.

6.4.2. Blade Design

Similar to the previous designs, the design wind speed for 25 kW wind turbine is chosen using Reference [26] as 7 m/s. Substituting rated power $P = 25\ kW$ and Betz

limit into Equation 5.2 and solving for *R*, the radius of the blade is found to be approximately 8 m. According to studies done by Bak et al. [27], the selection of the tip speed ratio λ is directly related with the airfoils used in the design. Therefore, similar to the previous ones, λ was assigned to be 6 and the resulting rotational speed is then becomes 5.25 rad/s or 50 rpm according to the mathematical definition of tip speed ratio. Basic design parameters of 25 kW wind turbine generator are given in Table 6.13.

Table 6.13.Basic design parameters of 25 kW wind turbine

Design Variable	Unit	Value
Number of blades	-	3
Rotor radius	m	8
Root extension	m	1.30
Tip speed ratio	-	6
Rotational speed	rpm	50
Design wind speed	m/s	7
Rated Power	kW	25

The output parameters of the modified BEM code, namely optimum chord and twist distributions and *Cp* obtained iteratively using the parameters summarized in Table 6.13 and the performance parameters of the airfoils, is listed in Table 6.14.

Table 6.14.Chord and twist distributions and Cp results of 25 kW wind turbine generator using modified BEM code, MATLAB

Section	r/R	chord (m)	twist (deg)	Cp
1	0.0	1.2700	24.4112	0
2	0.1	1.1696	21.7706	0.1195
3	0.2	1.0691	19.1259	0.1483
4	0.3	0.8277	12.8121	0.2384
5	0.4	0.7956	8.7164	0.3232
6	0.5	0.6599	5.9779	0.4075
7	0.6	0.5845	4.0471	0.4859
8	0.7	0.5046	2.6189	0.5581
9	0.8	0.4381	1.5157	0.6117
10	0.9	0.3661	0.6337	0.5891
11	1.0	0.3012	0.0000	0.3116

Using Equation 6.1, Cp according to modified BEM code becomes Cp = 0.5058 which is to be compared with the power output data obtained from CFD analysis.

6.4.3. Blade Analysis

Similar to the 10 kW wind turbine blade analysis case, the geometry created for the blade using AutoBlade™ module of Numeca and it is shown in Figure 6.30.

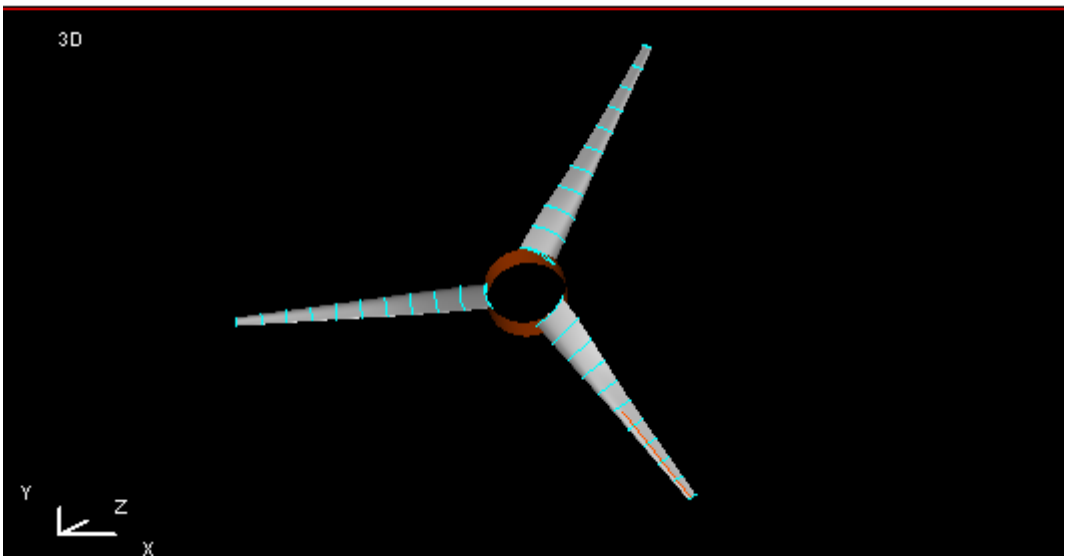

Figure 6.30.Geometry of 25 kW wind turbine blade, AutoBlade™

During the discretization performed in AutoGrid5^{TM} module of Numeca the settings were arranged as; rotational speed is 80 rpm, far-field domains are taken to be 5 times of the blade length both in upstream and downstream, spanwise expansion ratio was adjusted to be 1.26 along the layers and 1.30 for the controls of the far-field.

The grid quality measurements are done based on the studies of Hildebrandt et al. [36] and orthogonality and aspect ratio were found to be violated. However, it can be interpreted from Figure 6.31 that, only 0.0042% of the cells have Skewness angle less than 18^{o} and 2.53% have aspect ratios higher than 5000 which is the least important quality criterion. Therefore, the discretization was found to be adequate to proceed to the blade analysis of 25 kW wind turbine generator.

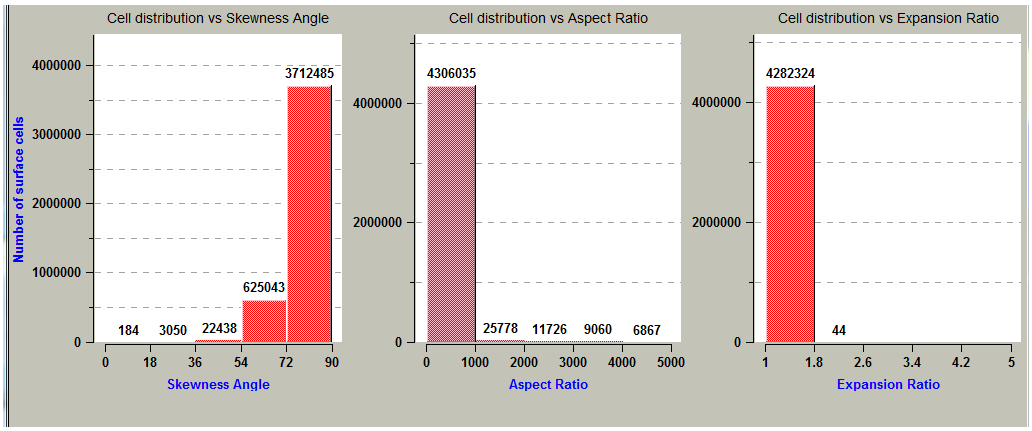

Figure 6.31.Grid quality report of 25 kW wind turbine blade, AutoGrid5^{TM}

The solution process performed by FINE™/Turbo starts with the constitution of the fluid flow model and it is taken as air. Also, the flow is considered to be steady, low speed i.e. Mach number < 0.3 and mathematically modeled as turbulent Navier-Stokes with turbulence model of Spalart-Allmaras. The external boundary conditions of static pressure, static temperature, velocity components along x, y and z directions and turbulent viscosity terms have been inputted as 101300 Pa or 1 atm, 293 K or 20^{o}C, V_x= V_y = 0 where V_z= 7 m/s and ν_t = 7.056x10^{-5} m^2/s, respectively. As initial solution, pressure, temperature and velocity component values have been taken equal to the external boundary conditions. Number of iterations was taken as 20000 and the program was started to run. After approximately 3000 iterations, the convergence criteria were satisfied and the resulting global residual and the behavior of torque output value is shown in Figure 6.32 and 6.33, respectively.

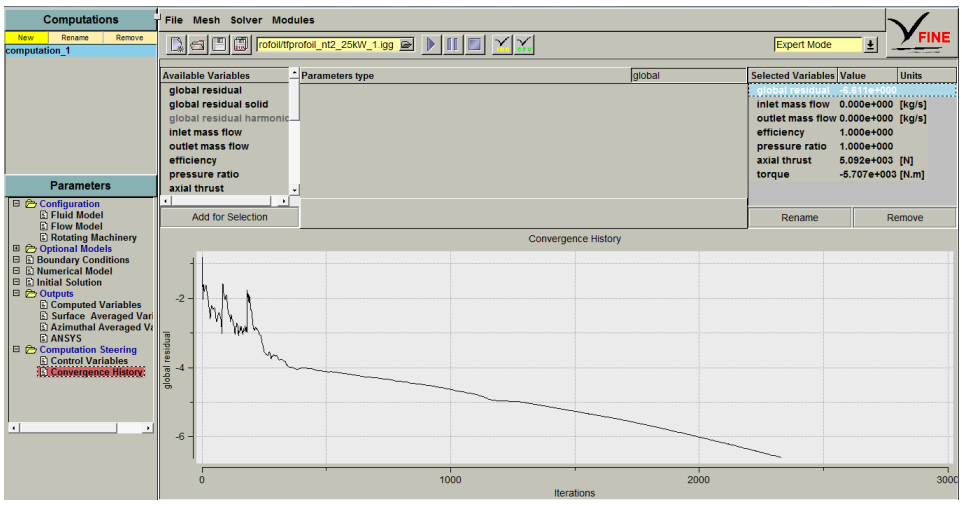

Figure 6.32.Global residual of 25 kW wind turbine rotor, FINE™/Turbo

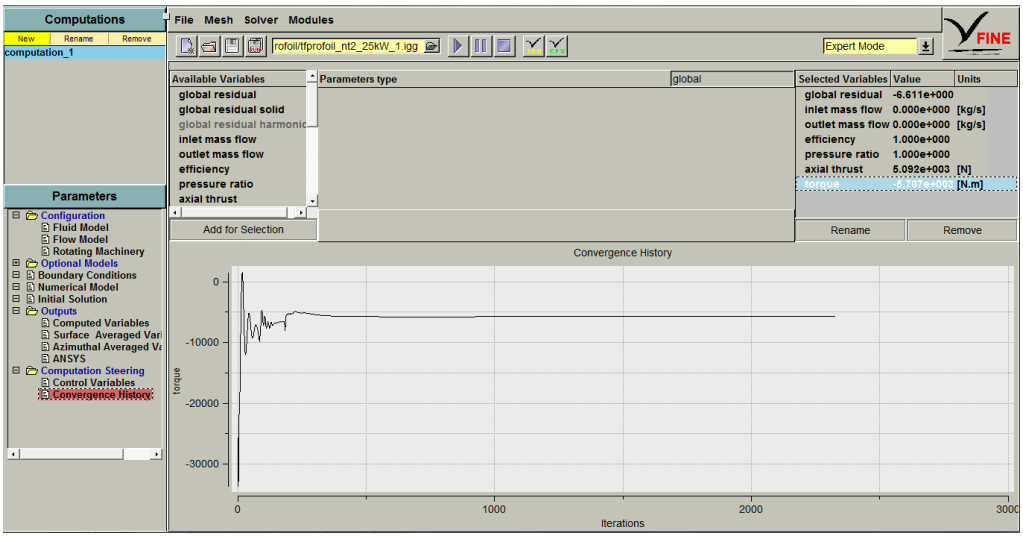

Figure 6.33.Torque output behavior of 25 kW wind turbine rotor, FINE™/Turbo

From Figure 6.33 the value of torque produced by designed 25 kW wind turbine rotor can be read as 5.707×10^3 Nm which corresponds to the power production of 21.572 kW using Equation 3.32 and transmission and gear box efficiencies taken to be 0.9 and 0.8 using the similar logic with the previous designs. The coefficient of performance *Cp* is calculated using Equation 3.15 as 0.5115. The values obtained for *Cp* from CFD and modified BEM codes are in a good agreement where there is only 1.11 % difference between those values.

The power curve of the designed 25 kW wind turbine rotor which is taken to be pitch-controlled can be seen from Figure 6.34.

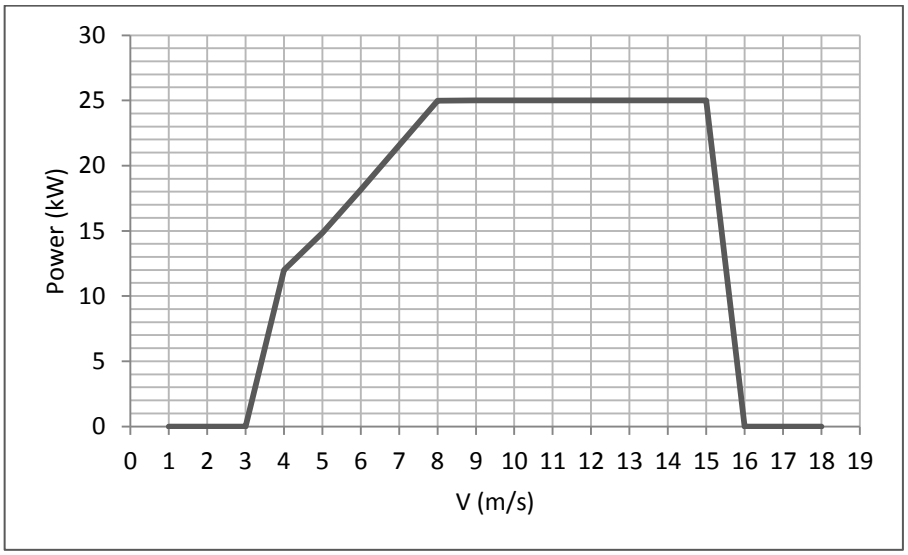

Figure 6.34.Power curve of 25 kW wind turbine generator

6.5. 50 kW Horizontal Axis Wind Turbine Generator

6.5.1. Airfoil Design

In design of 50 kW wind turbine generator, three design locations have been constructed such that from hub to 0.33 span, from 0.33 span to 0.66 span and from 0.66 span to tip. Consequently, three airfoil profiles have been used in these regions to overcome different considerations. For the first part, i.e. near hub region, the structural requirements for 50 kW wind turbine generator are more severe than those for the small wind turbines designed previously. For the second region, the combination of structural and aerodynamic concerns was taken into account. For the tip area, due to the fact that the structural constraints lessened, pure aerodynamically efficient geometries are to be used. Since tfprofoil_nt2 airfoil family was found to be efficient at their operating Reynolds number, they were decided to be used at region two and three. However, for the root section of the blade, importance of aerodynamic efficiencies has been subordinated and tfprofoil_nt2 has been thickened to compensate greater structural loads and it is named as "tfprofoil_nt2_root". The maximum thickness to chord ratio of tfprofoil_nt2_root is 24% at 20.8% of the chord and it maximum camber is 2.85% at 62.6% of the chord. The comparison between three profiles to be used in 50 kW wind turbine may be examined in Figure 6.35.

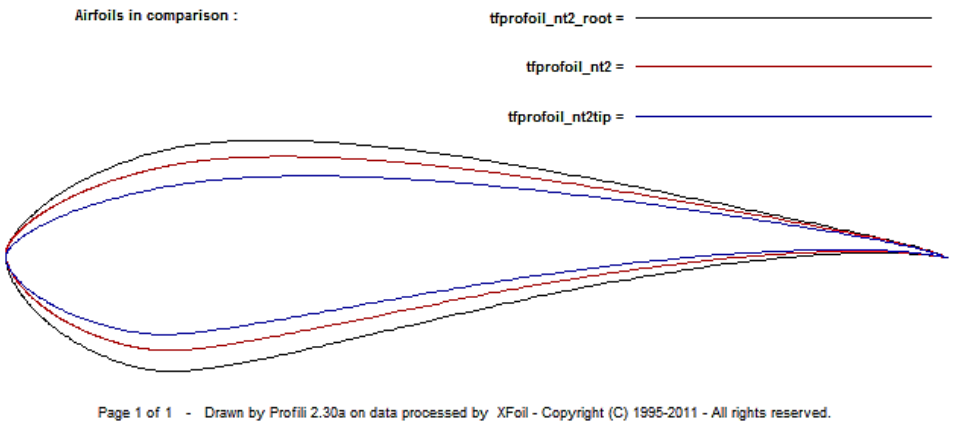

Figure 6.35.Geometrical comparison of tfprofoil_nt2_root, tfprofoil_nt2 and tfprofoil_nt2_tip, PROFILI

Newly generated airfoil has been analyzed at *Re = 400000* using XFOIL and its resulting performance parameters are presented in Table 6.15.

Table 6.15.Performance parameters of tfprofoil_nt2_root, XFOIL

$(c_L/c_D)_{max}$	64.9953
c_L	1.3779
c_D	0.0212
c_M	-0.1084
α (deg)	10

6.5.2. Blade Design

The design wind speed for 50 kW wind turbine design is chosen using Reference [26] as 7 m/s. Substituting rated power *P =50 kW* and Betz limit into Equation 5.2 and solving for *R*, the radius of the blade is found to be approximately 11.3 m. According to studies done by Bak et al. [27], λ was assigned to be 8 thus the resulting rotational speed becomes 4.96 rad/s or 47 rpm according to the mathematical definition of tip speed ratio. Basic design parameters of 50 kW wind turbine generator are given in Table 6.16.

Table 6.16.Basic design parameters of 50 kW wind turbine

Design Variable	Unit	Value
Number of blades	-	3
Rotor radius	m	11.3
Root extension	m	1.84
Tip speed ratio	-	8
Rotational speed	rpm	47
Design wind speed	m/s	7
Rated Power	kW	50

In Table 6.17, the optimum chord and twist distributions and *Cp* obtained iteratively using modified BEM code are presented.

Table 6.17.Chord and twist distributions and Cp results of 50 kW wind turbine generator using modified BEM code, MATLAB

Section #	r/R	chord (m)	twist (deg)	Cp
1	0	1.2052	23.6309	0
2	0.1	1.0977	19.8250	0.1506
3	0.2	0.9902	16.0202	0.2086
4	0.3	0.7270	10.2085	0.3222
5	0.4	0.5662	6.7930	0.4286
6	0.5	0.4613	4.6056	0.5293
7	0.6	0.3707	3.0992	0.6459
8	0.7	0.3194	2.0019	0.7427
9	0.8	0.2787	1.1644	0.8253
10	0.9	0.2376	0.4964	0.8307
11	1.0	0.1986	0	0.6513

Using tabulated values of Cp in Table 6.17 together with Equation 6.1, Cp according to modified BEM code becomes $\mathrm{Cp} = 0.5335$ which is to be compared with the power output data obtained from CFD analysis.

6.5.3. Blade Analysis

The geometry of the blade for 50 kW wind turbine blade is created in AutoBlade™ module of Numeca and then exported to AutoGrid5^{TM} to start the discretization process. The settings of that semi-automatic process were assigned as; rotational speed is 47 rpm, far-field domains are taken to be 5 times of the blade length both in upstream and downstream, spanwise expansion ratio was adjusted to be 1.30 along the layers and 1.31 for the controls of the far-field.

The grid quality is evaluated according to the studies of Hildebrandt et al. [36] and the orthogonality and aspect ratio were found to be violated. However, it can be interpreted from Figure 6.36 that, only 0.0185% of the cells have Skewness angle less than 18^{o} and 0.955% have aspect ratios higher than 5000 which is the least important quality criterion. As a result, no further computations were found to be required and the discretization was found to be adequate to proceed to the blade analysis of 50 kW wind turbine generator.

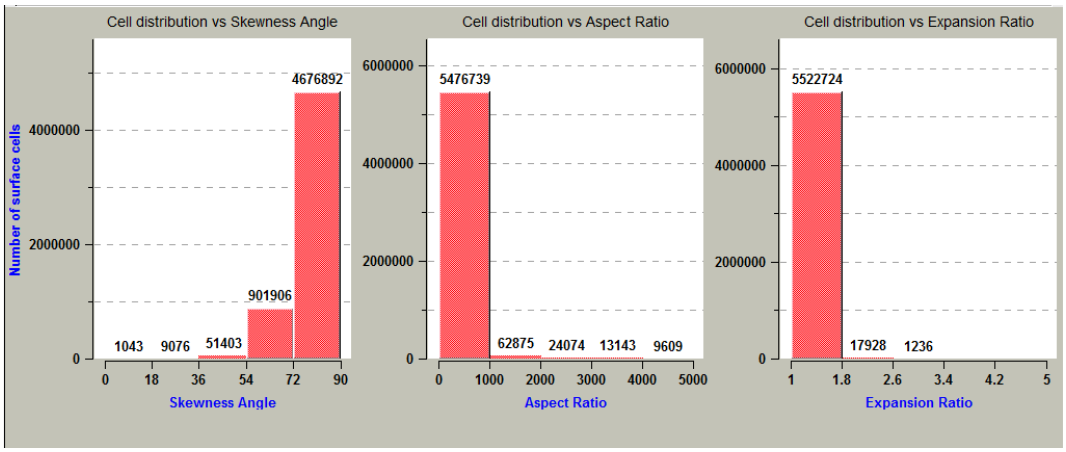

Figure 6.36.Grid quality report of 50 kW wind turbine blade, AutoGrid5™

The performance of the blade was analyzed using FINE™/Turbo where firstly the fluid flow model and is taken as air. Also, the flow is considered to be steady, low speed i.e. Mach number < 0.3 and mathematically modeled as turbulent Navier-Stokes with turbulence model of Spalart-Allmaras. The external boundary conditions of static pressure, static temperature, velocity components along x, y and z directions and turbulent viscosity terms have been inputted as 101300 Pa or 1 atm, 293 K or 20^{o}C, V_x= V_y = 0 where V_z= 7 m/s and ν_t = 7.056x10^{-5} m^2/s, respectively. As initial solution, pressure, temperature and velocity component values have been taken equal to the external boundary conditions. Number of iterations was taken as 20000 and the program was started to run. After approximately 3000 iterations, the convergence criteria were satisfied and the resulting global residual and the behavior of torque output value is shown in Figure 6.37 and 6.38, respectively.

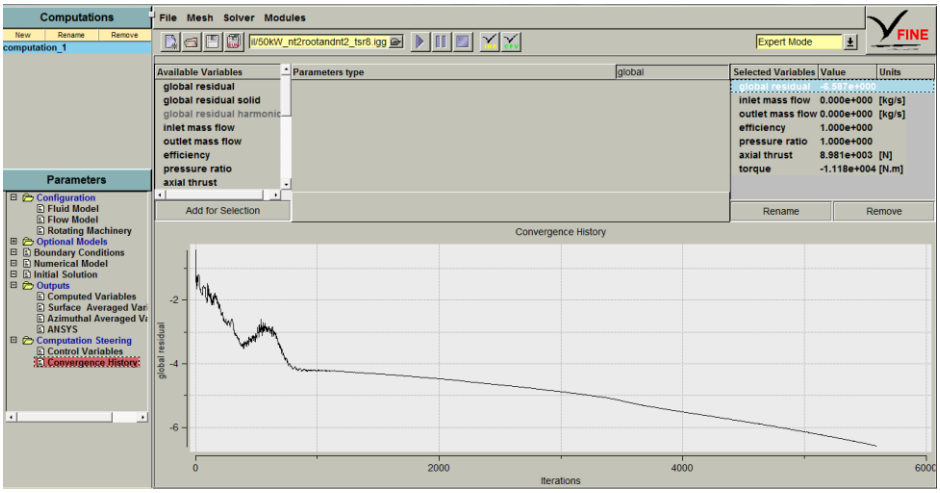

Figure 6.37.Global residual of 50 kW wind turbine rotor, FINE™/Turbo

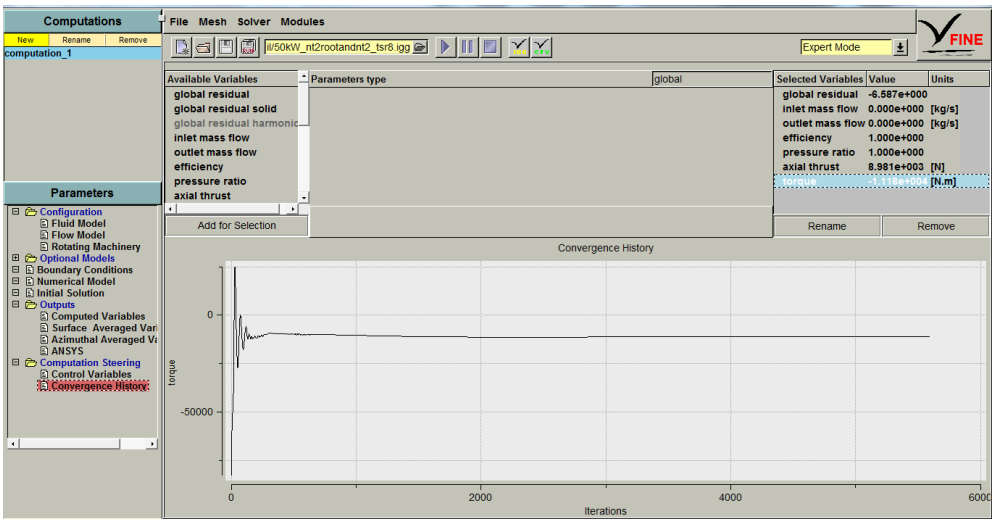

Figure 6.38.Torque output behavior of 50 kW wind turbine rotor, FINE™/Turbo

From Figure 6.38 the value of torque produced by designed 50 kW wind turbine rotor can be read as 11.18×10^3 Nm which corresponds to the power production of 44.9 kW using Equation 3.32 and transmission and gear box efficiencies taken to be 0.9 each. The coefficient of performance *Cp* is calculated using Equation 3.15 as 0.5338. The values obtained for *Cp* from CFD and modified BEM codes are in a very good agreement where there is only 0.056 % difference between those values.

The power curve of the designed 50 kW wind turbine rotor which is taken to be pitch-controlled can be seen from Figure 6.39.

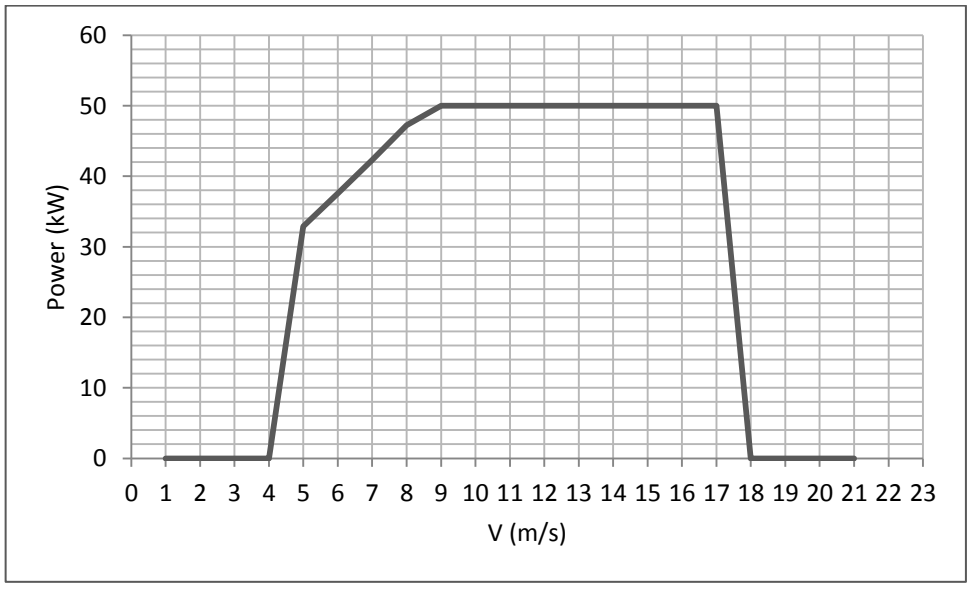

Figure 6.39.Power curve of 50 kW wind turbine generator

6.6. 100 kW Horizontal Axis Wind Turbine Generator

6.6.1. Airfoil Design

Since the structural and aerodynamic requirements of 100 kW wind turbine generator is similar to the 50 kW case, the airfoil profiles used at the corresponding locations were taken to be identical.

6.6.2. Blade Design

The design wind speed for 100 kW wind turbine generator is chosen to be higher than the previous designs since corresponding hub height is basically greater. With the help of Reference [26] it is taken to be 8 m/s. Substituting rated power $P = 100\ kW$ and Betz limit into Equation 5.2 and solving for R yields $R = 13.1\ m$. According to the research of Bak et al. [27], tip speed ratio λ was assigned to be 8 and the resulting rotational speed is found as 4.274 rad/s or 45 rpm. Basic design parameters of 100 kW wind turbine generator are given in Table 6.18.

Table 6.18.Basic design parameters of 100 kW wind turbine

Design Variable	Unit	Value
Number of blades	-	3
Rotor radius	m	13.1
Root extension	m	2.14
Tip speed ratio	-	8
Rotational speed	rpm	45
Design wind speed	m/s	8
Rated Power	kW	100

These parameters defined in Table 6.18 is then read by the modified BEM code created in MATLAB with the performance parameters of the designed airfoils for appropriate sections. The optimum chord and twist distributions and *Cp* attained iteratively are listed in Table 6.19.

Table 6.19.Chord and twist distributions and Cp results of 100 kW wind turbine generator using modified BEM code, MATLAB

Section #	r/R	chord (m)	twist (deg)	Cp
1	0	1.3748	23.6309	0
2	0.1	1.2613	19.8250	0.1506
3	0.2	1.1479	16.0202	0.2086
4	0.3	0.8428	10.2085	0.3222
5	0.4	0.6564	6.7930	0.4286
6	0.5	0.5347	4.6056	0.5293
7	0.6	0.4236	3.0992	0.6411
8	0.7	0.3650	2.0019	0.7362
9	0.8	0.3185	1.1644	0.8168
10	0.9	0.2715	0.4964	0.8205
11	1.0	0.2402	0	0.6513

Using Equation 6.1 and Table 6.19, Cp according to modified BEM code becomes $Cp = 0.5205$ which will be compared with the power output data obtained from CFD analysis.

6.6.3. Blade Analysis

In order to analyze the blade, the geometry is constructed using AutoBlade™ module of commercial CFD code, Numeca. The 3D modeled geometry of 100 kW wind turbine blade may be observed in Figures 6.40 and 6.41.

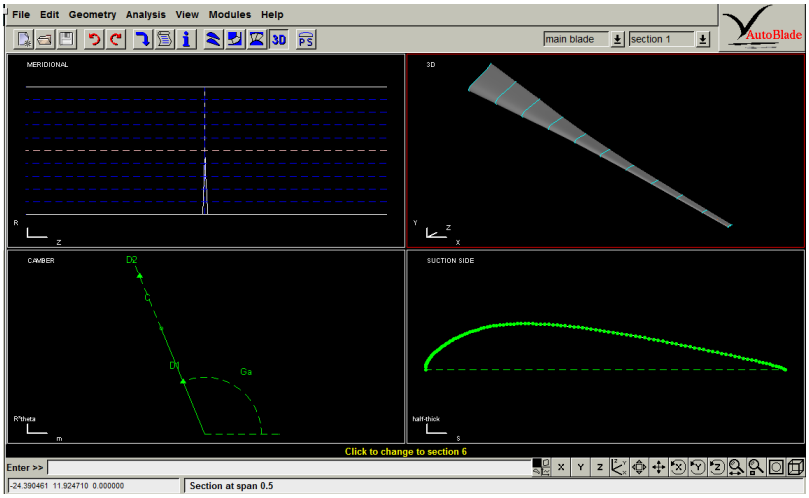

Figure 6.40.Geometry of 100 kW wind turbine blade, AutoBlade™

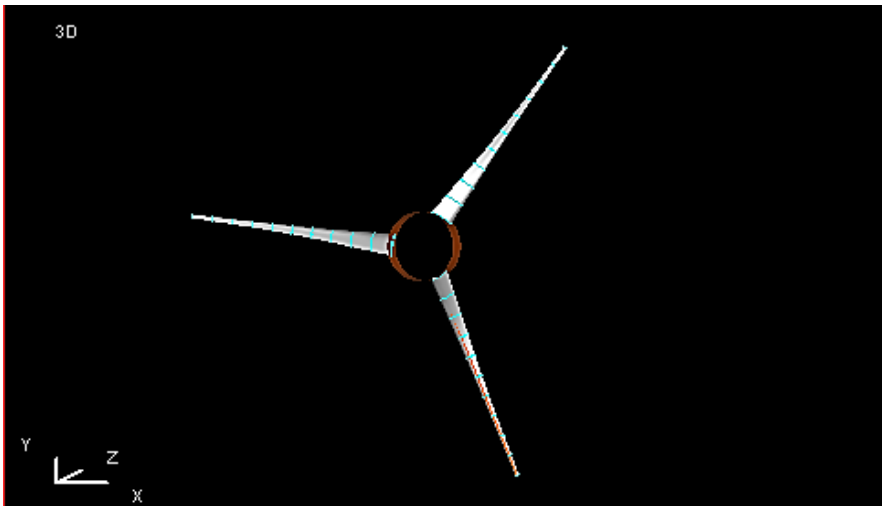

Figure 6.41.Geometry of 100 kW wind turbine rotor, AutoBlade™

In Figure 6.41, the length of the blade can be concluded by comparing the chord lengths belong to root and tip section whose ratio is called the aspect ratio of the blade. The twist distribution is also clearly visible.

The discretization of that geometry is performed using AutoGrid5™module of Numeca and mesh input parameters were inputted as the following; rotational speed, 40 rpm; far-field domain that is desired to be meshed, 4 times of the length of the blade, both upstream and downstream; spanwise expansion ratio, for layers 1.247; for far field, 1.316. 3D and blade to blade mesh distribution around 100 kW turbine blade may be seen in Figures 6.42 and 6.43, respectively.

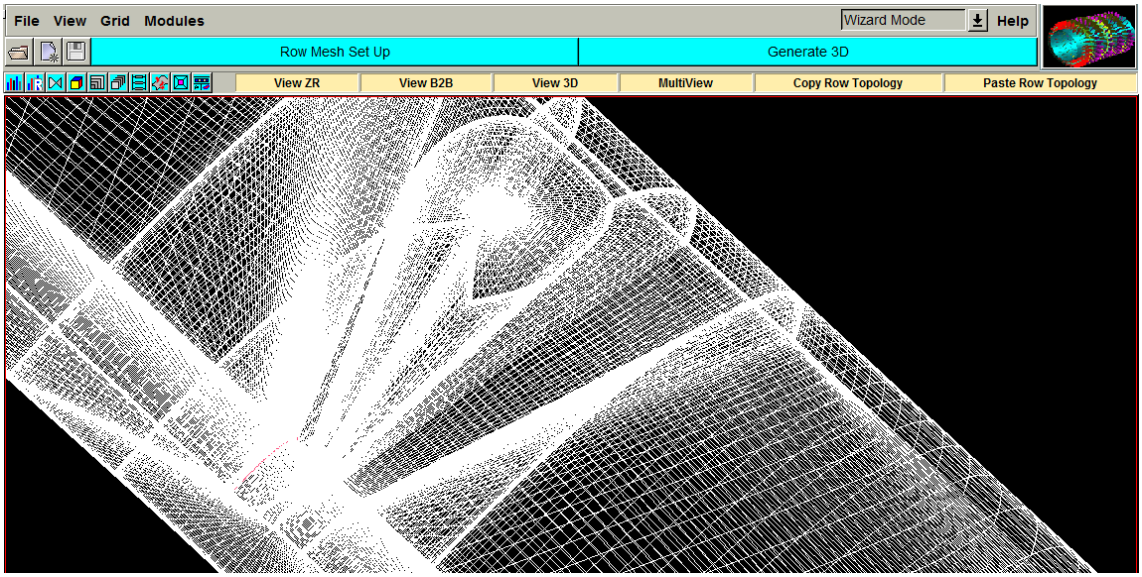

Figure 6.42.3D mesh distribution of 100 kW wind turbine blade, AutoGrid5™

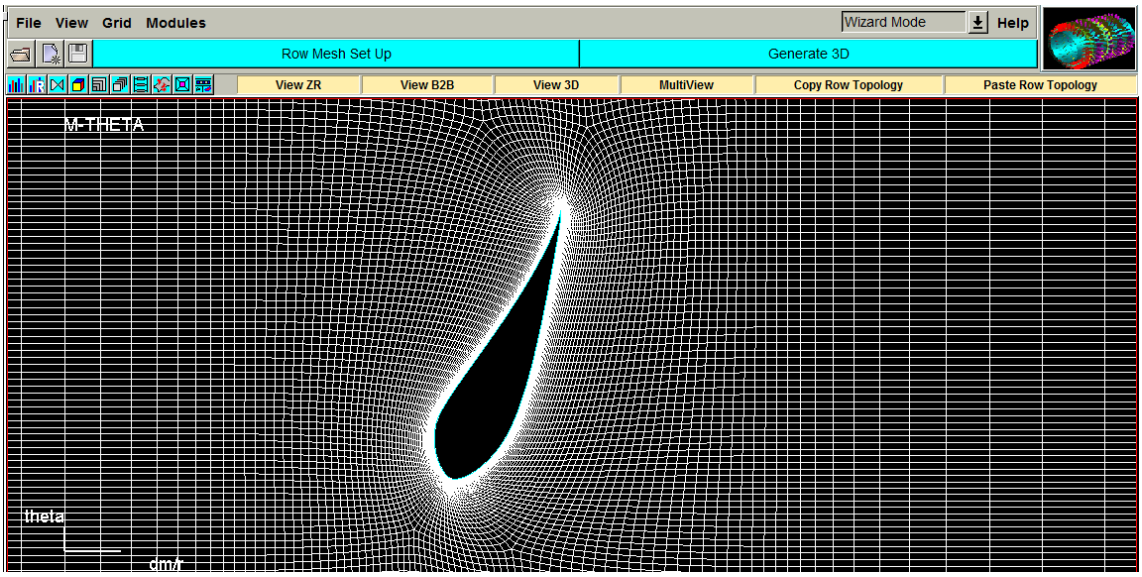

Figure 6.43.Blade to Blade (2D) mesh distribution of 100 kW wind turbine blade, AutoGrid5TM

Mesh quality report for 100 kW wind turbine blade discretization is reported in Table 6.20 from which the number of grids can be observed also.

Table 6.20.Grid quality report of 100 kW wind turbine blade

Number of Points	1,859,715
Minimal Skewness Angle (deg)	3.146
Maximal Skewness Angle (deg)	90
Average Skewness Angle (deg)	78.1435
Minimal Spanwise Skewness Angle (deg)	166.491
Maximal Spanwise Skewness Angle (deg)	180
Average Spanwise Skewness Angle (deg)	179.737
Minimal Spanwise Expansion Ratio	1
Maximal Spanwise Expansion Ratio	1.26839
Average Spanwise Expansion Ratio	1.15274
Minimal Aspect Ratio	1
Maximal Aspect Ratio	106914
Average Aspect Ratio	530.455
Minimal Expansion Ratio	1
Maximal Expansion Ratio	2.687
Average Expansion Ratio	1.40162

Similar to previous studies, while evaluating the grid, studies of Hildebrandt et al. will be taken as limiting values [36]. According to those studies, orthogonality and aspect ratio seems to be excessing the limits. However, it can be interpreted from Figure

6.44 that, only 0.0125% of the cells have Skewness angle less than 18^{o} and 0.87% have aspect ratios higher than 5000 which is the least important quality criterion. In order to avoid high computational costs, the discretization was considered to be sufficient to converge and give acceptable solutions.

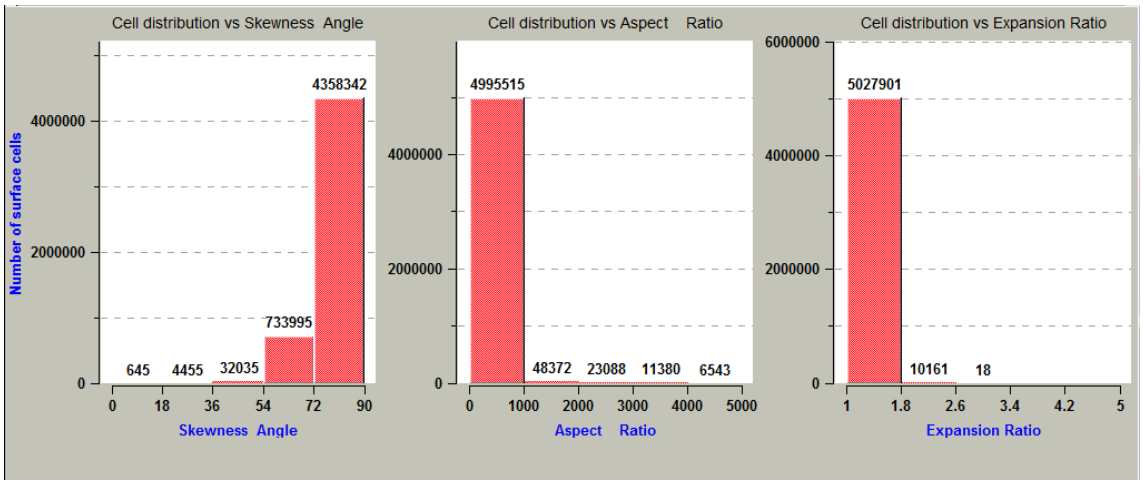

Figure 6.44.Grid quality report of 100 kW wind turbine blade, AutoGrid5^{TM}

The process of analysis continues with solution performed by FINE™/Turbo module. In the solution, similar to the previous cases, the fluid is taken as air, flow is considered to be steady, low speed i.e. Mach number < 0.3 and mathematically modeled as turbulent Navier-Stokes with turbulence model of Spalart-Allmaras. The external boundary conditions of static pressure, static temperature, velocity components along x, y and z directions and turbulent viscosity terms have been inputted as 101300 Pa or 1 atm, 293 K or 20^{o}C, V_x= V_y = 0 where V_z= 8 m/s and ν_t = 7.056x10^{-5} respectively. As initial solution, pressure, temperature and velocity component values have been taken equal to the external boundary conditions. Number of iterations was taken as 20000 and the program was started to run. After more than 5000 iterations, the program converged and the corresponding global residual and torque values are presented in Figures 6.45 and 6.46, respectively.

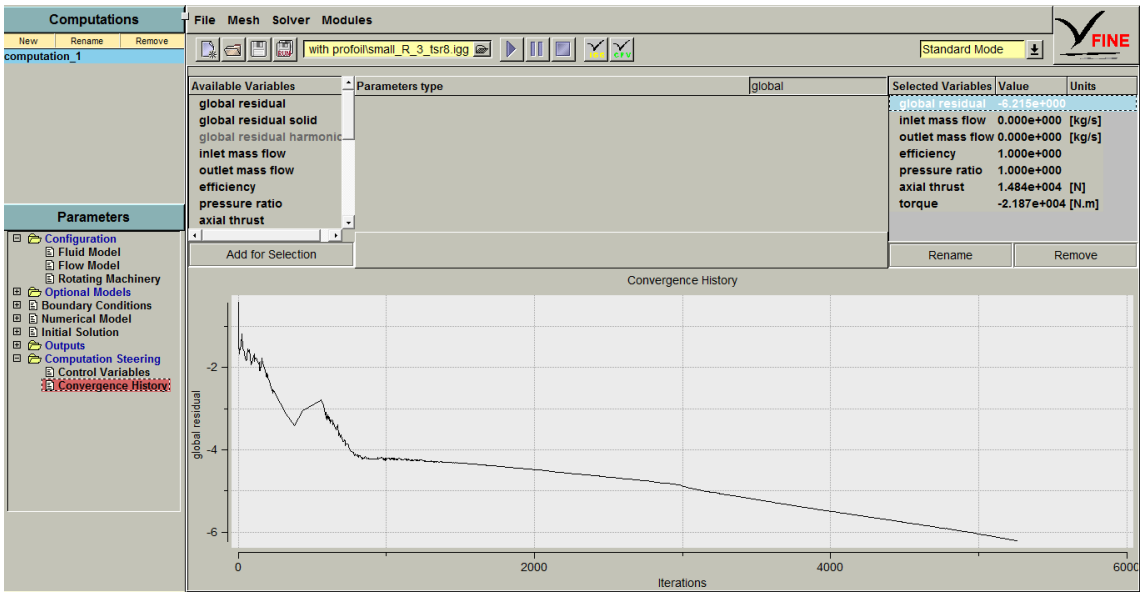

Figure 6.45.Global residual of 100 kW wind turbine rotor, FINE™/Turbo

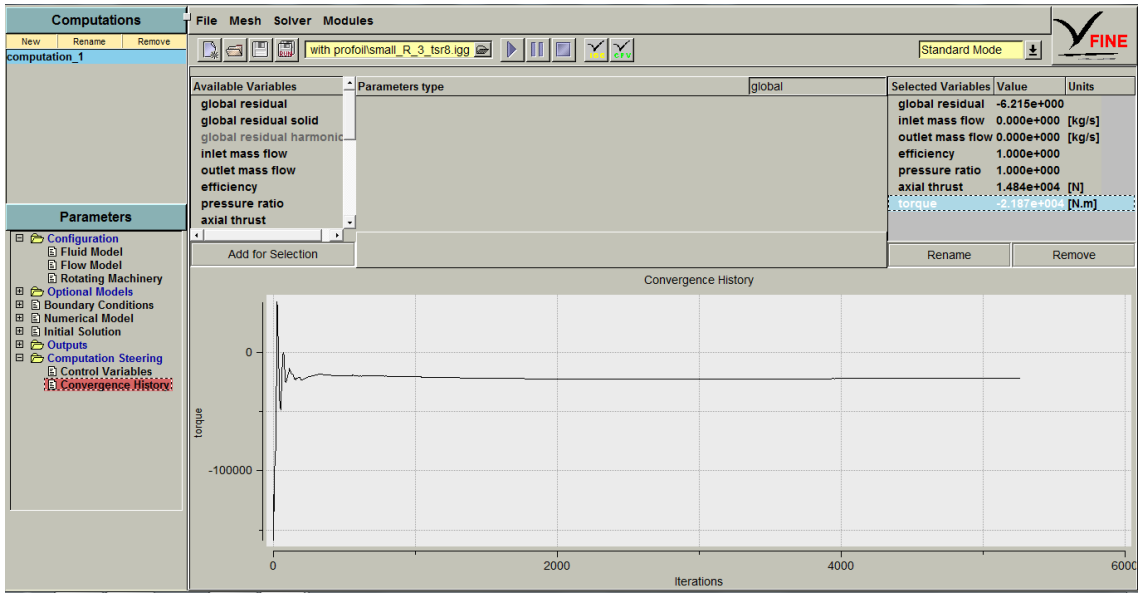

Figure 6.46.Torque output behavior of 100 kW wind turbine rotor, FINE™/Turbo

From Figure 6.46, it can be seen that torque produced by designed 100 kW wind turbine rotor is 21.87 kNm which corresponds to the power production of 86.448 kW using Equation 3.32 and transmission and gear box efficiencies taken to be 0.9 each since the angular rotation value is relatively low, the gear box may be considered to operate more efficiently. The coefficient of performance *Cp* is calculated using Equation 3.15 as 0.5121. The values obtained for *Cp* from CFD and modified BEM

codes are in a good agreement where there is only 1.64 % difference between those values. The velocity triangle obtained for the design around the cross-section taken at half span is presented in Figure 6.47.

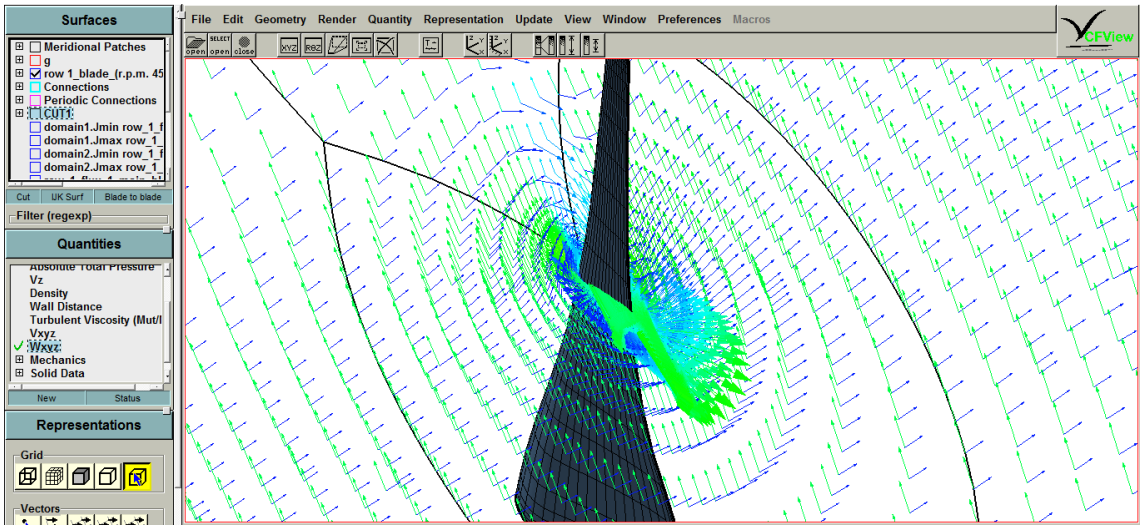

Figure 6.47.Velocity triangle formed around 100 kW wind turbine blade, CFView™

In Figure 6.47, the blue arrows correspond to the incoming velocity striking to the lower side of the blade whereas the green arrows represent the relative velocity formed by the vectoral summation of incoming and angular velocity.

The total pressure distribution around designed 100 kW wind turbine blade is presented in Figure 6.48.

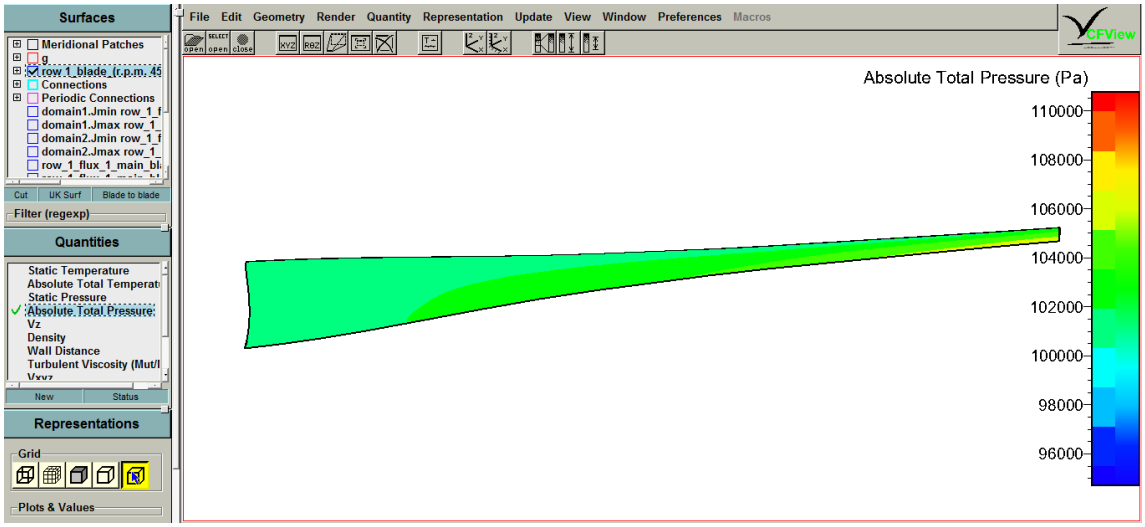

Figure 6.48.Absolute total pressure distribution around upper side of 100 kW wind turbine blade, CFView™

It can be seen from Figure 6.48 that, the highest pressure values can be read around the tip region of the blade; on the upper side near trailing edge which shows the critical area in terms of vibration due to aerodynamic and pressure forces.

The power curve of 100 kW wind turbine obtained using FINE™/Turbo is given in Figure 6.49 where cut-in wind speed can be observed as 4 m/s and cut-out wind speed is 15 m/s.

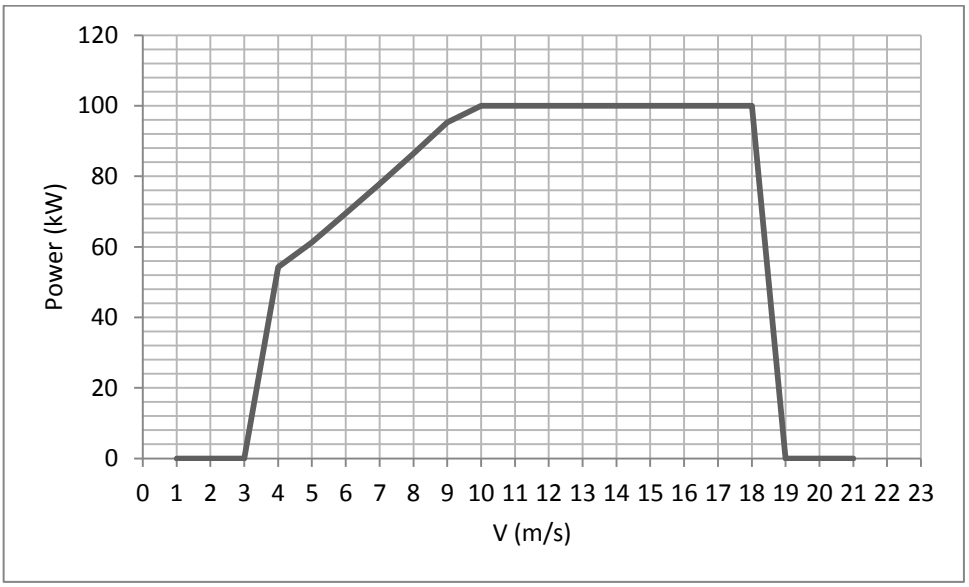

Figure 6.49.Power curve of 100 kW wind turbine

6.7. 250 kW Horizontal Axis Wind Turbine Generator

6.7.1. Airfoil Design

For the design of 250 kW wind turbine generator, creation of a whole new airfoil family was seen to be inevitable since the flow characteristics of the blade will be different than previous designs. Due to the fact that, the structural and aerodynamic loads on that particular design is expected to be higher, the profiles have been thickened and the points where the thickness and camber to chord ratios are maximum have been taken backwards in order to delay the separation which is likely to occur around the leading edge causing from relatively blunt nose. Also, the noise emission is a secondary problem since the distance between the turbine and urban area is decreased. Those demands have been inputted in PROFOIL as in Table 6.21.

Table 6.21.PROFOIL input parameters for 250 kW wind turbine generator airfoil

Parameters	Values
PHI 1	21.5
PHI 2	32.2
PHI 3	40
PHI 4	60
ALPHA 1 (deg)	8
ALPHA 2 (deg)	6
ALPHA 3 (deg)	-14
ALPHA 4 (deg)	14
Ks	0.35
Cm	-0.15

When compared to table 6.1, it can be seen that *ALPHA 2* and *3* which correspond to the upper and lower side of the leading edge is changed since the concerns about the thick leading edge or blunt nose is highly dominant. In addition to that, the trailing edge closure parameter *Ks* has been increased since noise emission rooting from trailing edge shape may relatively be neglected therefore the geometry of the trailing edge is able to be coarser than the previous designs.

The output for the parameters listed in Table 6.14 is given by PROFOIL as the geometrical shape shown in Figure 6.50 and it is named to be “tfprofoil_nt3”. It has the maximum thickness to chord ratio of 20.28 % at 23.6 % of the chord and its maximum camber is 2.69 % at 65.4 % of the chord. The coordinates of tfprofoil_nt3 is also presented in APPENDIX C.2.

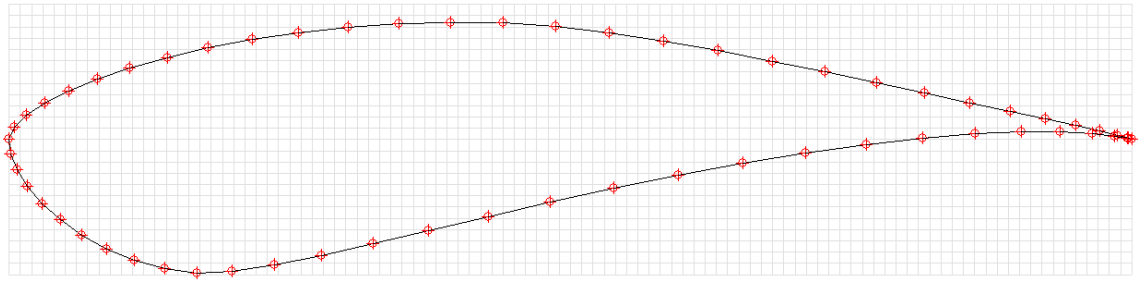

Figure 6.50.Geometry of tfprofoil_nt3

Similar to 100 kW wind turbine generator design, for 250 kW case, it is mandatory to divide the blade into design sections in order to overcome varying expectations and concerns along spanwise direction. Therefore, the blade is divided into 4 sections as near hub; from hub to 0.25 span, mid-section; from 0.25 to 0.50 span,

semi-section; from 0.50 to 0.70 span and tip region is taken to be from 0.70 span to the end of the blade. For the mid-section, tfprofoil_nt3 has been used and for the hub section it was modified to have a thickness to chord ratio of 24 % together with a decreased camber of 1.45 % in order to avoid manufacturing imperfections. For the semi-section the profile has slightly been modified to have 18 % thickness and for the tip, the thickness is reduced to the levels of 16 %.The airfoil family of tfprofoil_nt3 consists of four elements is given in Figure 6.51.

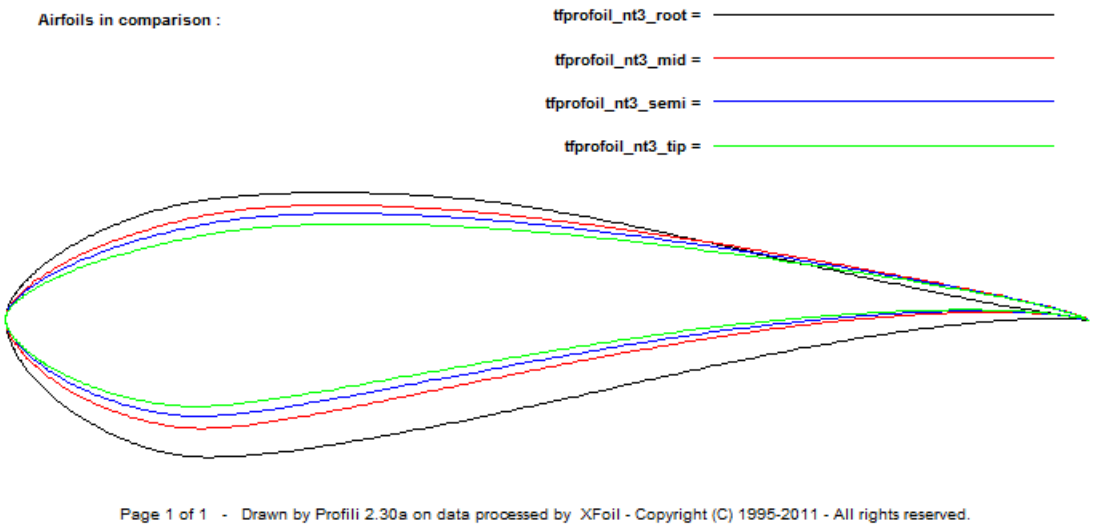

Figure 6.51.Geometrical comparison of tfprofoil_nt3 airfoil family, PROFILI

The airfoils in the family have been analyzed separately at *Re = 500000* where it is the maximum limit to be chosen using the interface of PROFILI. The possible errors rooting from that limit is to be discussed later. The resulting performance parameters of the profiles are presented in Tables 6.22, 6.23, 6.24 and 6.25.

Table 6.22.Performance parameters of tfprofoil_nt3_root, XFOIL

$(c_L/c_D)_{max}$	64.515
c_L	1.0774
c_D	0.0167
c_M	-0.0478
α (deg)	9

Table 6.23.Performance parameters of tfprofoil_nt3_mid, XFOIL

$(c_L/c_D)_{max}$	88.4873
c_L	1.3981
c_D	0.0158
c_M	-0.1005
α (deg)	9.5

Table 6.24.Performance parameters of tfprofoil_nt3_semi, XFOIL

$(c_L/c_D)_{max}$	90.4685
c_L	1.2937
c_D	0.0143
c_M	-0.1134
α (deg)	8

Table 6.25.Performance parameters of tfprofoil_nt3_tip, XFOIL

$(c_L/c_D)_{max}$	84.3468
c_L	1.0459
c_D	0.0124
c_M	-0.1217
α (deg)	5.5

6.7.2. Blade Design

The design wind speed for 250 kW wind turbine generator is chosen to 8 m/s similar to 100 kW case using Reference [26]. Substituting rated power *P = 250 kW* and Betz limit into Equation 5.2 and solving for *R* gives *R = 20.7 m*. According to the studies done by Bak et al. [27], tip speed ratio λ was assigned to be 8 and the resulting rotational speed is found as 3.092 rad/s or 30 rpm. Basic design parameters of 250 kW wind turbine generator are given in Table 6.26.

Table 6.26.Basic design parameters of 250 kW wind turbine generator

Design Variable	Unit	Value
Number of blades	-	3
Rotor radius	m	20.7
Root extension	m	3.3
Tip speed ratio	-	8
Rotational speed	rpm	30
Design wind speed	m/s	8
Rated Power	kW	250

These values listed in Table 6.26 are used as input parameters for the modified BEM code created in MATLAB. Also using the analysis results of the designed airfoils for appropriate sections, the optimum chord and twist distributions and *Cp* were found iteratively and they are listed in Table 6.27.

Table 6.27.Chord and twist distributions and Cp results of 250 kW wind turbine generator using modified BEM code, MATLAB

Section	r/R	chord (m)	twist (deg)	Cp
1	0	2.7996	23.6309	0
2	0.1	2.5597	19.8250	0.1508
3	0.2	2.3198	16.0202	0.2086
4	0.3	1.7033	10.2085	0.3220
5	0.4	1.3264	6.7930	0.4283
6	0.5	1.0806	4.6056	0.5289
7	0.6	0.7009	3.0992	0.6459
8	0.7	0.6038	2.0019	0.7427
9	0.8	0.5269	1.1644	0.8252
10	0.9	0.4491	0.4964	0.8306
11	1.0	0.4005	0	0.6823

Using Equation 6.1 and Table 6.27, the power coefficient Cp according to modified BEM code becomes $\mathrm{Cp} = 0.5365$ which will be compared with the power output data obtained from CFD analysis.

6.7.3. Blade Analysis

Similar to the other cases, to analyze the blade the geometry is formed in AutoBlade™ module of Numeca. The 3D modeled geometry of 250 kW wind turbine blade is presented in Figures 6.52 and 6.53.

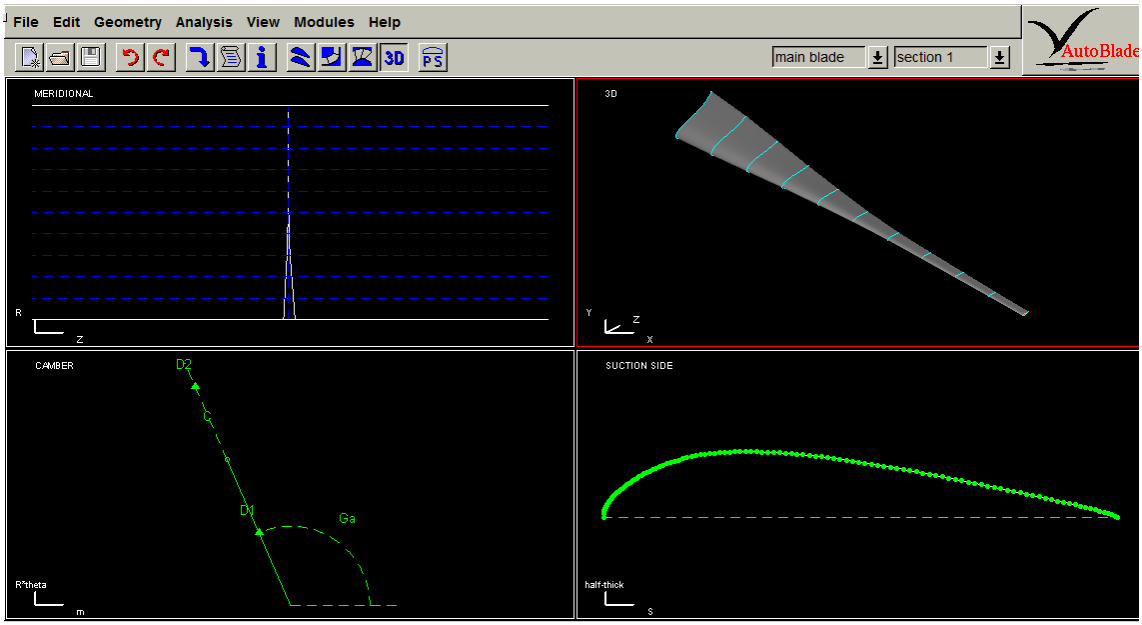

Figure 6.52.Geometry of 250 kW wind turbine blade, AutoBlade™

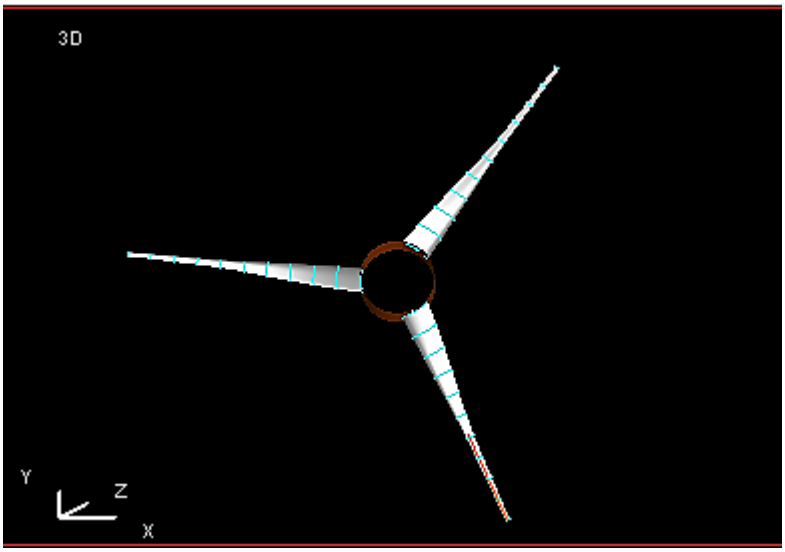

Figure 6.53.Geometry of 250 kW wind turbine rotor, AutoBlade™

In Figure 6.53, not only the observation of the length of the blade by comparing the chord lengths belong to root and tip sections can be made but also the twist distribution is clearly visualized.

The meshing process of 250 kW wind turbine blade geometry is performed using AutoGrid5^{TM}module of Numeca and the input parameters were selected as the following; rotational speed, 30 rpm; far-field domain that is desired to be meshed, 5 times of the blade length, upstream and downstream; spanwise expansion ratio, for layers 1.27; for far field, 1.35. 3D and 2D mesh distributions around 250 kW turbine blade can be observed from Figures 6.54 and 6.55, respectively.

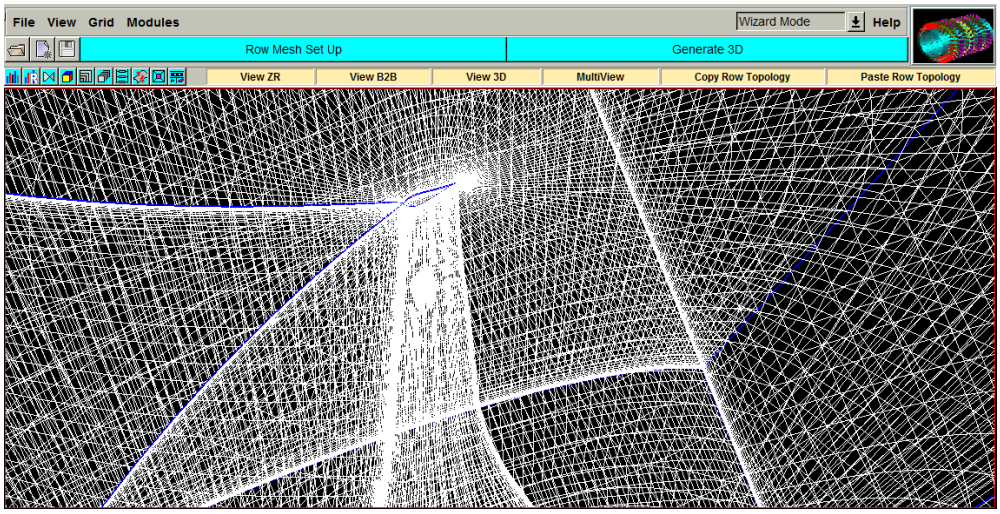

Figure 6.54.3D mesh distribution of 250 kW wind turbine blade, AutoGrid5^{TM}

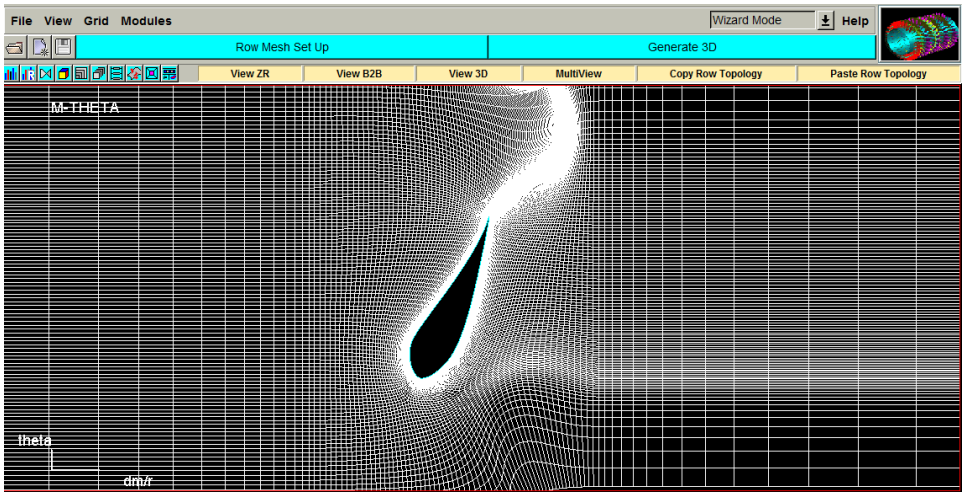

Figure 6.55.Blade to Blade (2D) mesh distribution of 250 kW wind turbine blade, AutoGrid5^{TM}

Mesh quality report for 250 kW wind turbine blade is tabulated in Table 6.28.

Table 6.28.Grid quality report of 250 kW wind turbine blade

Number of Points	1,509,651
Minimal Skewness Angle (deg)	4.031
Maximal Skewness Angle (deg)	90
Average Skewness Angle (deg)	78.2124
Minimal Spanwise Skewness Angle (deg)	169.997
Maximal Spanwise Skewness Angle (deg)	180
Average Spanwise Skewness Angle (deg)	179.710
Minimal Spanwise Expansion Ratio	1
Maximal Spanwise Expansion Ratio	1.35702
Average Spanwise Expansion Ratio	1.20626
Minimal Aspect Ratio	1
Maximal Aspect Ratio	224510
Average Aspect Ratio	538.228
Minimal Expansion Ratio	1
Maximal Expansion Ratio	2.859
Average Expansion Ratio	1.40237

In the evaluation of the grid construction, studies of Hildebrandt et al. will be considered as the limiting values [36]. According to those studies, orthogonality and aspect ratio seems to be excessing the limits. However, it can be interpreted from Figure 6.56 that, only 0.0148 % of the cells have Skewness angle less than 18^{o} and 1.12 % have aspect ratios higher than 5000 which is the least important quality criterion. In order not to increase the computational cost, the meshed geometry was considered to be sufficient to converge and give reasonable solutions.

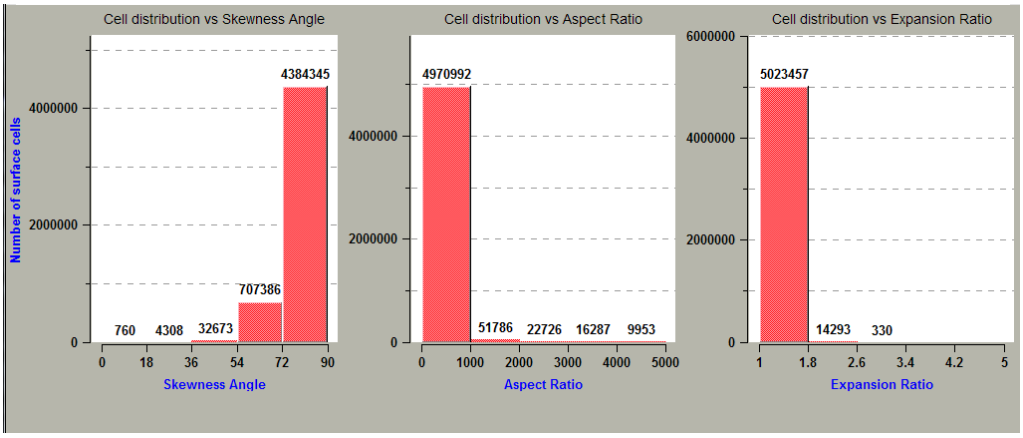

Figure 6.56.Grid quality report of 250 kW wind turbine blade, AutoGrid5^{TM}

The solution of the governing equations for the constructed elements was performed by FINE™/Turbo module. Similar to the previous cases, the fluid is taken as air, flow is considered to be steady, low speed i.e. Mach number < 0.3 and mathematically modeled as turbulent Navier-Stokes with turbulence model of Spalart-Allmaras. The external boundary conditions of static pressure, static temperature, velocity components along x, y and z directions and turbulent viscosity terms have been inputted as 101300 Pa or 1 atm, 293 K or 20^{o}C, V_x= V_y = 0 where V_z= 8 m/s and ν_t = 7.056x10^{-5}, respectively. As initial solution, pressure, temperature and velocity component values have taken to be equal to the external boundary conditions. Maximum number of iterations was taken as 20000 and the program was started to run. About 7000 iterations, the convergence is achieved. Global residual and torque values are presented in Figures 6.57 and 6.58, respectively.

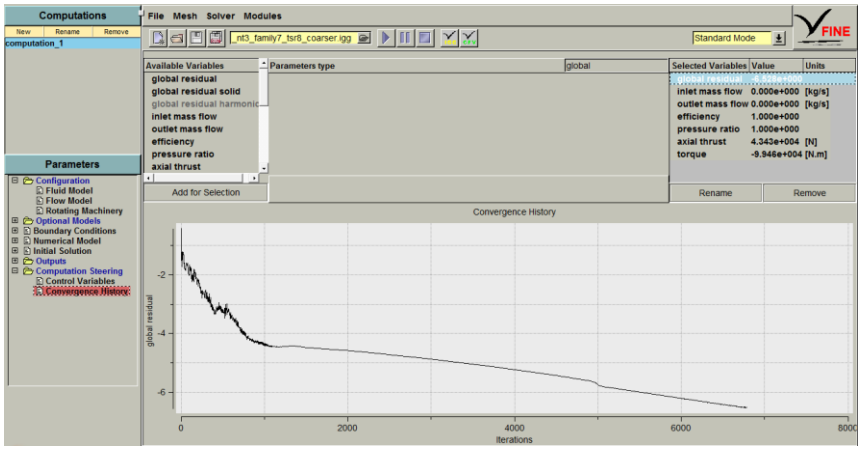

Figure 6.57.Global residual of 250 kW wind turbine rotor, FINE™/Turbo

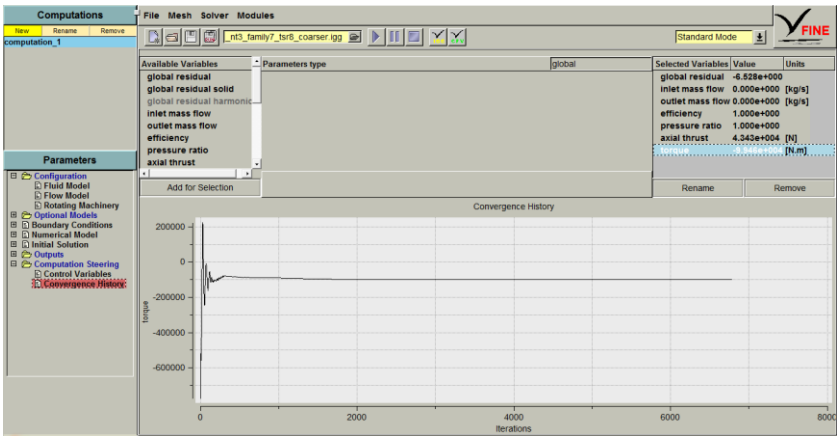

Figure 6.58.Torque output behavior of 250 kW wind turbine rotor, FINE™/Turbo

It can be interpreted from Figure 6.43 that torque produced by designed 250 kW wind turbine rotor is 99.46×10^3 Nm which corresponds to the power production of 249.083 kW using Equation 3.32 where transmission and gear box efficiencies are taken to be 0.9 each. *Cp* is calculated using Equation 3.15 as 0.5910 which is an over-estimated value. The reason for that value to be unrealistic is the lack of capability of XFOIL to analyze designed airfoils at their operating Reynolds number as mentioned in the airfoil design section of 250 kW wind turbine blade. Due to the fact that the resulting performance of the designed airfoil family is far from the real one, the geometry created by the modified BEM code is not sufficient. Moreover, the values of *Cp* calculated from CFD and modified BEM codes are not in a very good agreement where there is 10 % difference between those values. The velocity triangle obtained for the design around the cross-section taken at half span is presented in Figure 6.59.

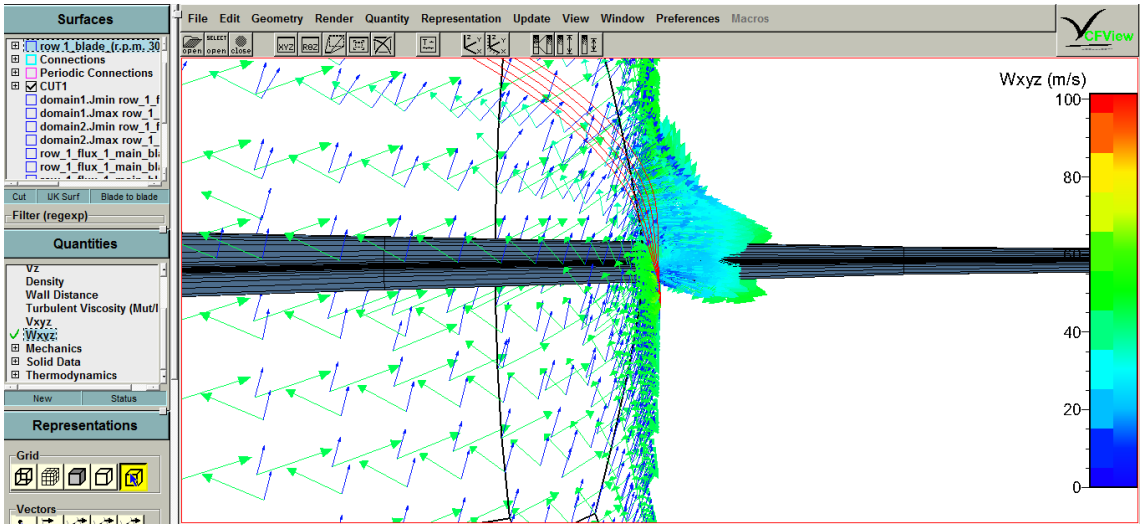

Figure 6.59.Velocity triangle formed around 250 kW wind turbine blade, CFView™

In Figure 6.59 which is side view of the blade seen from the trailing edge part, the blue arrows indicate the incoming velocity striking to the lower side of the blade whereas the green arrows represent the relative velocity constituted by the vectoral summation of incoming and angular velocity.

The static pressure distribution around half span 2D cross section of designed 250 kW wind turbine blade is presented in Figure 6.60.

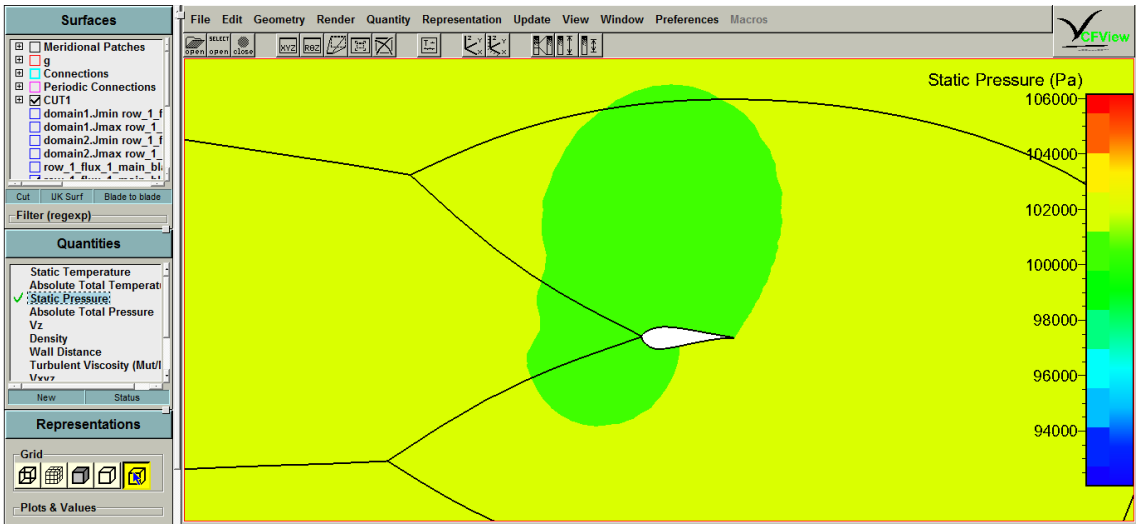

Figure 6.60.Static pressure distribution half span cross section of 250 kW wind turbine blade, CFView™

The low pressure regions being formed around the suction side of the blade can be observed from Figure 6.60 which consequently produce lift and rotate the turbine.

The power curve of 250 kW wind turbine obtained using FINE™/Turbo is given in Figure 6.61.

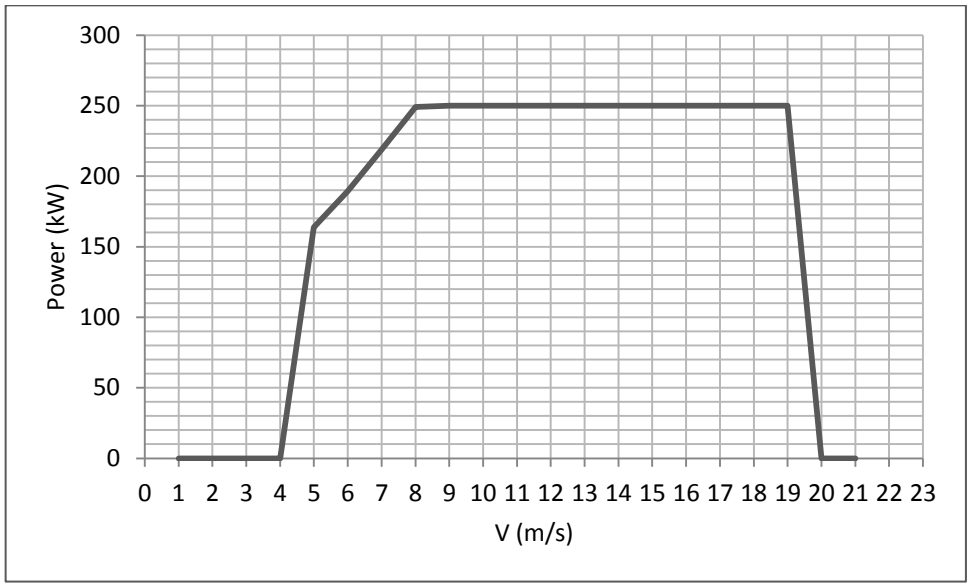

Figure 6.61.Power curve of 250 kW wind turbine

6.8. 500 kW Horizontal Axis Wind Turbine Generator

6.8.1. Airfoil Design

Since the aerodynamic and structural concerns for the design of 500 kW wind turbine generator may be considered to be similar to 250 kW design, the airfoil profiles used together with their corresponding design locations were taken to be identical. In summary, tfprofoil_nt3 airfoil family which consists of four sections; root, mid, semi and tip was used.

6.8.2. Blade Design

The design wind speed for 500 kW wind turbine generator is chosen to 8 m/s similar previous cases using Reference [26] and considering higher hub heights or altitudes. Substituting rated power $P = 500\ kW$ and Betz limit into Equation 5.2 and solving for R gives $R = 29.3\ m$. According to the studies done by Bak et al. [27], tip speed ratio λ was assigned to be 8 and the resulting rotational speed is found as 2.184 rad/s or approximately 20 rpm. Basic design parameters of 500 kW wind turbine generator are given in Table 6.29.

Table 6.29.Basic design parameters of 500 kW wind turbine generator

Design Variable	Unit	Value
Number of blades	-	3
Rotor radius	m	29.3
Root extension	m	4.7
Tip speed ratio	-	8
Rotational speed	rpm	20
Design wind speed	m/s	8
Rated Power	kW	500

These values listed in Table 6.29 are inserted to the modified BEM code created in MATLAB together with the analysis results of the designed airfoils for appropriate sections, the optimum chord and twist distributions and *Cp* were found iteratively and they are listed in Table 6.30.

Table 6.30.Chord and twist distributions and Cp results of 500 kW wind turbine generator using modified BEM code, MATLAB

Section	r/R	chord (m)	twist (deg)	Cp
1	0	4.0000	23.6309	0
2	0.1	3.6618	19.8250	0.1508
3	0.2	3.2836	16.0202	0.2086
4	0.3	2.4109	10.2085	0.3220
5	0.4	1.8775	6.7930	0.4283
6	0.5	1.5296	4.6056	0.5289
7	0.6	0.9921	3.0992	0.6459
8	0.7	0.8547	2.0019	0.7427
9	0.8	0.7458	1.1644	0.8252
10	0.9	0.6357	0.4964	0.8306
11	1.0	0.5486	0	0.6823

Using Equation 6.1 and Table 6.30, the power coefficient Cp according to modified BEM code becomes $\mathrm{Cp} = 0.5365$ which will be compared with the power output data obtained from CFD analysis. Note that, the value obtained for power coefficient using Table 6.30 is identical to the value obtained for 250 kW design since the profiles used and design tip speed ratios are the same.

6.8.3. Blade Analysis

The analysis of designed 500 kW wind turbine blade starts with the construction of the geometry which has been performed using AutoBlade™ and followed by the discretization process done in AutoGrid5^{TM} module of Numeca. The input parameters for that semi-automatic meshing process were inserted as; rotational speed, 20 rpm; far-field domain that is desired to be meshed, 5 times of the blade length upstream and downstream; spanwise expansion ratio, for layers 1.28; for far field, 1.29. While evaluating the grid, studies of Hildebrandt et al. are considered as the limiting values [36]. According to those studies, orthogonality and aspect ratio seems to be violated. However, it can be interpreted from Figure 6.62 that, only 0.0178 % of the cells have Skewness angle less than 18^{o} and 1.291 % have aspect ratios higher than 5000 which is the least important quality criterion. In order to avoid higher computational costs, the discretization was considered to be sufficient to converge and give reasonable solutions.

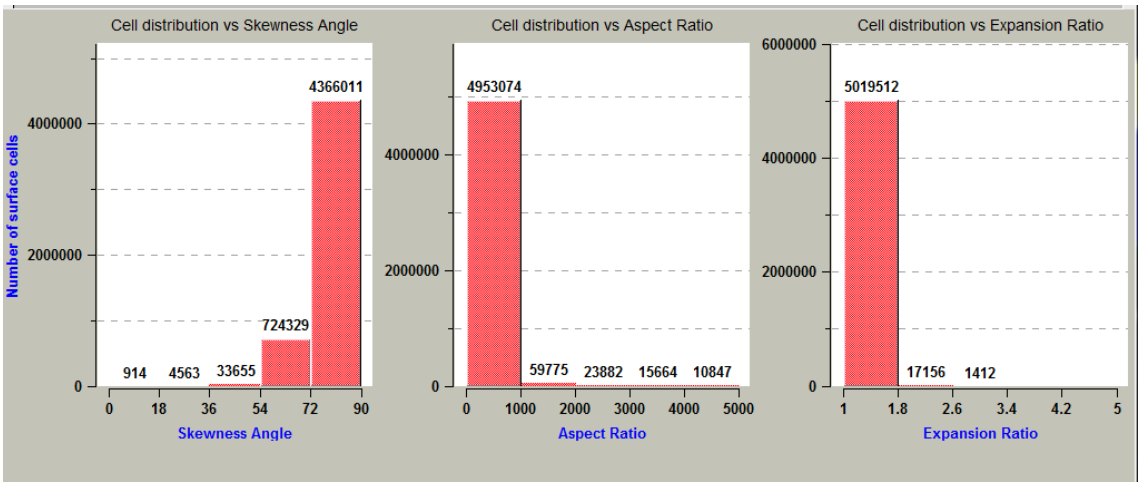

Figure 6.62.Grid quality report of 500 kW wind turbine blade, AutoGrid5^{TM}

The solution of the governing equations for the constructed elements was performed by FINE™/Turbo module. Similar to the previous cases, the fluid is taken as air, flow is considered to be steady, low speed i.e. Mach number < 0.3 and mathematically modeled as turbulent Navier-Stokes with turbulence model of Spalart-Allmaras. The external boundary conditions of static pressure, static temperature, velocity components along x, y and z directions and turbulent viscosity terms have been inputted as 101300 Pa or 1 atm, 293 K or 20^{o}C, $V_x = V_y = 0$ where $V_z = 8$ m/s and $\nu_t = 7.056x10^{-5}$, respectively. As initial solution, pressure, temperature and velocity component values have taken to be equal to the external boundary conditions. Maximum number of iterations was taken as 20000 and the program was started to run. About 5500 iterations, the convergence is achieved. Global residual and torque values are presented in Figures 6.63 and 6.64, respectively.

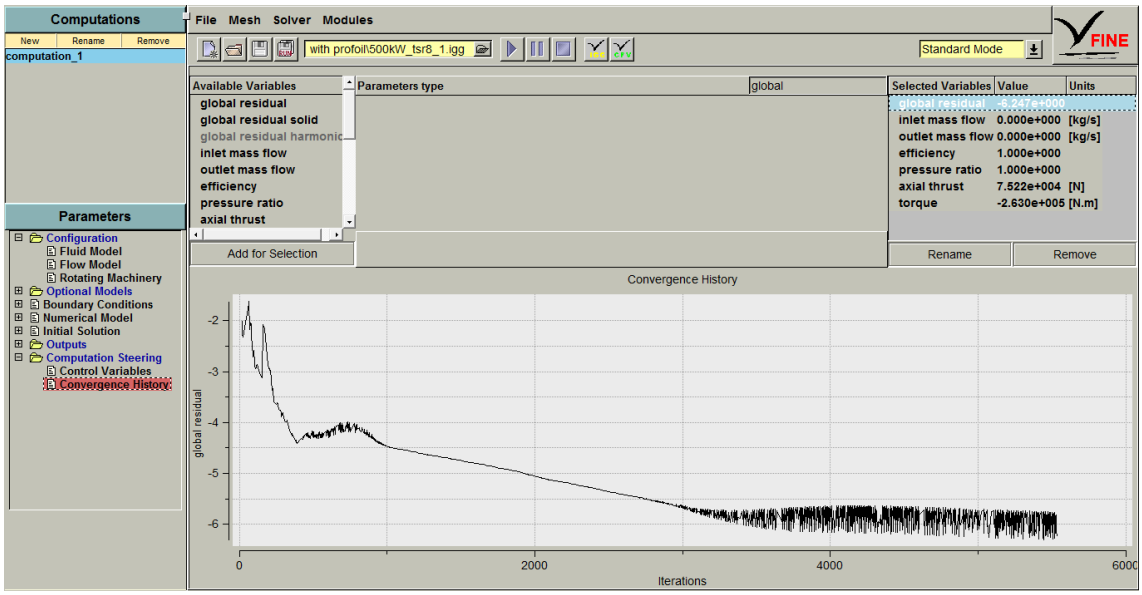

Figure 6.63.Global residual of 500 kW wind turbine rotor, FINE™/Turbo

It can be observed from Figure 6.63 that the global residual of the program starts oscillating after performing approximately 3000 iterations. The reason for that behavior is the fact that the analysis of airfoils was made at much lower Reynolds number than the actual case due to the limitations of the analysis code XFOIL.

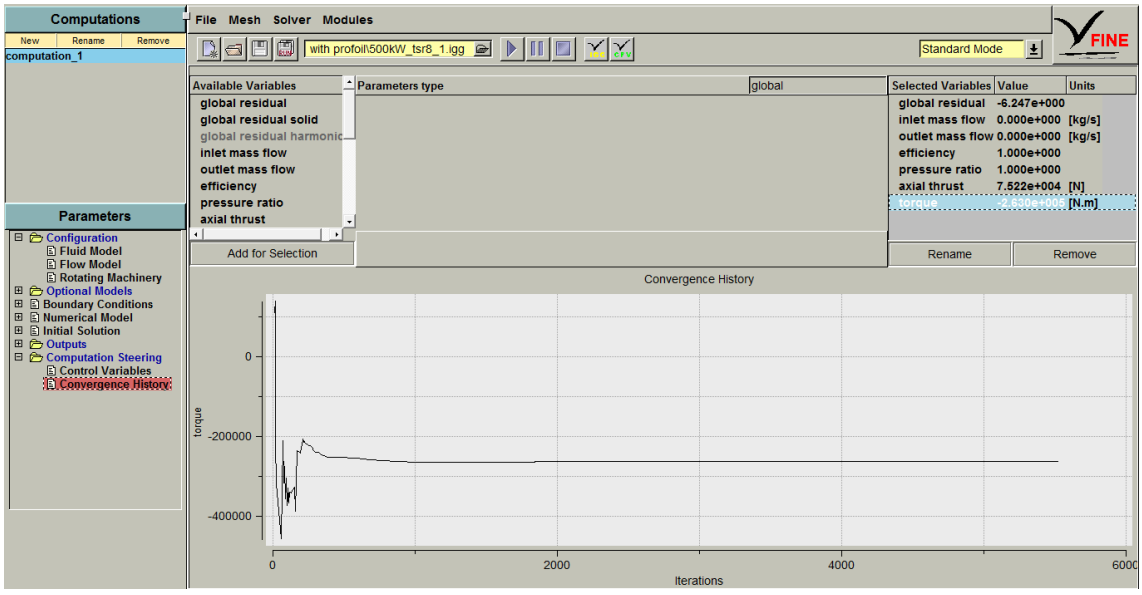

Figure 6.64.Torque output behavior of 500 kW wind turbine rotor, FINE™/Turbo

It can be interpreted from Figure 6.64 that torque produced by designed 500 kW wind turbine rotor is 2.63×10^5 Nm which corresponds to the power production of

465.26 kW using Equation 3.32 where transmission and gear box efficiencies are taken to be 0.9 each. *Cp* is calculated using Equation 3.15 as 0.552 which may be found as an over-estimated or unrealistic value which occurred from the same reason as the oscillations mentioned above.

The power curve of 500 kW wind turbine obtained using FINE™/Turbo is given in Figure 6.65. Note that, it has been constructed with the consideration of brakes both aerodynamic and mechanical and pitch control.

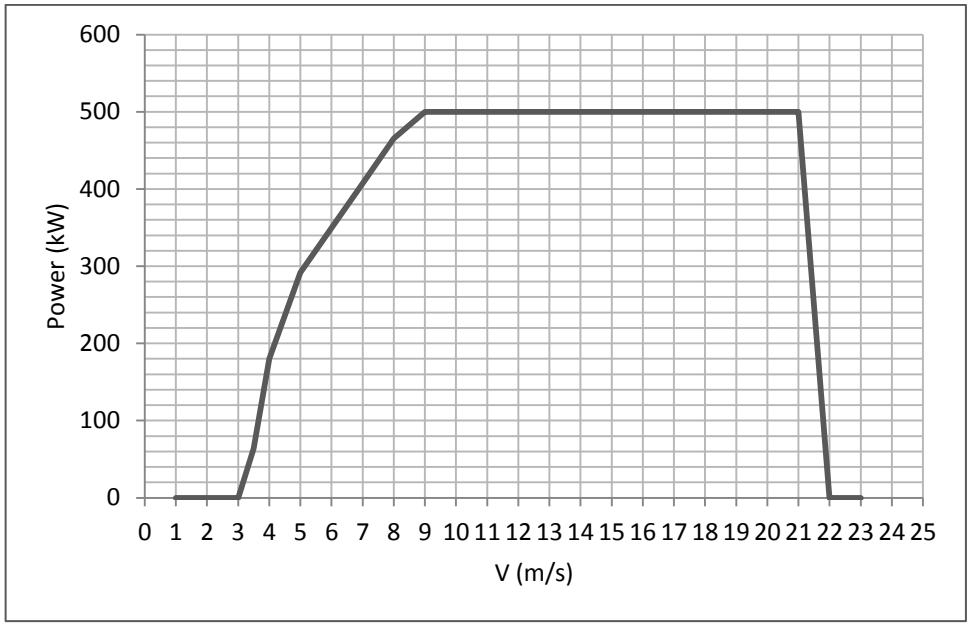

Figure 6.65.Power Curve of 500 kW wind turbine generator

CHAPTER 7

CONCLUSION

In this study, aerodynamic design of horizontal axis small scale wind turbine blades has been performed. The blades have been designed and analyzed for wind turbines with rated powers of 1, 5, 10, 25, 50, 100, 250 and 500 kW by applying different strategies.

The process starts with design and analysis of the airfoil which is done by PROFOIL and a user interface for XFOIL called PROFILI, respectively. After obtaining the results from the designed airfoil such as its maximum lift to drag ratio point, they are put as inputs to a code developed using modified blade element momentum theory on MATLAB. The design tool is validated using MIE wind turbine with rated power of 8 kW developed in Mie University, Japan. The program is designed to read the airfoil data and rotor characteristics such as number of blades, desired radius and tip speed ratio and give the geometric characteristics of the blade such as chord and twist distribution and the expected coefficient of power as outputs. Those geometrical data of the blade are then inputted to CFD software called NUMECA which gives the power output of the design.

All the wind turbine designs are three bladed and design wind speeds were selected using the wind atlas prepared for the campus area of Izmir Institute of Technology, IZTECH.

For the design of 1 kW wind turbine generator, only one airfoil profile which was designed using PROFOIL was used due to the manufacturing considerations. The blade radius for that design was calculated to be 1.78 m. The resulting coefficient of power Cp was obtained as 0.5004 according to the modified BEM code where CFD analysis gives 0.4593 because of high mechanical losses taken into consideration.

In 5 kW wind turbine blade design, tfprofoil_nt2 the airfoil designed in 1 kW case was modified using PROFOIL to achieve 20 % thickness around hub region where 16 % thickness was maintained around tip. The radius of that rotor was obtained as 3.6 m and Cp calculated using modified BEM code is 0.5054 where using CFD, Cp may be found as 0.5072.

In the aerodynamic design of 10 and 25 kW wind turbine blades, the same spanwise design sections were used with 5 kW case since the considerations are similar. The radius of that rotor was obtained as 5 m for 10 kW and 8 m for 25 kW case. For 10 kW design, Cp calculated using modified BEM code is 0.5072 where using CFD, Cp may be found as 0.4903 whereas for 25 kW, Cp calculated using modified BEM code is 0.5058 where using CFD, Cp may be found as 0.5115 .

In rated power of 50 kW and 100 kW wind turbine blade designs, three design locations were constructed and three airfoil profiles were used such that tfprofoil_nt2 was modified to have 24 % thickness in order to support the hub structurally. The resulting blade length of 50 kW was found to be 11.3 m where for 100 kW case it was 13.1 m. Cp calculated using modified BEM code is 0.5335 for 50 kW and 0.5205 for 100 kW design where using CFD, Cp may be found as 0.5338 for 50 kW and 0.5121 for 100 kW rotor.

For the design of 250 kW and 500 kW wind turbine blades, a new airfoil was designed using PROFOIL and it was named as tfprofoil_nt3. It was modified to obtain an airfoil family appropriate for four separate design points. The radius of the rotor was attained to be 20.7 m for 250 kW and 29.3 m for 500 kW design. Cp calculations yields 0.5365 for both of the designs using modified BEM code and 0.5910 for 250 kW and 0.5520 for 500 kW case using the results obtained from CFD.

Consequently, it was seen that, the values of Cp is increasing with increasing number of design points since it provides the usage of appropriate airfoil sections which are designed for the particular segment along the blade span. Also, the importance of operating Reynolds number for airfoils was highlighted since it leads to miscalculated geometrical properties and therefore over estimated Cp values.

To sum up, the developed process is performed successfully for both design and analysis of horizontal axis small scale wind turbines. Considering the practicality, applicability, robustness and computational cost this process may be regarded as sufficient. It is possible to strengthen the methodology by the usage of more powerful and capable design and analysis tools.

REFERENCES

[1] United Nations, 2012. *Kyoto Protocol*. Available: http://unfccc.int/kyoto_protocol/items/2830.php

[2] E. Hau and E. Hau, *Wind turbines : fundamentals, technologies, application, economics*, 2nd English ed. Berlin ; New York: Springer, 2006.

[3] J. F. Manwell, J. G. McGowan, and A. L. Rogers, *Wind energy explained: theory, design and application*, 2nd ed. Chichester, U.K.: Wiley, 2009.

[4] P. Gipe, *Wind energy comes of age*. New York: Wiley, 1995.

[5] Global Wind Energy Council. 2012, Global Wind Statistics 2011.

[6] Republic of Turkey Energy Market Regulatory Authority. 2011, Legislation of the Change in Regulations for Electricity Market.

[7] D. A. Spera, *Wind turbine technology : Fundamental concepts of wind turbine engineering*, 2nd ed. New York, NY: ASME Press, 2009.

[8] S. Eriksson, H. Bernhoff, and M. Leijon, "Evaluation of different turbine concepts for wind power," *Renewable and Sustainable Energy Reviews*, vol. 12, pp. 1419-1434, 2008.

[9] J. Wata, M. Faizal, B. Talu, L. Vanawalu, P. Sotia, and M. R. Ahmed, "Studies on a low Reynolds number airfoil for small wind turbine applications," *Science China-Technological Sciences*, vol. 54, pp. 1684-1688, Jul 2011.

[10] J. C. C. Henriques, F. Marques da Silva, A. I. Estanqueiro, and L. M. C. Gato, "Design of a new urban wind turbine airfoil using a pressure-load inverse method," *Renewable Energy*, vol. 34, pp. 2728-2734, 2009.

[11] P. Fuglsang and C. Bak, "Development of the Riso wind turbine airfoils," *Wind Energy*, vol. 7, pp. 145-162, Apr-Jun 2004.

[12] R. K. Singh, M. R. Ahmed, M. A. Zullah, and Y. H. Lee, "Design of a low Reynolds number airfoil for small horizontal axis wind turbines," *Renewable Energy*, vol. 42, pp. 66-76, Jun 2012.

[13] K. Ameku, B. M. Nagai, and J. N. Roy, "Design of a 3 kW wind turbine generator with thin airfoil blades," *Experimental Thermal and Fluid Science*, vol. 32, pp. 1723-1730, Sep 2008.

[14] L. Dong, M. F. Liao, Y. F. Li, X. P. Song, and K. Xu, "Study on Aerodynamic Design of Horizontal Axis Wind Turbine Generator System," *Iceet: 2009 International Conference on Energy and Environment Technology, Vol 1, Proceedings*, pp. 841-844, 2009.

[15] Y. Hu and S. S. Rao, "Robust Design of Horizontal Axis Wind Turbines Using Taguchi Method," *Journal of Mechanical Design,* vol. 133, Nov 2011.

[16] E. Benini and A. Toffolo, "Optimal Design of Horizontal-Axis Wind Turbines Using Blade-Element Theory and Evolutionary Computation," *Journal of Solar Energy Engineering,* vol. 124, p. 357, 2002.

[17] K. Y. Maalawi and M. A. Badr, "A practical approach for selecting optimum wind rotors," *Renewable Energy,* vol. 28, pp. 803-822, Apr 2003.

[18] A. Vitale and A. Rossi, "Computational method for the design of wind turbine blades," *International Journal of Hydrogen Energy,* vol. 33, pp. 3466-3470, 2008.

[19] L. Baffisti, G. Soraperra, R. Fedrizzi, and L. Zanne, "Inverse design-momentum, a method for the preliminary design of horizontal axis wind turbines - art. no. 012013," *Science of Making Torque from Wind,* vol. 75, pp. 12013-12013, 2007.

[20] J. F. Walker and N. Jenkins, *Wind energy technology*. hichester, England; New York: John Wiley, 1997.

[21] J. D. Anderson, *Fundamentals of aerodynamics*, 4th ed. Boston: McGraw-Hill Higher Education, 2007.

[22] M. S. Selig and M. D. Maughmer, "Multipoint Inverse Airfoil Design Method Based on Conformal Mapping," *Aiaa Journal,* vol. 30, pp. 1162-1170, May 1992.

[23] M. S. Selig and M. D. Maughmer, "Generalized Multipoint Inverse Airfoil Design," *Aiaa Journal,* vol. 30, pp. 2618-2625, Nov 1992.

[24] M. Drela. XFOIL: an analysis and design system for low Reynolds number airfoils. *Low Reynolds numbers aerodynamics, Lecture Notes in Engineering 54(1),* 1989.

[25] E. Hoogedoorn, G. B. Jacobs, and A. Beyene, "Aero-elastic behavior of a flexible blade for wind turbine application: A 2D computational study," *Energy,* vol. 35, pp. 778-785, 2010.

[26] Ç. Ünveren, "Wind Resource Assessment on the Campus Area of Izmir Institute of Technology: Use of Multi Point Data Source " Master's, İzmir Institute of Technology, İzmir, 2010.

[27] C. Bak, "Sensitivity of key parameters in aerodynamic wind turbine rotor design on power and energy performance - art. no. 012008," *Science of Making Torque from Wind,* vol. 75, pp. 12008-12008, 2007.

[28] S. Rajakumar and D. Ravindran, "Iterative approach for optimising coefficient of power, coefficient of lift and drag of wind turbine rotor," *Renewable Energy,* vol. 38, pp. 83-93, Feb 2012.

[29] H. Glauert, *Airplane Propellers : Aerodynamic Theory*. Berlin: Springer Verlag, 1935.

[30] J. G. Schepers, "Final Report of IEA Annex XVIII: Enhanced Field Rotor Aerodynamics Database," Energy Research Centre of Netherlands2002.

[31] "Fine / Turbo Theory Manual," N. International, Ed., ed, 2010.

[32] P. R. Spalart and S. R. Allmaras, "A One-Equation Turbulence Model for Aerodynamic Flows," *Recherche Aerospatiale*, pp. 5-21, 1994.

[33] P. K. G. Ashford G.A. (1996, An unstructured grid generation and adaptative solution technique for high-Reynolds number compressible flow.

[34] D. Choi and C. L. Merkle, "The application of preconditioning in viscous flows," *Journal of Computational Physics*, vol. 105, pp. 207-223, 1993.

[35] R. P. J. O. M. Rooij and W. Timmer, "Roughness sensitivity considerations for thick rotor blade airfoils," *Journal of Solar Energy Engineering-Transactions of the Asme*, vol. 125, pp. 468-478, Nov 2003.

[36] T. Hildebrandt. 2008, Ingenieurbüro.

APPENDIX A

MODIFIED BEM THEORY ITERATIVE MATLAB CODE

```
clear all
clc
i=1;
B=3;
cl=1.4321;
cd=0.0209;
alpha=10.5;
R=3.6;
t=0.5;
tsr=6;
tsrl=t*tsr;
% w1 = inital "angle of relative wind"
w1=2/3*(atand(1/tsrl));
% c1= initial "local chord"
c1=8*pi*R*t/(B*cl)*(sin(w1)/(3*tsrl));
% s1= "initial solidity"
s1=B*c1/(2*pi*R*t);
% a= initial "axial induction factor"
a=1/(1+(4*(sind(w1))^2/(s1*cl*cosd(w1))));
% an= a'= initial "angular induction factor"
an=(1-3*a)/(4*a-1);
maxiter=1000;
for iter=1:maxiter;
    i=i+1;
    % w = "angle of relative wind"
    w(i-1)=atand((1-a(i-1))/((1+an(i-1))*tsrl));
    % spitch = "section pitch"
    spitch(i-1)= atand((1-a(i-1))/((1+an(i-1))*tsr))-alpha;
    % c = "local chord"
    c(i-1)=8*pi()*R*t*sind(w(i-1))/(3*B*cl*tsrl);
    % s = "solidity"
    s(i-1)=B*c(i-1)/(2*pi()*R*t);
    %ct= "thrust coefficient"
    ct(i-1)=s(i-1)*(1-a(i-1))^2*(cl*cosd(w(i-1))+cd*sind(w(i-
1)))/(sind(w(i-1)))^2;
    % F = "relative tip loss factor"
    F(i)=(2/pi)*acos(exp(-(B/2)*(1-t)/(t*sind(w(i-1)))));
    if ct(i-1)<0.96;
    % a = "axial induction factor"
    a(i)=1/(1+4*F(i)*(sind(w(i-1)))^2/(s(i-1)*cl*cosd(w(i-1))));
    else
    a(i)=1/F(i)*(0.143+(0.0203-0.6427*(0.889-ct(i-1)))^0.5);
    end
    % an = "angular induction factor"
    an(i)=1/(4*cosd(w(i-1))/(s(i-1)*cl)-1);
    errora=max(abs(a(i)-a(i-1)));
    erroran=max(abs(an(i)-an(i-1)));
    Cp(i)=F(i)*(sind(w(i-1)))^2*(cosd(w(i-1))-tsrl*sind(w(i-
1)))*(sind(w(i-1))+tsrl*cosd(w(i-1)))*(1-(cd/cl)*cotd(w(i-1)))*tsrl^2;
    if errora<1E-9;
        if erroran<1E-9;
        break;
```

```
        end
    end
end
    if iter==maxiter;
    warning('Convergence not reached')
    end
twist=w-alpha-spitch;
twist=twist(end)
c=c(end)
Cp=Cp(end)
errora
erroran
```

APPENDIX B

COMPARISON OF CHORD DISTRIBUTIONS BETWEEN MIE TURBINE AND MODIFIED BEM THEORY OUTPUT

Table B.1. Comparison of chord distributions between MIE turbine and modified BEM theory output

local radius(m)	spanwise position	MIE chord (m)	BEM code chord (m)
0.433	0.0866	0.255	0.685
0.804	0.1608	0.320	0.592
1.269	0.2538	0.438	0.475
1.361	0.2722	0.447	0.4524
1.625	0.325	0.410	0.3863
2.500	0.500	0.294	0.2576
2.7970	0.559	0.246	0.2273
3.500	0.700	0.209	0.1793
3.960	0.792	0.178	0.1560
4.500	0.900	0.139	0.1178
4.703	0.9406	0.126	0.1073
4.827	0.9654	0.115	0.0960
4.923	0.9846	0.104	0.0896
5.000	1	0.030	0.0845

APPENDIX C

COORDINATES OF CONSTRUCTED AIRFOILS

C.1. Coordinates of tfprofoil_nt2

Table C.1. Coordinates of tfprofoil_nt2

Upper		Lower	
x/c	y/c	x/c	y/c
0	0	0	0
0.00133	0.011468	0.004531	-0.01263
0.008871	0.023019	0.013242	-0.02622
0.021253	0.035277	0.025794	-0.04003
0.037996	0.047653	0.041886	-0.05351
0.058779	0.059789	0.061279	-0.06622
0.083293	0.071323	0.083663	-0.07766
0.111257	0.081929	0.108746	-0.08733
0.142331	0.091285	0.13618	-0.09464
0.176146	0.098994	0.165345	-0.09819
0.212682	0.104355	0.19805	-0.09695
0.252238	0.107258	0.236095	-0.09193
0.294744	0.108142	0.278792	-0.08453
0.339791	0.107178	0.325659	-0.07539
0.386988	0.104539	0.376126	-0.0651
0.435885	0.100405	0.429534	-0.05419
0.486033	0.094997	0.485143	-0.04317
0.536881	0.088528	0.542131	-0.03249
0.587878	0.081257	0.59963	-0.02258
0.638426	0.073408	0.656709	-0.01375
0.687933	0.065242	0.712397	-0.0063
0.73574	0.05696	0.765725	-0.00039
0.781227	0.048785	0.815722	0.003834
0.823774	0.040877	0.861439	0.006389
0.862789	0.0334	0.901975	0.007329
0.897705	0.026453	0.936481	0.006854
0.928029	0.02012	0.964175	0.005199
0.953293	0.01446	0.984198	0.002884
0.973136	0.009495	0.996119	0.000861
0.987368	0.005025	1	0
0.99651	0.00139	-	-
1	0	-	-

C.2. Coordinates of tfprofoil_nt3

Table C.2. Coordinates of tfprofoil_nt3

Upper		Lower	
x/c	y/c	x/c	y/c
0	0	0	0
0.004481	0.01097	0.001521	-0.01274
0.015565	0.021533	0.007142	-0.02702
0.03186	0.032415	0.016545	-0.04192
0.052896	0.043224	0.029489	-0.05688
0.078294	0.053719	0.045754	-0.07138
0.107722	0.063698	0.06509	-0.08492
0.140802	0.07295	0.087246	-0.09703
0.177173	0.081314	0.111914	-0.1072
0.216415	0.088608	0.138752	-0.11479
0.258107	0.09468	0.16712	-0.11836
0.301771	0.099399	0.19895	-0.1168
0.346954	0.102583	0.236131	-0.11113
0.393128	0.10408	0.278003	-0.1028
0.439742	0.103639	0.324117	-0.09246
0.486676	0.100527	0.373932	-0.08075
0.53438	0.094808	0.426838	-0.06825
0.582835	0.08739	0.482105	-0.05552
0.63147	0.078803	0.538922	-0.04305
0.679694	0.069495	0.596429	-0.03132
0.726868	0.059872	0.653676	-0.02073
0.772342	0.050313	0.709683	-0.01161
0.815415	0.041116	0.763459	-0.0042
0.855397	0.032568	0.813994	0.001349
0.891597	0.024846	0.860298	0.004977
0.923367	0.018109	0.90142	0.006736
0.950135	0.012384	0.936501	0.006783
0.971381	0.007689	0.964609	0.005264
0.986776	0.003833	0.984665	0.002806
0.996479	0.001018	0.996279	0.000757
1	0	1	0